AD_____

Award Number: W81XWH-08-1-0377

TITLE: Unraveling the Molecular Mechanism(s) Underlying Er+/PR-Breast Tumorigenesis Using a Novel Genetically Engineered Mouse Model

PRINCIPAL INVESTIGATOR: Dr. Hua Xiao

CONTRACTING ORGANIZATION: Michigan State University
East Lansing, MI 48824

REPORT DATE: November 2011

TYPE OF REPORT: Final

PREPARED FOR: U.S. Army Medical Research and Materiel Command
Fort Detrick, Maryland 21702-5012

REPORT DOCUMENTATION PAGE

Form Approved
OMB No. 0704-0188

1. REPORT DATE *(DD-MM-YYYY)*	**2. REPORT TYPE**	**3. DATES COVERED** *(From - To)*
01-11-2011	Final	1 SEP 2008 - 31 AUG 2011

4. TITLE AND SUBTITLE
Unraveling the Molecular Mechanism(s) Underlying Er+/PR-Breast Tumorigenesis Using a Novel Genetically Engineered Mouse Model

5a. CONTRACT NUMBER

5b. GRANT NUMBER
W81XWH-08-1-0377

5c. PROGRAM ELEMENT NUMBER

6. AUTHOR(S)
Dr. Hua Xiao

E-Mail: xiaoh@msu.edu

5d. PROJECT NUMBER

5e. TASK NUMBER

5f. WORK UNIT NUMBER

7. PERFORMING ORGANIZATION NAME(S) AND ADDRESS(ES)
Michigan State University
East Lansing, MI 48824

8. PERFORMING ORGANIZATION REPORT NUMBER

9. SPONSORING / MONITORING AGENCY NAME(S) AND ADDRESS(ES)
U.S. Army Medical Research and Materiel Command
Fort Detrick, Maryland 21702-5012

10. SPONSOR/MONITOR'S ACRONYM(S)

11. SPONSOR/MONITOR'S REPORT NUMBER(S)

12. DISTRIBUTION / AVAILABILITY STATEMENT
Approved for Public Release; Distribution Unlimited

13. SUPPLEMENTARY NOTES

14. ABSTRACT
ES

Abstract on next page.

15. SUBJECT TERMS
Subject terms on next page.

16. SECURITY CLASSIFICATION OF:			**17. LIMITATION OF ABSTRACT**	**18. NUMBER OF PAGES**	**19a. NAME OF RESPONSIBLE PERSON**
a. REPORT	**b. ABSTRACT**	**c. THIS PAGE**			USAMRMC
U	U	U	UU	51	**19b. TELEPHONE NUMBER** *(include area code)*

14. ABSTRACT

Estrogen-receptor alpha (ERα)-positive and progesterone receptor negative (ER+/PR-) breast ductal carcinomas comprise approximate15-25% of human breast cancers. However, molecular mechanisms underlying the development of this subtype of breast cancer remain poorly understood. This project is to study the molecular mechanism(s) underlying ER+/PR- breast tumorigenesis. Specifically, we proposed to determine genetic and epigenetic alterations in the initiation and progression of ER+/PR- mammary tumors arising in Tip30-/-/MMTV-Neu mice. We demonstrated that *Tip30* deletion in MMTV-Neu mice significantly accelerates the formation of ER+/PR- mammary tumors. An unbiased DNA microarray analysis revealed that Tip30 deletion resulted in increased activation of cAMP-mediated signaling, EGF signaling, IGF signaling and PI3K/AKT signaling in ER+/PR- mammary tumors. Moreover, we reported that the growth of ER+/PR- mammary tumors arising in our mouse models depends not only on estrogen, but also on progesterone, despite the absence of detectable PR by immunohistochemistry, providing a rationale for targeting PR signaling for the inhibition of ER+/PR- breast cancer development. Here we report that loss of Tip30 cooperates with Neu activation to enhance the activation of Akt signaling and ERα through delaying EGFR degradation and sustaining EGFR signaling. In addition, we demonstrate that treatment of ER+/PR- mammary tumor cells with NVP-BEZ235 in combination with tamoxifen significantly inhibited cell proliferation compared to treatment with either NVP-BEZ235 or tamoxifen alone. Together, our data suggest NVP-BEZ235 in combination with tamoxifen as a potential therapeutic strategy for treating ER+/PR- breast cancers that are resistant to tamoxifen or trastuzumab.

15. SUBJECT TERMS

Estrogen receptor, progesterone receptor, breast cancer, tumorigenesis

Table of Contents

Introduction:

It is estimated that 15-25% of all human breast cancers are ER+/PR- with more aggressive malignant characteristics and poorer response to SERMs compared to ER+/PR+ breast cancers (*1-3*). However, the molecular mechanism underlying development of ER+/PR- breast cancers still remains elusive (*1*). Our data indicates that deletion of *Tip30*, a tumor suppressor, leads to development of ER+/PR- in MMTV-Neu mouse model. The objective of this research project was to determine the molecular basis of ER+/PR- breast tumor development promoted by *Tip30* deletion. Our rationale for these studies was that elucidation of molecular basis of ER+/PR- breast tumor development has the potential to identify new therapeutic targets and strategies in the treatment, or even prevention, of breast cancers that are resistant to anti-estrogen therapy (*2, 4*). Specifically, we wanted to determine genetic and epigenetic alterations in the initiation and progression of ER+/PR- mammary tumors arising in *Tip30*-/-/MMTV-Neu mice; and to evaluate IGF-I and Wisp-2 as potential therapeutic targets for ER+/PR- mammary tumors developed in *Tip30-/-* MMTV-Neu mice.

Body:

Task 1. **Determine specific genetic and epigenetic alterations in the initiation and progression of ER+/PR- mammary tumors arising in *Tip30*-/-/MMTV-Neu and *Tip30*+/-/MMTV-Neu mice.** The experiments proposed in Task 1 were completed. We have demonstrated that deletion of *Tip30* leads to progressively increased numbers of p-Akt positive cells in the mammary glands from MMTV-Neu mice. Our data indicate that the relatively earlier onset of enhanced activation p-Akt in the mammary glands due to *Tip30* loss may contribute to accelerated mammary tumorigenesis in *Neu+/Tip30*$^{-/-}$ mice. We also found that the genes affected by Tip30 loss in breast tumors are involved in ion and protein transportation, cell adhesion, cell proliferation and apoptosis signaling pathways (see Appendices). Ingenuity pathway analysis of altered gene profiles revealed that cancer-associated pathways including EGF, IGF-I and PI3K/AKT signaling pathways were affected by *Tip30* deletion in Neu+ mammary tumors. Importantly, we have unraveled a novel mechanism in which TIP30 deletion increases EGFR signaling pathway (*5, 6*). These results have been included in three research articles, which were published in 2010 and 2011 (see Appendices). Together, our results indicate that besides increasing IGF-I signaling, enhancing other growth factor signaling pathways such as EGF signaling in mammary epithelial cells could also contribute to the development of ER+/PR- mammary tumors.

Tip30 **deletion leads to delayed EGFR degradation and sustained EGFR signaling.** Upon binding EGF, EGFR proteins are rapidly internalized and localized in early endosomes, where they are either sent back to the plasma membrane or sorted into late endosomes and lysosomes for destruction (*7, 8*). Early endosomes serve as a platform for signaling receptors to activate specific downstream signaling until ligand-receptor dissociation occurs due to early endosomal acidification mediated by vacuolar (H^+)-ATPases (*9, 10*). We have demonstrated that TIP30 regulates EGFR signaling by controlling endocytic downregulation of EGFR in primary hepatocytes and liver cancer cells. *Tip30* deletion impairs the fusion of Rab5 vesicles carrying vacuolar (H^+)-ATPases with early endosomes that contain internalized EGF and EGFR, leading to delayed EGFR degradation and sustained EGFR signaling (*5*). Therefore, we questioned whether the increased phosphorylation of Akt and ERα in *Neu+/Tip30*$^{-/-}$ mammary gland are also caused by a similar mechanism. First, we measured the protein levels of EGFR in mammary tumors cells isolated from *Neu+/Tip30*$^{-/-}$ and *Neu+/Tip30*$^{+/+}$ mammary tumors in response to EGF treatment at various times after EGF internalization. We used an experimental approach that eliminates the interference from continuous ligand internalization and nascent protein synthesis to measure endocytic degradation of EGFR. The comparison revealed that endocytic degradation of EGFR was significantly delayed in

Neu+/Tip30$^{-/-}$ mammary tumors cells compared to *Neu+/Tip30*$^{+/+}$ mammary tumors cells, indicating that *Tip30* deletion impairs endocytic degradation of EGFR (Fig. 1A and B).

To determine whether *Tip30* deletion can block EGFR trafficking from early endosomes to lysosomes for degradation, we tracked Alexa-488 conjugated EGF (Alexa^{488}-EGF) and EGFR in normal primary MECs isolated from *Tip30*$^{-/-}$ and *Tip30*$^{+/+}$ mice. The majority of internalized EGF dissociated from EGFR in wild type MECs two hours after EGF internalization. In contrast, they remained associated with EGFR in *Tip30*$^{-/-}$ MECs (EGF-EGFR colocalization in wild type primary MECs: 11%; EGF-EGFR colocalization in *Tip30*$^{-/-}$ primary MECs: 55%; n = 20, $P = 0.004$; Fig. 1C and D), indicating that *Tip30* deletion causes the trapping of EGF-EGFR complex in endosomes and sustained endosomal EGFR signaling. To rule out the possibility that *Tip30* deletion increased Neu transgene expression at the level of transcription, we used quantitative RT-PCR to examine the mRNA expression of Neu transgene in 5- to 9-week-old *Neu+/Tip30*$^{+/+}$ and *Neu+/Tip30*$^{-/-}$ mice and found no significant difference (data not shown). Together, these results suggest that Tip30 loss may prolong EGFR signaling, which cooperates with Neu activation to accelerate Akt activation and to promote the formation of ER+/PR- tumors. These results were published in *Cancer Research* (*11*).

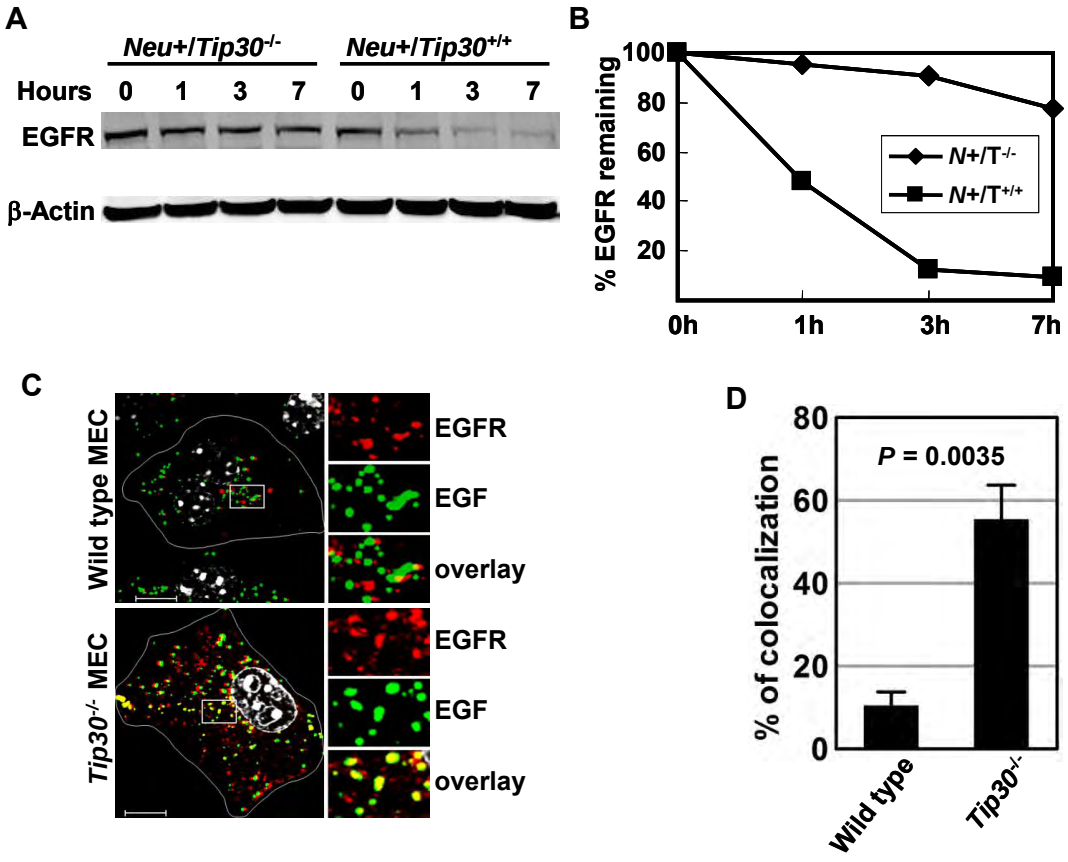

Fig. 1. Deletion of *Tip30* in MECs leads to delayed EGFR degradation. *A*, Mammary tumor cells isolated from *Neu+/Tip30*$^{-/-}$ and *Neu+/Tip30*$^{+/+}$ mice were incubated with 100 ng/ml of EGF for 1 hour on ice followed by washing with cold PBS and then incubated in serum-free medium containing 20 μg/ml of cycloheximide for the indicated times. Whole cell lysates were blotted with the indicated antibodies. *B*, Quantification of EGFR protein levels in (*A*) using Odyssey 2.1 software. *C*, Primary *Tip30*$^{+/+}$ and *Tip30*$^{-/-}$ MECs were subjected to EGFR internalization analysis. Representative confocal microscope images show the localization of EGFR (red) in endosomes after two hours of Alexa^{488}-EGF (green) internalization. Results are typical and representative of three experiments on primary cells from two mice of each genotype. Boxed areas are magnified. Representative cells are outlined in white. The colocalization of EGF and EGFR (yellow) in *Tip30*$^{-/-}$ cells is indicative of delayed endocytic degradation of EGFR; the nucleus was stained with DAPI (Grey). Scale bar, 10 μm.

D, Quantitative analysis of EGF and EGFR colocalization. Twenty cells in each group were analyzed using MBF_imageJ. Pearson's colocalization coefficients were calculated and converted to percentages. $P = 0.035$; *t* test.

Task 2. Evaluate IGF-I and Wisp-2 as potential therapeutic targets for ER+/PR- mammary tumors developed in *Tip30-/-* MMTV-Neu mice. We have completed the experiments proposed in Task 2. Our results suggest that PI3K, ER and PR are better therapeutic targets for ER+/PR- mammary tumors.

AG1024, an IGF-IR inhibitor, can not effectively inhibit ER+/PR- mammary tumors developed in *Tip30*$^{-/-}$/MMTV-Neu mice. Our previous results showed IGF-1 and Wisp2 expression are increased in *Neu+/Tip30*$^{-/-}$ tumors; therefore, we have generated ER-/PR- and ER+/PR-*Tip30*$^{+/+}$/MMTV-Neu and *Tip30*$^{-/-}$/MMTV-Neu mammary tumor cell lines for testing whether IGF-1 and Wisp2 (Task 2c) in year 2. The growth of ER+/PR- cells at the initial passages requires EGF and E2 (data not shown), but after cultured in vitro for 20 passages, the growth of these cells was independent of E2 (Figure 2. left panel). Based on our recent evidence that Tip30 loss also increases EGF signaling, we anticipate that inhibition of IGF-I and IGF-IR may not efficiently inhibit proliferation of ER+/PR- tumor cells. Indeed, addition of AG1024, an IGF-IR inhibitor, in the culture medium containing tamoxifen did not further affect proliferation of ER+/PR- mammary tumor cells derived from *Tip30-/-*/MMTV-Neu mice (Figure 2, right panel).

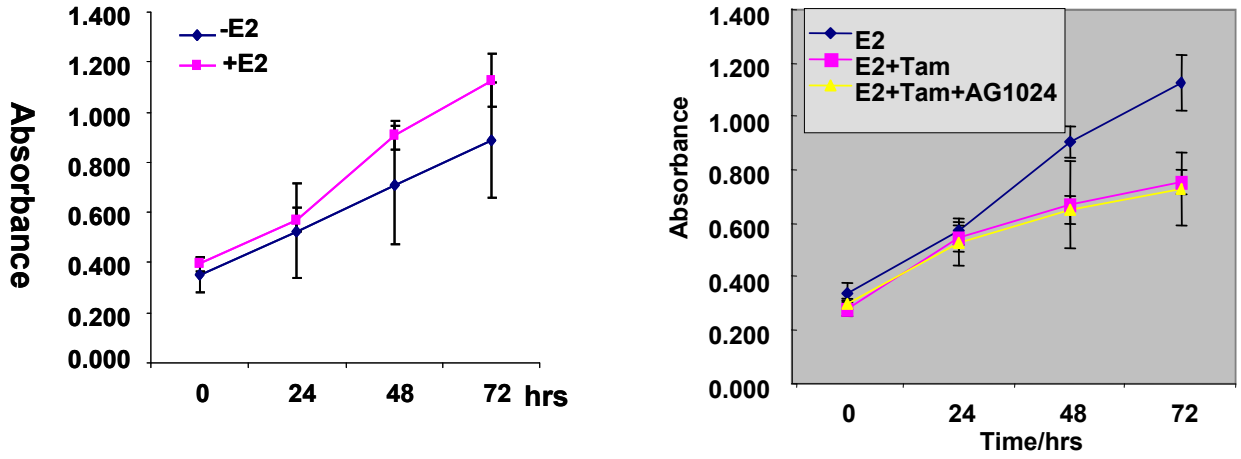

Fig. 2. Effect of AG1024 on the proliferation of ER+/PR- tumor cells. Cells were plated into 96-well culture plate in DMEM medium with 10% FBS. After 24 hrs, medium was replaced with phenol red-free DMEM supplemented with 10% charcoal-stripped FBS (Gibico). After starvation overnight, 10 nM E2 (left panel), or 10 nM E2, 1 uM tamoxifen plus nM E2, 1 μM tamoxifen plus nM E2 and 1uM AG1024 (right panel) were added to the indicated wells. Ethanol was used as vehicle control. Cell Counting Kit-8 (Dojindo, Japan) was used to measure cell proliferation at indicated times. Absorbance at 450 nm was measured using Fluostar Optima (BMG Labtech).

A combination of NVP-BEZ235 and tamaxifen has a better inhibitory effect on proliferation of ER+/PR- mammary tumor cells compared to use of either NVP-BEZ235 or tamoxifen alone. A functional property of breast stem/progenitor cells is their ability to grow as non-adherent mammospheres. Consistently, we also found that *Neu+Tip30*$^{-/-}$ primary mammary epithelial cells (MECs) gave rise to higher numbers and larger size of mammospheres compared to *Neu+Tip30*$^{+/+}$ primary MECs (Fig.4. A and B). Intriguingly, *Neu+Tip30*$^{-/-}$ tumor cells also gave rise to higher numbers

of tumorospheres compared to *Neu+Tip30*$^{+/+}$ tumor cells (Fig. 4C); the growth of tumorospheres was inhibited by NVP-BEZ235, a dual pan PI3K/mTOR inhibitor (Novartis)**.** It appeared that *Neu+Tip30*$^{-/-}$ tumor cells are more sensitive to NVP-BEZ235 compared to *Neu+Tip30*$^{+/+}$ tumor cells (Fig. 4D). NVP-BEZ235 effectively blocks phosphorylation of Akt and induces apoptosis of breast cancer cells having either HER2 amplification and/or PIK3CA mutation. This inhibitor is currently used in phase I–II clinical trials for treating advanced solid tumors including advanced HER2+ breast cancers.

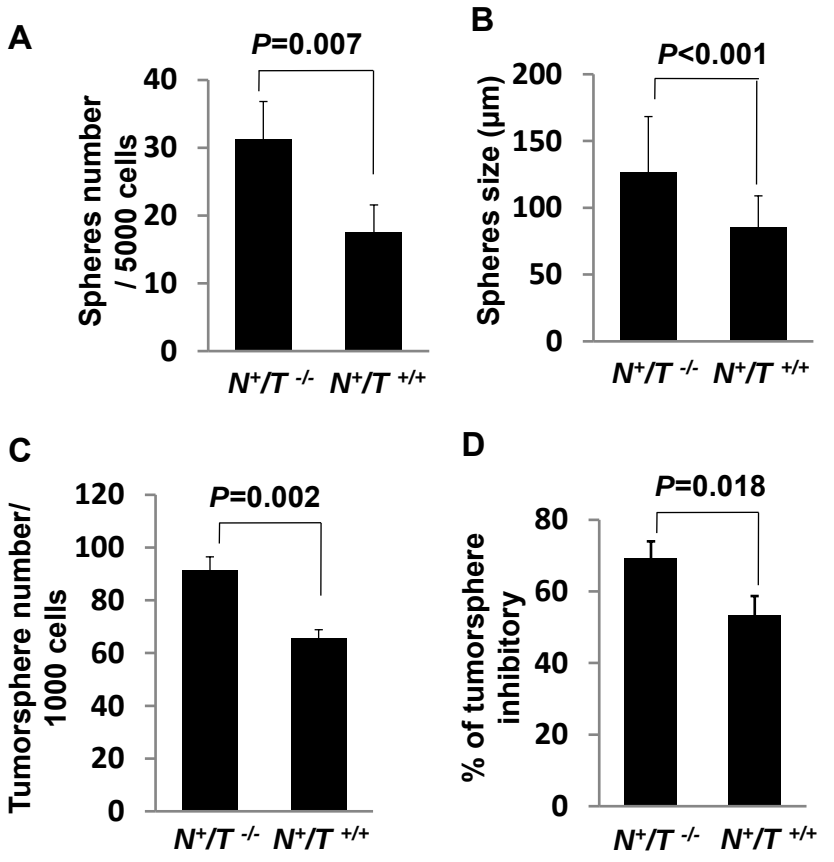

Fig. 4. A and B, Mammosphere forming capacity of MECs from *Neu+/Tip30* $^{-/-}$ and *Neu+/Tip30* $^{+/+}$ mice. MECs were isolated from *Neu+/Tip30* $^{-/-}$ and *Neu+/Tip30* $^{+/+}$ mice of 5 months old (n=3). Histogram showing total numbers (A) and size (B) of mammosphere forming from 5000 MECs seeded. C, Tumorsphere forming capacity from tumor cell lines derived from *Neu+/Tip30* $^{-/-}$ and *Neu+/Tip30* $^{+/+}$ mice. Histogram showing total numbers of tumorsphere forming from 1000 cells of *Neu+/Tip30*$^{-/-}$ and *Neu+/Tip30*$^{+/+}$ cell lines. D, Data showing the percentage of tumorsphere inhibitory *in vitro* of *Neu+/Tip30*$^{-/-}$ and *Neu+/Tip30*$^{+/+}$ mice tumor cell lines treated with NVB-BEZ235 (250nM) for a week.

We have established primary tumor cell lines from HER2+/ER+/PR- and HER2+/ER-/PR- mouse tumors and tested the effect of trastuzumab on the proliferation of these two primary tumor cell lines. We found that HER2+/ER+/PR- tumor cells were significantly less sensitive to trastuzumab inhibition compared to HER2+/ER-/PR- tumor cells (data not show). Similarly, knockdown of TIP30 in human HER2 positive breast cancer SKBr3 cells (HER2+/ER-/PR-) resulted in cells resistance to growth inhibition by trastuzumab (data not show). These results suggest that TIP30 down-regulation leads to resistance of cancer cells to trastuzumab. Previous studies suggested that patients with ER+ positive tumors containing an enhanced PI3K signaling, and patients who relapse on endocrine therapy, may benefit from therapeutics targeting both the ER and the PI3K pathways (*12*); therefore, we tested whether NVP-BEZ235 alone or in combination with tamoxifen affects proliferation of ER+/PR- tumor cells derived

from *Neu+Tip30*$^{-/-}$ mice. Simultaneous treatment of ER+/PR- tumor cells with NVP-BEZ235 and tamoxifen robustly inhibits cell proliferation in vitro, whereas NVP-BEZ235 or tamoxifen alone treatment has only moderate or no inhibition of proliferation of the cells in vitro (Fig. 5). These results suggest that a combined NVP-BEZ235 and tamoxifen treatment is a potentially effective strategy for treatment of ER+/PR- breast cancers. Therefore, we propose the following experiments to further test the working hypothesis.

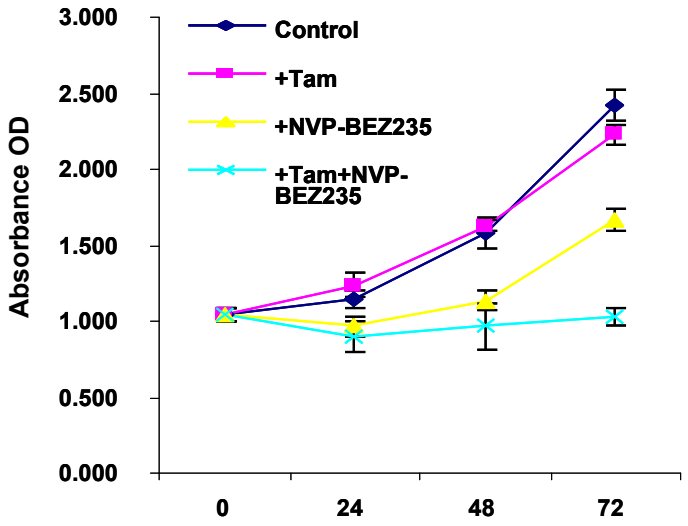

Fig. 5. Effect of NVP-BEZ235 and/or tamoxifen on growth of mouse HER2+/ER+/PR- tumor cells. Tumor cells were seeded in 96-well plates in DMEM, in the presence of DMSO, tamoxifen (1μm), NVP-BEZ235 (250 nM) or tamoxifen (1μm) plus NVP-BEZ235 (250 nM) at 0 hr. Proliferation was analyzed using cell counting Kit-8 assay (Dojindo, Kumamoto, Japan) at indicated time points and absorbance at 485 nm was measured. Data are mean of ± s.e. from three experiments. Statistical significance was analyzed by a t-test, $P < 0.05$; NVP-BEZ235 and tamoxifen versus control vehicle treatment.

In summary, the outcomes of this idea grant demonstrate that Tip30 deletion resulted in enhanced EGFR/PI3K/AKT signaling, proliferation of ER+ MECs and development of ER+ mammary tumors. Moreover, HER2+/ER+/PR- mammary tumor cells derived from *Tip30*$^{-/-}$/MMTV-Neu mice were resistant to trastuzumab and tamoxifen but sensitive to NVP-BEZ235 plus tamoxifen.

Key research Accomplishments:

1. Our data suggest that loss of Tip30 cooperates with Neu activation to enhance the activation of Akt signaling, leading to the development of ER+/PR- mammary tumors.

2. Our data demonstrate that *Tip30* deletion leads to delayed EGFR degradation and sustained EGFR signaling through impairing EGFR intracellular trafficking.

3. A combined NVP-BEZ235 and tamoxifen treatment has a better inhibitory effect on proliferation of ER+/PR- mammary tumor cells compared to the use of either NVP-BEZ235 or tamoxifen alone.

Reportable outcomes:

1. Part of this work was included in three research articles that have been published.

a. Zhang, C-L, Mori, M., Gao, S., Li, A-M., Hoshino, I., Aupperlee, M.D., Haslam, S. Z., and Xiao, H., (2010).Tip30 Deletion in MMTV-Neu Mice Leads to Enhanced EGFR Signaling and Development of Estrogen Receptor-Positive and Progesterone Receptor-Negative Mammary Tumors. *Cancer Res.* Dec. 15, 70:10224-10233

b. Zhang C, Li A, Zhang X, Xiao H. (2011) A novel TIP30 protein complex regulates EGF receptor signaling and endocytic degradation. *J Biol Chem.* Mar 18;286 (11):9373-81.Jan 20. [Epub ahead of print]

c. Zhang C, Li A, Gao S, Zhang X, Xiao H. (2011) The TIP30 Protein Complex, Arachidonic Acid and Coenzyme A Are Required for Vesicle Membrane Fusion. *PLoS One*.;6(6):e21233. Epub 2011 Jun 24.

2. Part of this work is included in the PH.D. dissertation by Chengliang Zhang, a graduate student supported by this award, and his thesis has been defended successfully on Sept. 7, 2010.

3. Part of this work was presented as a poster in Era Hope conference at Orlando, Florida in Aug. 2011.

4. A Breast Cancer DOD Idea expansion award application entitled "Elucidation and targeting of novel oncogenic pathways essential for ER+/PR+ and ER+/PR- breast cancers" is submitted based on work supported by this award.

Conclusions: Our data suggest that enhanced EGFR signaling induced by TIP30 deletion contributes to ER+/PR- breast cancers and a combined NVP-BEZ235 with tamoxifen treatment has a better inhibitory effect on proliferation of ER+/PR- mammary tumor cells compared to the use of either PI3K or tamoxifen alone.

References:

1. G. Arpino *et al.*, Estrogen receptor-positive, progesterone receptor-negative breast cancer: association with growth factor receptor expression and tamoxifen resistance. *J Natl Cancer Inst* 97, 1254 (Sep 7, 2005).
2. R. Ponzone *et al.*, Clinical outcome of adjuvant endocrine treatment according to PR and HER-2 status in early breast cancer. *Ann Oncol* 17, 1631 (Nov, 2006).
3. H. J. Kim, X. Cui, S. G. Hilsenbeck, A. V. Lee, Progesterone receptor loss correlates with human epidermal growth factor receptor 2 overexpression in estrogen receptor-positive breast cancer. *Clin Cancer Res* 12, 1013s (Feb 1, 2006).
4. P. E. Goss *et al.*, Efficacy of letrozole extended adjuvant therapy according to estrogen receptor and progesterone receptor status of the primary tumor: National Cancer Institute of Canada Clinical Trials Group MA.17. *J Clin Oncol* 25, 2006 (May 20, 2007).
5. C. Zhang, A. Li, X. Zhang, H. Xiao, A novel TIP30 protein complex regulates EGF receptor signaling and endocytic degradation. *The Journal of biological chemistry* 286, 9373 (Mar 18, 2011).
6. C. Zhang, A. Li, S. Gao, X. Zhang, H. Xiao, The TIP30 protein complex, arachidonic acid and coenzyme a are required for vesicle membrane fusion. *PLoS One* 6, e21233 (2011).
7. J. Hutchinson, J. Jin, R. D. Cardiff, J. R. Woodgett, W. J. Muller, Activation of Akt (protein kinase B) in mammary epithelium provides a critical cell survival signal required for tumor progression. *Mol Cell Biol* 21, 2203 (Mar, 2001).

8. D. C. Allred, P. Brown, D. Medina, The origins of estrogen receptor alpha-positive and estrogen receptor alpha-negative human breast cancer. *Breast Cancer Res* 6, 240 (2004).
9. M. Forgac, Vacuolar ATPases: rotary proton pumps in physiology and pathophysiology. *Nat Rev Mol Cell Biol* 8, 917 (2007).
10. A. M. Murphy, Mammography screening for breast cancer: a view from 2 worlds. *JAMA* 303, 166 (Jan 13, 2010).
11. C. Zhang *et al.*, Tip30 deletion in MMTV-Neu mice leads to enhanced EGFR signaling and development of estrogen receptor-positive and progesterone receptor-negative mammary tumors. *Cancer research* 70, 10224 (Dec 15, 2010).
12. T. W. Miller *et al.*, Hyperactivation of phosphatidylinositol-3 kinase promotes escape from hormone dependence in estrogen receptor-positive human breast cancer. *J Clin Invest* 120, 2406 (Jul 1, 2010).

Upregulated genes

Gene symbol	Gene name	GenBank Accession#	Function	Fold change
Transport				
Rbp7	Retinoid binding protein 7	NM_022020	Transport	10.77
Slc38A1	Solute carrier family 38, member 1	NM_012038	Ion/amino acid Transport	9.04
Gabra4	Gamma-aminobutyric acid (GABA) A receptor, alpha 4	NM_010251	Transport	3.74
Gria4	Glutamate receptor ionotropic, AMPA 4	NM_019691	transport ion transport	3.00
Slc2a1	solute carrier family 2,member 1	NM_011400	transport	2.86
Scp2	Sterol carrier protein 2	NM_011327	lipid transport	2.40
Signal transduction				
Pik3cg	Phosphoinositide-3-kinase, catalytic, gamma polypeptide	NM_020272	Phosphorylation	2.73
Tacr3	Tachykinin receptor 3	NM_021382	G-protein coupled receptor protein signaling pathway	2.70
Mknk1	MAP kinase interacting serine/threonine kinase 1	NM_021461	protein kinase cascade	2.67
EGF	Epidermal growth factor	NM_010113	epidermal growth factor receptor signaling pathway	2.41
Arl4d	ADP-ribosylation factor-like 4D	NM_025404	small GTPase mediated signal transduction	2.30
Rab1b	Ras-related protein Rab-1B	NM_029576	small GTPase mediated signal transduction	2.30

Cell adhesion and cell cycle control				
Glycam1	Glycosylation-dependent cell adhesion molecule-1	NM_008134	Cell adhesion	8.02
G0s2	G0/G1 switch regulatory protein 2	NM_008059	cell cycle	5.27
Smoc1	Secreted modular calcium-binding protein 1	NM_022316	Cell adhesion	3.63
Crispld2	Cysteine-rich secretory protein LCCL domain containing 2	NM_030209	extracellular matrix organization	3.23
Spink5	Serine peptidase inhibitor, Kazal type 5	NM_001081180	regulation of cell adhesion/negative regulation of proteolysis	2.87
Cdkn1c	Cyclin-dependent kinase inhibitor 1C	NM_009876	cell cycle arrest	2.26
Casp6	Caspase 6, apoptosis-related cysteine peptidase	NM_009811	induction of apoptosis	2.13
Regulation of Transcription				
Cited4	CBP/p300-interacting transactivator 4	NM_019563	regulation of transcription	2.97
Barx2	BARX homeobox 2	NM_013800	regulation of transcription, DNA-dependent	2.46
Cdkn1c	Cyclin-dependent kinase inhibitor 1C (p57, Kip2)	NM_009876	negative regulation of transcription from RNA polymerase II promoter	2.25
Txnip	Thioredoxin interacting protein	NM_001009935	regulation of transcription, DNA-dependent	2.01
Protein degradation				
Lao1	L-amino acid oxidase 1	NM_133892	amino acid catabolic process	5.99

Ctsf	Cathepsin F	NM_019861	proteolysis	3.11
Spop	Speckle-type POZ protein	NM_025287	ubiquitin-dependent protein catabolic process	2.07
Rnf20	Ring finger protein 20	NM_182999	ubiquitin-dependent protein catabolic process // chromatin modification	2.03
Fbxo31	F-box protein 31	NM_133765	ubiquitin-dependent protein catabolic process	2.03

Downregulated genes

Gene symbol	Gene name	GenBank Accession#	Function	Fold change
Transport				
Apod	Apolipoprotein D	NM_007470	transport	16.38
Slc35f1	Solute carrier family 35, member F1	NM_178675	transport	4.78
Mup1	Major urinary protein 1	NM_031188	transport	3.69
Slc26a9	Solute carrier family 26, member 9	NM_177243	transport	3.19
Trpv6	Transient receptor potential cation channel, subfamily V, member 6	NM_022413	transport	3.15
Regulation of transcription				
Ifi205	Interferon activated gene 205	NM_172648	regulation of transcription, DNA-dependent	3.90
Ifi204	Interferon activated gene 204	NM_008329	regulation of transcription	3.63
Lass6	LAG1 homolog, ceramide synthase 6	NM_172856	regulation of transcription	2.90
Rbm39	RNA binding motif protein 39	AY061882	transcription	2.59
Signal transduction				
Serpina3f	serine (or cysteine) peptidase inhibitor	NM_001033335	response to cytokine stimulus	7.65

Il18r1	Interleukin 18 receptor 1	NM_008365	signal transduction	3.09
Rasgrp1	RAS guanyl releasing protein 1	NM_011246	intracellular signaling cascade	2.98
Angpt1	Angiopoietin 1	NM_009640	signal transduction	2.95
Gpr64	G protein-coupled receptor 64	NM_178712	signal transduction	2.77
Gprc5b	G protein-coupled receptor, family C, group 5, member B	NM_022420	signal transduction	2.65
Rassf9	Ras association (RalGDS/AF-6) domain family (N-terminal) member 9	NM_146240	signal transduction	2.55
Fgf13	Fibroblast growth factor 13	NM_010200	MAPKKK cascade	2.50
Vipr2	Vasoactive intestinal peptide receptor 2	NM_009511	G-protein coupled receptor protein signaling pathway	2.46
Gpr97	G protein-coupled receptor 97	NM_173036	G-protein coupled receptor protein signaling pathway	2.22
Cell adhesion and cycle control				
Htatip2	HIV-1 Tat interactive protein 2, 30kDa	NM_016865	cell cycle	5.37
Fmnl2	Formin homology 2 domain containing 2	NM_172409	cellular component organization	4.20
Vcan	Chondroitin sulfate proteoglycan	NM_001081249	cell adhesion	3.8
Protein degradation				

Cpe	carboxypeptidase E	NM_013494	proteolysis	6.52
St8sia6	ST8 alpha-N-acetyl-neuraminide alpha-2,8-sialyltransferase 6	NM_145838	protein amino acid glycosylation	5.83
Dpp10	Dipeptidyl peptidase IV-related protein 3	NM_199021	proteolysis	5.29
Rnf125	Ring finger protein 125	NM_026301	ubiquitin-dependent protein catabolic process	2.50
Ube2l6	Ubiquitin-conjugating enzyme E2L 6	NM_019949	ubiquitin-dependent protein catabolic process	2.33
Other biological process				
Tacstd2	Tumor-associated calcium signal transducer 2	NM_020047	biological_process	5.74
Adipoq	Adiponectin, C1Q and collagen domain containing	NM_009605	glucose metabolic process	5.62
Cxcl10	Chemokine (C-X-C motif) ligand 10	NM_021274	inflammatory response	3.75
Cyp2e1	Cytochrome P450, family 2, subfamily E, polypeptide 1	NM_021282	oxidation reduction	3.49

DOI:10.1158/0008-5472.CAN-10-3057

Cancer Research

Tip30 Deletion in MMTV-Neu Mice Leads to Enhanced EGFR Signaling and Development of Estrogen Receptor –Positive and Progesterone Receptor –Negative Mammary Tumors

Chengliang Zhang, Mikito Mori, Shenglan Gao, et al.

Cancer Res 2010;70:10224-10233. Published online December 14, 2010.

DOI:10.1158/0008-5472.CAN-10-3057

Cancer Research

Tip30 Deletion in MMTV-Neu Mice Leads to Enhanced EGFR Signaling and Development of Estrogen Receptor–Positive and Progesterone Receptor–Negative Mammary Tumors

Chengliang Zhang[1,2], Mikito Mori[1], Shenglan Gao[1,3], Aimin Li[1,4], Isamu Hoshino[1], Mark D. Aupperlee[1], Sandra Z. Haslam[1], and Hua Xiao[1,2]

Abstract

Estrogen receptor–positive and progesterone receptor–negative (ER+/PR−) breast cancers account for 15% to 25% of all human breast cancers and display more aggressive malignant characteristics than ER+/PR+ cancers. However, the molecular mechanism underlying development of ER+/PR− breast cancers still remains elusive. We show here that *Tip30* deletion dramatically accelerated the onset of mammary tumors in the MMTV-Neu mouse model of breast cancer. The mammary tumors arising in *Tip30*$^{-/-}$/MMTV-Neu mice were exclusively ER+/PR−. The growth of these ER+/PR− tumors depends not only on estrogen but also on progesterone despite the absence of detectable PR. *Tip30* is predominantly expressed in ER+ mammary epithelial cells, and its deletion leads to an increase in the number of phospho-ERα–positive cells in mammary glands and accelerated activation of Akt in MMTV-Neu mice. Moreover, we found that *Tip30* regulates the EGFR pathway through controlling endocytic downregulation of EGFR protein level and signaling. Together, these findings suggest a novel mechanism in which loss of *Tip30* cooperates with Neu activation to enhance the activation of Akt signaling, leading to the development of ER+/PR− mammary tumors. *Cancer Res; 70(24); 10224–33. ©2010 AACR.*

Introduction

Despite considerable success in the treatment of estrogen receptor–positive and progesterone receptor–positive (ER+/PR+) breast cancers with therapies directed at targeting estrogen and ERα, a substantial fraction of patients with ER+/PR− tumors do not benefit significantly from these therapies (1, 2). It is estimated that 15% to 25% of all human breast cancers are ER+/PR− with more aggressive malignant characteristics and poorer response to selective estrogen receptor modulators than ER+/PR+ breast cancers (2–4). Moreover, 25% of ER+/PR− tumors are found to have HER2/Neu overexpression; patients with this subtype of ER+/PR− breast cancer have an extremely poor response to endocrine treatment. While several lines of evidence suggest that ER+/PR− tumors can be derived from ER+/PR+ tumors by the loss of PR expression due to anti-hormone therapy, studies indicate that ER+/PR− tumors could arise *de novo* from other etiologic factors (5). To date, the mechanisms underlying *de novo* and acquired ER+/PR− breast cancer remain poorly defined. Thus, elucidation of the molecular basis of ER+/PR− breast tumor development has the potential to reveal new therapeutic targets for the treatment, and even prevention of the resistance to anti-estrogen therapy in breast cancer patients.

There are several hypotheses to explain the development of ER+/PR− breast cancers. These include inhibition of PR transcription by aberrant ER cofactors or nonfunctional ER, reduced ER activity due to lower circulating estrogen levels, hypermethylation of PR promoter, or by growth factor signaling pathways (6). Of particular interest are growth factor signaling pathways, in which aberrations are common in many human cancers (7, 8). Among the growth factor receptors, HER2/Neu is the most frequently altered receptor in breast cancers. While most of HER2 positive breast cancers are ER−/PR−, only a small fraction are ER+/PR+ or ER+/PR−, suggesting that HER2 may inhibit ER expression as well as PR expression (6). This hypothesis is supported by the observation that mouse models of breast cancer harboring a HER2/Neu transgene almost exclusively develop ER−/PR− mammary tumors. In addition, when transfected with HER2-expressing vectors, ER+/PR+ breast cancer cells exhibited a significant decrease in ER and PR expression (8). Nevertheless, the mechanism by

Authors' Affiliations: [1]Department of Biomedical and Integrative Physiology, [2]Genetics Program, and [3]Department of Biochemistry and Molecular Biology, Michigan State University, East Lansing, Michigan; and [4]Department of Oncology, Nanfang Hospital, Southern Medical University, Guangzhou, China

Note: Supplementary data for this article are available at Cancer Research Online (http://cancerres.aacrjournals.org/).

C. Zhang and M. Mori contributed equally to this work.

Corresponding Author: Hua Xiao, Department of Biomedical and Integrative Physiology, College of Human Medicine, Michigan State University, 3193 Biomedical and Physical Sciences Building, East Lansing, MI 48824-3320. Phone: 517-884-5127; Fax: 517-355-5125. E-mail: xiaoh@msu.edu

doi: 10.1158/0008-5472.CAN-10-3057

DOI:10.1158/0008-5472.CAN-10-3057

which activation of HER2/Neu leads to the development of ER−/PR− but not ER^{+} breast cancer remains poorly understood.

TIP30, also known as CC3, is a 30-kDa human cellular protein that was purified as a HIV-1 Tat interacting protein (9) and its expression is altered in human liver, lung, and breast cancers (10–13). Our previous studies showed that *Tip30*-deficient mice spontaneously develop tumors in several tissues and mammary preneoplastic lesions, suggesting that TIP30 acts as a tumor suppressor (10, 14). Its tumor suppressor activity is probably due to multiple mechanisms. TIP30 functions as a transcription cofactor to repress expression of genes that are involved in proliferation and apoptosis (15, 16) and it can induce apoptosis as an inhibitor of nuclear import (17). In particular, TIP30 can act as a repressor of ERα-mediated c-Myc transcription in mammary glands and breast cancer cells (15). In addition, recent evidence has highlighted that TIP30 controls endocytic downregulation of the EGFR signaling pathway in primary hepatocytes and hepatocellular carcinoma cells (C. Zhang, A. Li, X. Zhang, and H. Xiao, submitted manuscript).

The multiple functions of TIP30 have prompted the speculation that its loss may contribute to mammary tumorigenesis induced by activation of oncogenes. Therefore, we aimed to determine whether *Tip30* deletion enhances mammary tumorigenesis in MMTV-Neu mice. We report here that *Tip30* deletion cooperates with HER2/Neu activation to promote the development of ER+/PR− mammary tumors, in part, through upregulation of the EGFR signaling pathway. The growth of these ER+/PR− tumors seemed to depend upon both estrogen and progesterone. Thus, the *Neu*$^{+}$/*Tip30*$^{-/-}$ mouse model may help decipher the mechanisms leading to ER+/PR− mammary tumors and identify therapeutic targets for this subgroup of tumors.

Materials and Methods

Mice, primary MECs, and tumor cells

Tip30$^{+/-}$ mice in FBV genetic background were generated by backcrossing *Tip30*$^{+/-}$ C57BL/6 mice (14) 7 times with FBV mice. *Tip30*$^{+/-}$ mice in FBV background were bred with MMTV-Neu mice (FVB/N-Tg; Jackson Laboratory) to generate *Neu*$^{+}$/*Tip30*$^{-/-}$, *Neu*+/*Tip3*$^{+/-}$ and *Neu*$^{+}$/*Tip30*$^{+/+}$ mice. Primary MECs and tumor cells were isolated and cultured as described previously (43). For tumor transplantation assays, all recipient mice were 8-week-old *Nu/Nu* female nude mice (Charles River). For ovariectomized mice, both ovaries were removed under anesthesia. Placebo (25 mg, 90-day release), 17-estradiol or estrogen (0.1 mg E2, 90-day release), progesterone (35 mg P4, 21-day release), or E2 + P4 pellets (0.1 mg E2 + 32.5 mg P4, 90-day release) were purchased from Innovative Research of America and implanted subcutaneously in the front flanks of each mouse. RU486 was purchased from Calbiochem. Mice were sacrificed at the end of 3 months or when the tumor volume reached 1 cm^{3}. All mice were housed and cared for in the Animal Facility at Michigan State University according to institutional guidelines.

Immunofluorescence and immunohistochemistry

Immunofluorescent staining of mouse mammary tissues was carried out as follow. After deparaffinization and rehydration, tissue sections were autoclaved and then incubated with primary antibody specific for ERα (MC-20, 1:50; Santa Cruz Biotechnology), p-ERα (Santa Cruz Biotechnology), PR-A (hPRa7, 1:50; Labvision), PR-B (hPRa6, 1:50; Labvision), or β-Gal (Promega) at 4°C overnight. After PBS rinse, tissue sections were sequentially incubated for 30 minutes at room temperature with diluted goat anti-rabbit or mouse Alexa-488- or Alexa-594–conjugated secondary antibody (1:200; Molecular Probes). Nuclei were counterstained with 4',6-diamidino-2-phenylindole (DAPI). Immunohistochemical staining of mouse mammary tissues was described previously (44). Immunohistochemical analysis of p-Akt at Ser473 (1:50; Cell Signaling Technologies) and p-ERα (Santa Cruz Biotechnology) were carried out as described previously (44).

EGFR internalization assay

Tip30$^{+/+}$ and *Tip30*$^{-/-}$ primary mammary epithelial cells were isolated from 2-month-old *Tip30*$^{+/+}$ and *Tip30*$^{-/-}$ female mice and cultured as previously described (14) and then serum-starved for 3 hours. Cells were incubated with 100 ng/mL of Alexa^{488}-EGF (Invitrogen) and 20 μg/mL of cycloheximide on ice for 1 hour and then washed 4 times with cold PBS before being incubated in DMEM with 20 μg/mL of cycloheximide at 37°C for 2 hours. Cells were fixed in 4% paraformaldehyde in PBS for 15 minutes, permeabilized with 0.1% Triton X-100 for 2 minutes, and stained for EGFR. Images were obtained with a Zeiss LSM 510 Meta confocal microscope (Carl Zeiss), using Plan-Apochromat 63×/1.40 Oil objective. Pinhole size was set to 1 airy unit for all channels. All images are representative of single optical sections.

Statistical analysis

Comparisons among groups were analyzed by 2-sided *t* test or Fisher's exact test. A difference of $P < 0.05$ was considered to be statistically significant. All analyses were done with SPSS software, Version 11.5. Data are expressed as mean ± SEM.

Results

Tip30 deletion significantly accelerates mammary tumorigenesis in MMTV-Neu mice

To investigate whether *Tip30* deletion cooperates with HER2/Neu to promote mammary tumorigenesis, we generated *Tip30*-knockout mice with overexpression of Neu by crossing the MMTV-Neu transgene from MMTV-Neu mice (FVB/N-Tg; ref. 18) into *Tip30*$^{-/-}$ FBV mice. *Neu*$^{+}$/*Tip30*$^{-/-}$ mice appeared similar to *Neu*$^{+}$/*Tip30*$^{+/+}$ mice in size and reached weaning age at the expected Mendelian frequency. A cohort of *Neu*$^{+}$/*Tip30*$^{-/-}$, *Neu*$^{+}$/*Tip30*$^{+/-}$, and *Neu*$^{+}$/*Tip30*$^{+/+}$ female mice were monitored for 75 weeks. Mammary tumors were noted to appear earlier in *Neu*$^{+}$/*Tip30*$^{-/-}$ mice than in *Neu*$^{+}$/*Tip30*$^{+/+}$ mice. Kaplan–Meier survival curves (Fig. 1A) were generated on the basis of the time of palpable tumor formation. We observed that 50% of *Neu*$^{+}$/*Tip30*$^{+/+}$ mice developed mammary tumors with a relatively long median latency of 58 weeks. The relatively longer

DOI:10.1158/0008-5472.CAN-10-3057

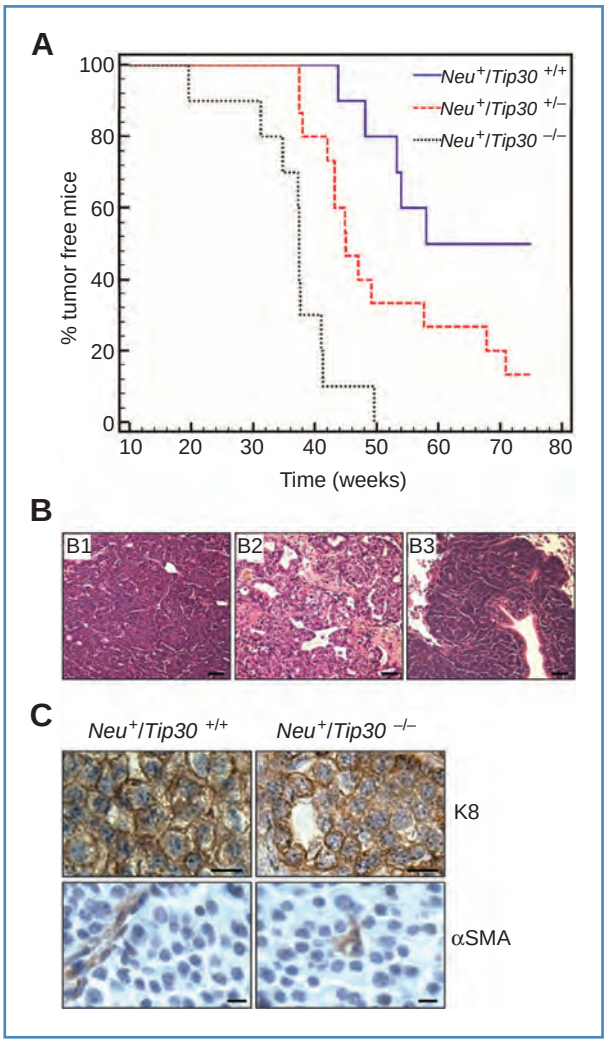

Figure 1. *Tip30* deletion significantly accelerates the onset of mammary tumors in MMTV-Neu mice. $Neu^+/Tip30^{+/+}$ ($n = 10$), $Neu^+/Tip30^{+/-}$ ($n = 15$), and $Neu^+/Tip30^{-/-}$ ($n = 10$) female mice were monitored weekly for a period of 75 weeks and sacrificed at the endpoint or when tumor volume reached 0.5 cm^3. A, Kaplan–Meier analysis of survival as the function of palpable tumor. The data were plotted as percentage of tumor-free animals against the time in weeks. $P \leq 0.0001$; log-rank test. B, representative hematoxylin and eosin-stained mammary tumors arising in $Neu^+/Tip30^{-/-}$ mice. A poorly differentiated adenocarcinoma with solid growth pattern (B1); a moderately differentiated adenocarcinoma with glandular growth pattern (B2); and a pulmonary metastasis (B3). Scale bar, 50 μm. C, representative immunohistochemical staining of mammary tumors for K8 (brown staining indicates presence of K8) and αSMA (lack of brown staining indicates the lack of αSMA). Scale bar, 10 μm.

median latency and lower frequency of tumors arising in $Neu^+/Tip30^{+/+}$ mice than those in MMTV-Neu mice (18) are possibly due to only 1 MMTV-Neu wild-type transgene allele in $Neu^+/Tip30^{+/+}$ mice. In contrast, all $Neu^+/Tip30^{-/-}$ mice developed tumors at a median age of 37 weeks and 87% of $Neu^+/Tip30^{+/-}$ mice developed tumors at a median age of 45 weeks. Histologic analysis showed that $Neu^+/Tip30^{-/-}$ tumors were poorly or moderately differentiated mammary tumors with solid or glandular growth patterns, which are morphologically similar to the mammary tumors arising in MMTV-Neu mice (Fig. 1B1 and B2). Immunohistochemical staining of paraffin-embedded tumor sections revealed that $Neu^+/Tip30^{-/-}$ or $Neu^+/Tip30^{+/+}$ tumor cells were mostly Keratin (K8)-positive and α-smooth muscle actin (αSMA)-negative (Fig. 1C), indicating that $Neu^+/Tip30^{-/-}$ tumors are of the luminal cell type similar to MMTV-Neu tumors (19). The presence of metastasis in the lung was observed in 4 of 10 $Neu^+/Tip30^{-/-}$ mice, whereas metastasis was detected in 1 of 10 $Neu^+/Tip30^{+/+}$ mice. These results suggest that *Tip30* loss accelerates the onset of mammary luminal tumors in MMTV-Neu mice and possibly increases metastasis.

Deletion of *Tip30* results in a shift from development of ER^-/PR^- tumors to ER^+/PR^- tumors in the MMTV-Neu mouse model

It is well known that MMTV-Neu transgenic mice develop mammary tumors composed almost exclusively of ER−/PR− luminal epithelial cells. Surprisingly, we found that all $Neu^+/Tip30^{-/-}$ tumors ($n = 8$) and 50% of $Neu^+/Tip30^{+/-}$ tumors ($n = 6$) examined showed an ER+/PR− staining pattern (Fig. 2B) whereas 89% $Neu^+/Tip30^{+/+}$ tumors ($n = 9$) were

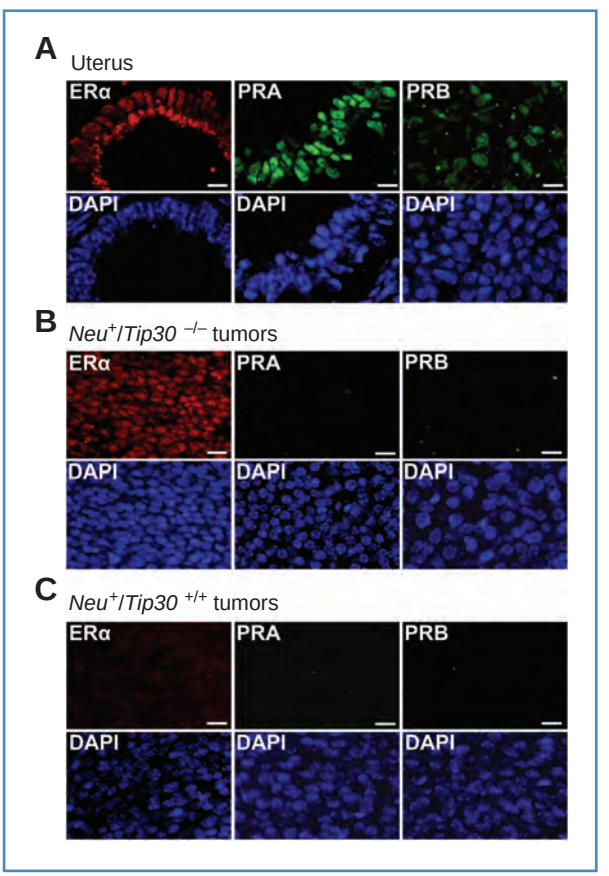

Figure 2. Mammary tumors arising in $Neu^+/Tip30^{-/-}$ mice are exclusively ER+/PR−. A–C, representative immunofluorescent staining of ERα (red), PR-A (green), and PR-B (green) in the positive control uterus (A) and mammary tumors arising in $Neu^+/Tip30^{-/-}$ mice (B) or $Neu^+/Tip30^{+/+}$ mice (C). Tumor sections were stained with anti-ERα-, anti-PR-A (hPRa7)-, or anti-PR-B (hPRa6)-specific antibodies, followed by counterstaining with DAPI. Scale bar, 10 μm.

DOI:10.1158/0008-5472.CAN-10-3057

Table 1. ERα and PR staining in mammary tumors

Tumors	ER+/PR−	ER−/PR−
Neu^{+}/*Tip30*$^{-/-}$	100% (8/8)	0% (0/8)
Neu^{+}/*Tip30*$^{+/-}$	50% (3/6)	50% (3/6)
Neu^{+}/*Tip30*$^{+/+}$	11% (1/9)	89% (8/9)

ER−/PR− (Fig. 2C), indicating that *Neu*$^{+}$/*Tip30*$^{-/-}$ mice were more likely to develop ER+/PR− mammary tumors than *Neu*$^{+}$/*Tip30*$^{+/+}$ mice (Table 1, 100% vs. 11%; $P = 0.004$). These results suggest that *Tip30* loss combined with the activation of Neu promotes development of ER+/PR− mammary tumors.

Estrogen and progesterone promote growth of *Neu*$^{+}$/*Tip30*$^{-/-}$ mammary tumors

To determine whether ER+/PR− mammary tumors arising in *Neu*$^{+}$/*Tip30*$^{-/-}$ were ovarian hormone dependent, we first transplanted small pieces of freshly dissected tumors into ovary-intact (non-OVX) and ovariectomized (OVX) nude mice and then monitored the growth of transplanted tumor tissues. Remarkably, removal of both ovaries from recipient mice drastically reduced growth and progress of transplanted tumors, suggesting that ER+/PR− mammary tumors that developed in *Neu*$^{+}$/*Tip30*$^{-/-}$ mice are ovary dependent (Fig. 3A). Next, we transplanted small pieces of freshly dissected tumors into OVX mice supplemented with placebo, estrogen, progesterone, or estrogen plus progesterone pellets (Fig. 3B and Supplementary Fig. 1). Surprisingly, estrogen plus progesterone strongly promoted tumor growth compared with placebo ($P = 0.04$) whereas estrogen or progesterone

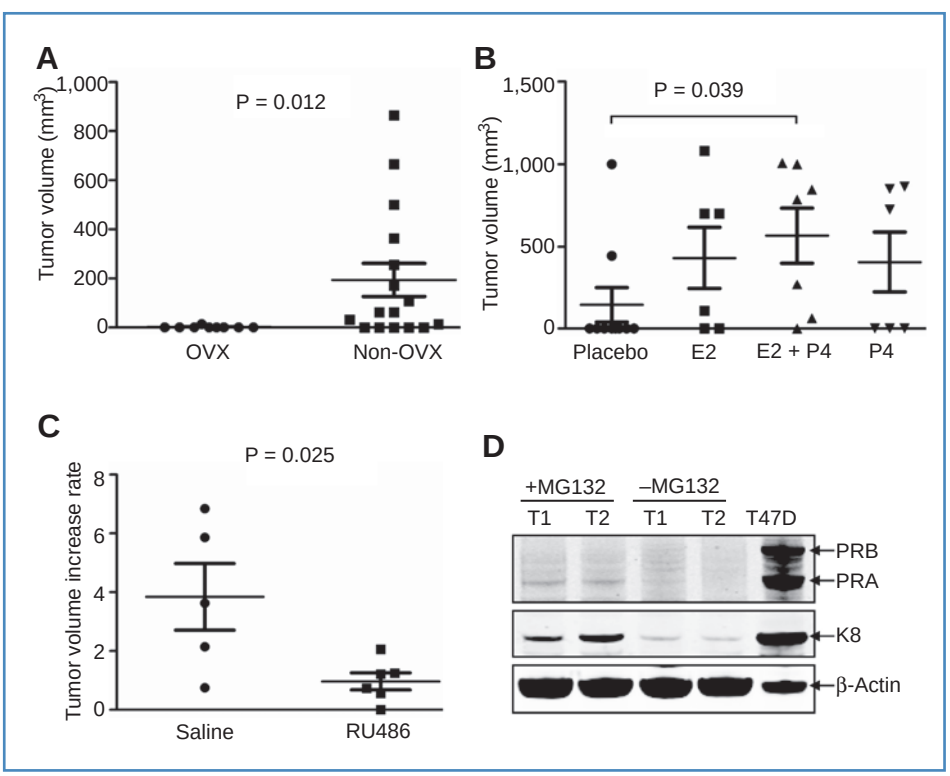

Figure 3. Growth of ER+/PR− tumors arising in *Neu*$^{+}$/*Tip30*$^{-/-}$ mice depends upon estrogen and progesterone. A, two ER+/PR− mammary tumors from *Neu*$^{+}$/*Tip30*$^{-/-}$ mice were minced and inoculated subcutaneously (s.c.) in the front flanks of ovary-intact ($n = 16$) or ovariectomized ($n = 9$) mice. The graph represents the measurements of tumors by the end of 3 months after transplantations or when the tumor volume reaches 1 cm^3. $P = 0.012$. B, two ER+/PR− mammary tumors from *Neu*$^{+}$/*Tip30*$^{-/-}$ mice were minced and inoculated s.c. in the front flanks of ovariectomized mice supplemented with placebo ($n = 10$), estrogen (E2, $n = 6$), progesterone (P4, $n = 6$), or E2 plus P4 ($n = 7$) pellets. The graphs show the measurements of tumor volumes by the end of 3 months after transplantations or when the tumor volume reaches 1 cm^3. $P = 0.039$ (placebo vs. E2 + P4). Note that tumor growth in 2 mice of the placebo group was independent of ovarian hormones. C, growth of ER+/PR− tumors after being treated with saline/ethanol vehicle or RU486. Two ER+/PR− tumors arising in *Neu*$^{+}$/*Tip30*$^{-/-}$ female mice were minced and inoculated s.c. to nude mice. After transplanted tumors reached approximately 0.5 cm in diameter, mice were divided into 2 groups to be treated with either RU486 (6.5 mg/kg of body weight) or saline/ethanol vehicle solution s.c. daily for 7 days. Tumor size was measured by caliper (length and width) for another 7 days. Tumor increase rate was calculated by comparing tumor volume (1/2 × length × width^2) before and after treatment. $P = 0.025$. D, primary tumor cells derived from 2 ER+/PR− tumors (T1 and T2) were serum-starved and cultured in the presence or absence of 10 μmol/L MG132 for 6 hours. Cell lysates were subjected to Western blot analysis with the anti-PR antibody hPRa7 that detects both PR-A and PR-B. K8 is degraded by proteasomes (45) and was blotted as a positive control for MG132 inhibition.

DOI:10.1158/0008-5472.CAN-10-3057

alone only slightly increased tumor growth compared with placebo ($P > 0.05$). Moreover, the progesterone antagonist RU486 could significantly delay the growth of *Neu*$^{+}$/*Tip30*$^{-/-}$ tumors (Fig. 3C). These results suggest that both estrogen and progesterone are required for promoting growth of ER+/PR− tumors arising in *Neu*$^{+}$/*Tip30*$^{-/-}$ mice.

The effect of progesterone on the growth of ER+/PR− tumors from *Neu*$^{+}$/*Tip30*$^{-/-}$ mice raises the question of whether these tumor cells express any PR proteins. Because previous studies have suggested that active PRs are rapidly degraded in breast cells (20), we speculated that PR was expressed and then degraded rapidly in ER+/PR− tumors. To test this hypothesis, we examined PR-A and PR-B expression in cultured tumor cells derived from ER+/PR− tumors. Indeed, PR-A, but not PR-B, was clearly detected by Western blot analysis after cells were serum-starved and treated for 6 hours with the proteasome inhibitor MG132 (Fig. 3D), implying that PR-A is expressed but rapidly turned over in these tumors. Together, these results suggest that estrogen and progesterone play stimulating roles in the development of ER+/PR− mammary tumors in *Neu*$^{+}$/*Tip30*$^{-/-}$ mice.

Deletion of *Tip30* leads to a progressively increased numbers of phospho-ERα- and phospho-Akt–positive cells in the mammary gland from MMTV-Neu mice

The preceding data imply that *Tip30* may play a key role in suppressing tumorigenesis in ERα-positive (ER+) epithelial cells. To test whether the *Tip30* gene promoter is active in ER^{+} epithelial cells and ER+/PR− tumors, we carried out immunofluorescent double staining for ERα and β-galactosidase in the mammary glands and tumors derived from *Neu*$^{+}$/*Tip30*$^{+/-}$ mice harboring a knock-in β-galactosidase (β-*Gal*) gene at the *Tip30* gene locus under the control of *Tip30* promoter. The β-Gal protein was predominantly detected in ER+ mammary epithelial cells and tumor cells (Fig. 4A), indicating that the *Tip30* promoter is activated mainly in ER+ mammary epithelial cells (MEC) and tumor cells. Given that ERα is activated through ligand binding and phosphorylation in response to estrogen- and growth factor–induced signaling and that *Tip30*$^{-/-}$ mice do not exhibit a significant increase in the number of ERα-positive cells in the mammary gland at the age of 4 months (14), we therefore asked whether the proportion of phospho-ERα (p-ERα)-positive cells is altered in *Neu*$^{+}$/*Tip30*$^{-/-}$ mammary glands. Immunohistochemical analysis was used to examine phosphorylation of ERα at Ser171 (equivalent to Ser167 in human) in mammary glands and tumors from *Neu*$^{+}$/*Tip30*$^{-/-}$ and *Neu*$^{+}$/*Tip30*$^{+/+}$ mice (Fig. 4B). No significant difference in the numbers of p-ERα–positive cells was detected between 2-month-old mammary glands from *Neu*$^{+}$/*Tip30*$^{-/-}$ and *Neu*$^{+}$/*Tip30*$^{+/+}$ mice (Fig. 4C). Strikingly, 12-month-old *Neu*$^{+}$/*Tip30*$^{-/-}$ mammary glands and tumors displayed an increase in the number of p-ERα–positive cells compared with *Neu*$^{+}$/*Tip30*$^{+/+}$ mammary glands and tumors ($P < 0.05$). These results suggest that *Tip30* deletion preferentially increases the number of p-ERα–positive luminal cells in the mammary gland of MMTV-Neu mice.

Akt is one of the most important downstream factors in HER2/Neu and EGFR signaling pathways that can phosphorylate ERα and regulate MEC apoptosis (21, 22). Previous studies have shown that the expression of a constitutively active form of Akt-1 accelerates HER2/Neu-mediated mammary tumor formation (23) whereas disruption of Akt-1 delays HER2/Neu-mediated mammary tumorigenesis (24–26). To examine whether the deletion of *Tip30* affects the activation of Akt (phospho-Akt, p-Akt) in preneoplastic mammary glands from MMTV-Neu mice, we carried out the immunohistochemical analysis for p-Akt in preneoplastic mammary glands from *Neu*$^{+}$/*Tip30*$^{-/-}$ and *Neu*$^{+}$/*Tip30*$^{+/+}$ mice at the age of 2 and 12 months. MECs at the different ages exhibit negative, weak, intermediate, or strong staining for p-Akt (Fig. 5; A1, A2, A3, or A4, respectively). No significant difference in p-Akt expression levels and numbers of p-Akt–positive cells ($P = 0.678$ or 0.972, respectively) was detected between *Neu*$^{+}$/*Tip30*$^{-/-}$ and *Neu*$^{+}$/*Tip30*$^{+/+}$ mammary glands at 2 months of age (Fig. 5B). However, at 12 months, the number of MECs having strongly positive p-Akt staining in *Neu*$^{+}$/*Tip30*$^{-/-}$ mammary glands was significantly increased compared with that in *Neu*$^{+}$/*Tip30*$^{+/+}$ mammary glands (strong staining in *Neu*$^{+}$/*Tip30*$^{-/-}$ mammary gland: 41.4%; strong staining in *Neu*$^{+}$/*Tip30*$^{+/+}$ mammary gland: 9.9%; $P = 0.02$; Fig. 5C). However, there was no significant difference in the levels of p-Akt between mammary tumors from *Neu*$^{+}$/*Tip30*$^{-/-}$ and *Neu*$^{+}$/*Tip30*$^{+/+}$ mice (Fig. 5D). These data indicate that the relatively earlier onset of enhanced Akt activation in the mammary glands due to *Tip30* loss may contribute to accelerated mammary tumorigenesis in *Neu*$^{+}$/*Tip30*$^{-/-}$ mice.

Tip30 deletion leads to delayed EGFR degradation and sustained EGFR signaling

Upon binding EGF, EGFR proteins are rapidly internalized and localized in early endosomes, where they are either sent back to the plasma membrane or sorted into late endosomes and lysosomes for destruction (27, 28). Early endosomes serve as a platform for signaling receptors to activate specific downstream signaling until ligand–receptor dissociation occurs due to early endosomal acidification mediated by vacuolar (H^{+})-ATPases (29, 30). Recently, we have shown that TIP30 regulates EGFR signaling by controlling endocytic downregulation of EGFR in primary hepatocytes and liver cancer cells. *Tip30* deletion impairs the fusion of Rab5 vesicles carrying vacuolar (H^{+})-ATPases with early endosomes that contain internalized EGF and EGFR, leading to delayed EGFR degradation and sustained EGFR signaling (C. Zhang, A. Li, X. Zhang, and H. Xiao, submitted manuscript). Therefore, we questioned whether the increased phosphorylation of Akt and ERα in *Neu*$^{+}$/*Tip30*$^{-/-}$ mammary gland is also caused by a similar mechanism. First, we measured the protein levels of EGFR in mammary tumors cells isolated from *Neu*$^{+}$/*Tip30*$^{-/-}$ and *Neu*$^{+}$/*Tip30*$^{+/+}$ mammary tumors in response to EGF treatment at various time points after EGF internalization. We used an experimental approach that eliminates the interference from continuous ligand internalization and nascent protein synthesis to measure endocytic degradation of EGFR. The comparison revealed that endocytic degradation of EGFR was significantly delayed in *Neu*$^{+}$/*Tip30*$^{-/-}$ mammary tumors cells compared with *Neu*$^{+}$/*Tip30*$^{+/+}$ mammary tumors cells,

DOI:10.1158/0008-5472.CAN-10-3057

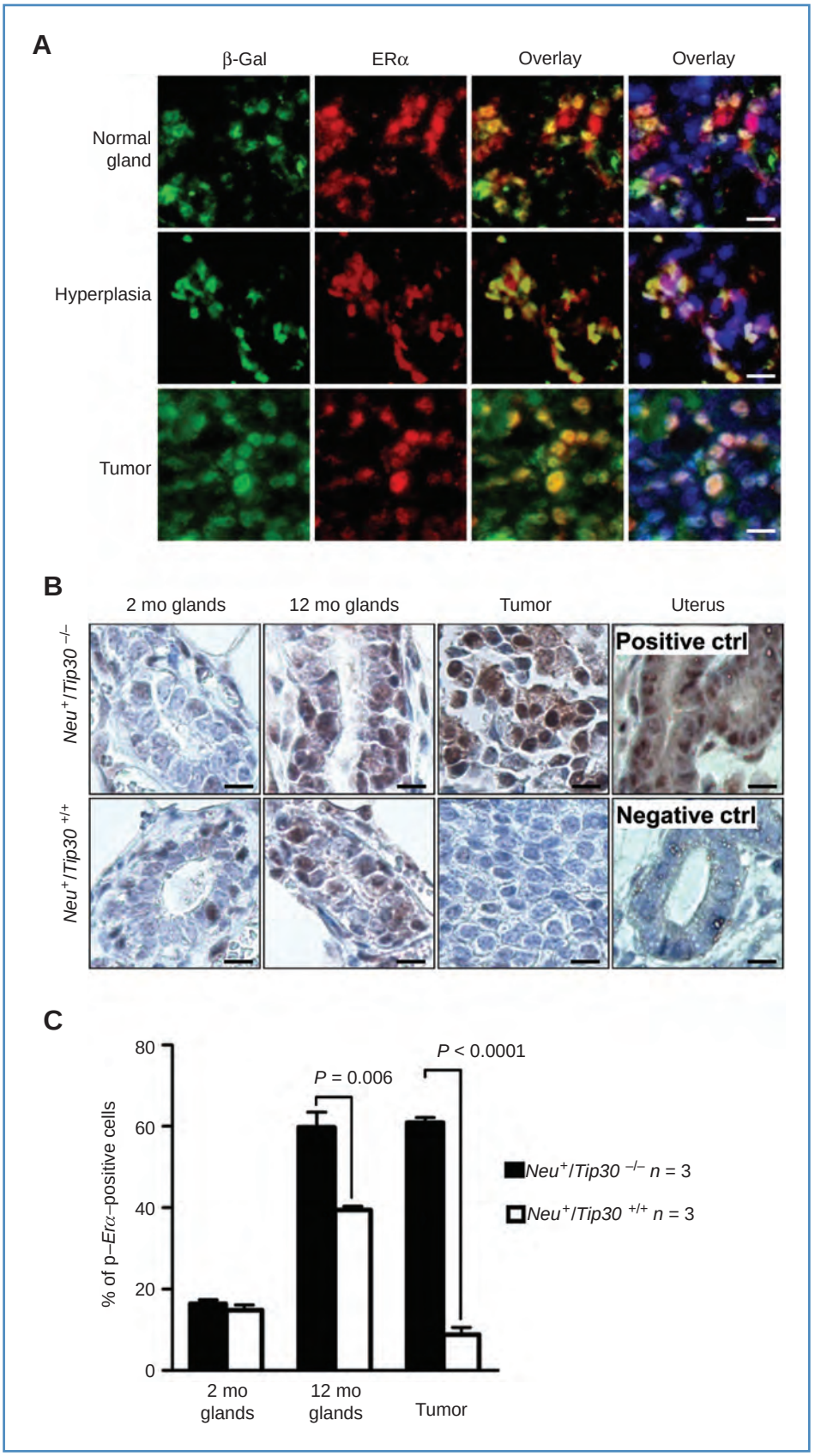

Figure 4. Representative immunohistochemical staining of p-ERα in mammary glands and mammary tumors from *Neu*$^{+}$/*Tip30*$^{-/-}$ and *Neu*$^{+}$/*Tip30*$^{+/+}$ mice. A, representative immunofluorescent double staining of mammary gland and tumor sections from a *Neu*$^{+}$/*Tip30*$^{+/-}$ mouse for ERα (red) and β-Gal (green), followed by counterstaining with DAPI (blue). Scale bar, 10 μm. B, representative immunohistochemical staining of p-ERα in 2- and 12-month-old mammary glands and mammary tumors from *Neu*$^{+}$/*Tip30*$^{-/-}$ and *Neu*$^{+}$/*Tip30*$^{+/+}$ mice. As a negative control (ctrl), a uterus section was stained without using the primary antibody (anti–p-ERα). Scale bar, 10 μm. C, data represent means ± SEM of the percentage of p-ERα–positive cells in the mammary glands and tumors derived from *Neu*$^{+}$/*Tip30*$^{-/-}$ and *Neu*$^{+}$/*Tip30*$^{+/+}$ mice. Positive p-ERα cells were counted in the sections of mammary glands and tumors derived from 3 mice of each genotype (randomly selected fields per section). Fifty cells were counted per field and 10 fields were counted per mouse.

DOI:10.1158/0008-5472.CAN-10-3057

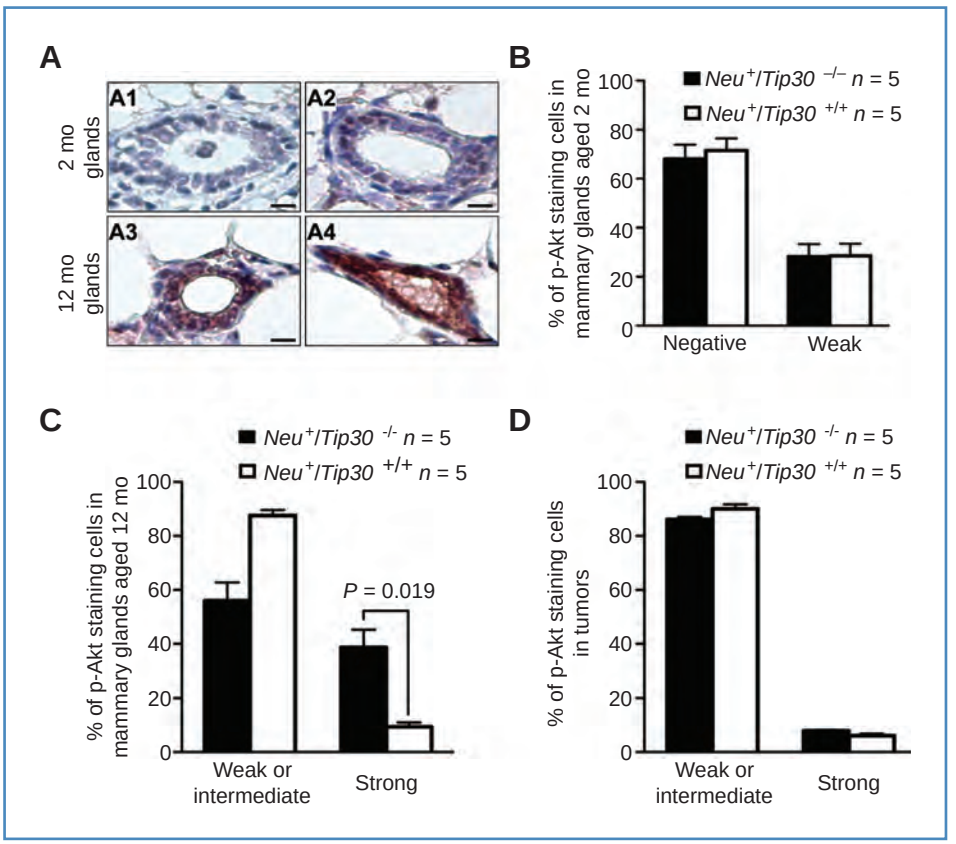

Figure 5. Representative immunohistochemical staining for p-Akt in mammary tumors and mammary glands from *Neu*$^{+}$/*Tip30*$^{-/-}$ and *Neu*$^{+}$/*Tip30*$^{+/+}$ mice. A, representative immunohistochemical staining of p-Akt in mammary glands. Staining of p-Akt in 2-month-old mammary glands ranges from negative to weak (A1 and A2) and is more intense in 12-month-old mammary glands (A3 and A4, intermediate and strong, respectively). Scale bar, 10 μm. B–D, data represent means ± SEM of the percentage of cells that were stained positive or negative for p-Akt in 2-month-old (B) and 12-month-old (C) mammary glands and tumors (D) derived from *Neu*$^{+}$/*Tip30*$^{-/-}$ and *Neu*$^{+}$/*Tip30*$^{+/+}$ mice. Fifty cells were counted per field and 10 fields were counted per mouse. Data were analyzed by 2-tailed *t* test.

indicating that *Tip30* deletion impairs endocytic degradation of EGFR (Fig. 6A and B).

To determine whether *Tip30* deletion can block EGFR trafficking from early endosomes to lysosomes for degradation, we tracked Alexa-488–conjugated EGF (Alexa^{488}-EGF) and EGFR in normal primary MECs isolated from *Tip30*$^{-/-}$ and *Tip30*$^{+/+}$ mice. The majority of internalized EGFs dissociated from EGFR in wild-type MECs 2 hours after EGF internalization. In contrast, they remained associated with EGFR in *Tip30*$^{-/-}$ MECs (EGF-EGFR colocalization in wild-type primary MECs: 11%; EGF–EGFR colocalization in *Tip30*$^{-/-}$ primary MECs: 55%; $n = 20$, $P = 0.004$; Fig. 6C and D), indicating that *Tip30* deletion causes the trapping of EGF–EGFR complex in endosomes and sustained endosomal EGFR signaling. To rule out the possibility that *Tip30* deletion increased Neu transgene expression at the level of transcription, we used quantitative reverse transcription-PCR (RT-PCR) to examine the mRNA expression of Neu transgene in 5- to 9-week-old *Neu*$^{+}$/*Tip30*$^{+/+}$ and *Neu*$^{+}$/*Tip30*$^{-/-}$ mice and found no significant difference (data not shown). Together, these results suggest that *Tip30* loss may prolong EGFR signaling, which cooperates with Neu activation to enhance Akt activation and to promote the formation of ER+/PR− tumors.

Discussion

This study was designed to investigate the relationship between HER2/Neu overexpression and *Tip30* deletion in mammary tumorigenesis by using genetically engineered mice containing both *Tip30* deletion and an MMTV-Neu transgene. Strikingly, the data show that *Tip30* deletion cooperates with Neu overexpression to promote exclusive development of ER+/PR− mammary tumors in mice. In addition, we show that *Tip30* loss impairs endocytic trafficking of EGF–EGFR, delays EGFR degradation in primary MECs and tumor cells, and enhances Akt and ERα phosphorylation in the mammary gland. These findings, combined with our recent observation that TIP30 formed a protein complex with ACSL4 and EndoB1 to control EGF–EGFR endocytic trafficking in hepatocytes (C. Zhang, A. Li, X. Zhang, and H. Xiao, submitted manuscript), strongly suggest a novel mechanism by which the loss of *Tip30* contributes to the development of ER+/PR− tumors, at least in part, through enhancing EGFR signaling in ER+ MECs.

It is not immediately obvious why *Tip30* deletion combined with Neu overexpression causes the exclusive development of ER+/PR− mammary tumors. The observation that the promoter of *Tip30* was predominantly active in ER+ MECs suggest that *Tip30* deletion may mainly affect the proliferation of ER+ cells by inducing enhanced ERα activities, thereby selecting ER+ cells to initiate tumorigenesis. Indeed, ER+/PR+ mammary tumors developed spontaneously in 22% of aged *Tip30*-knockout female mice in the BALB/c genetic background (A. Li, C. Zhang, S. Gao, R. Luo, and H. Xiao, unpublished data) and TIP30 could inhibit ERα-mediated transcription (15). The correlation between progressively increased p-Akt and p-ERα–positive cells in *Neu*$^{+}$/*Tip30*$^{-/-}$ mammary glands observed in this study implies that *Tip30*

DOI:10.1158/0008-5472.CAN-10-3057

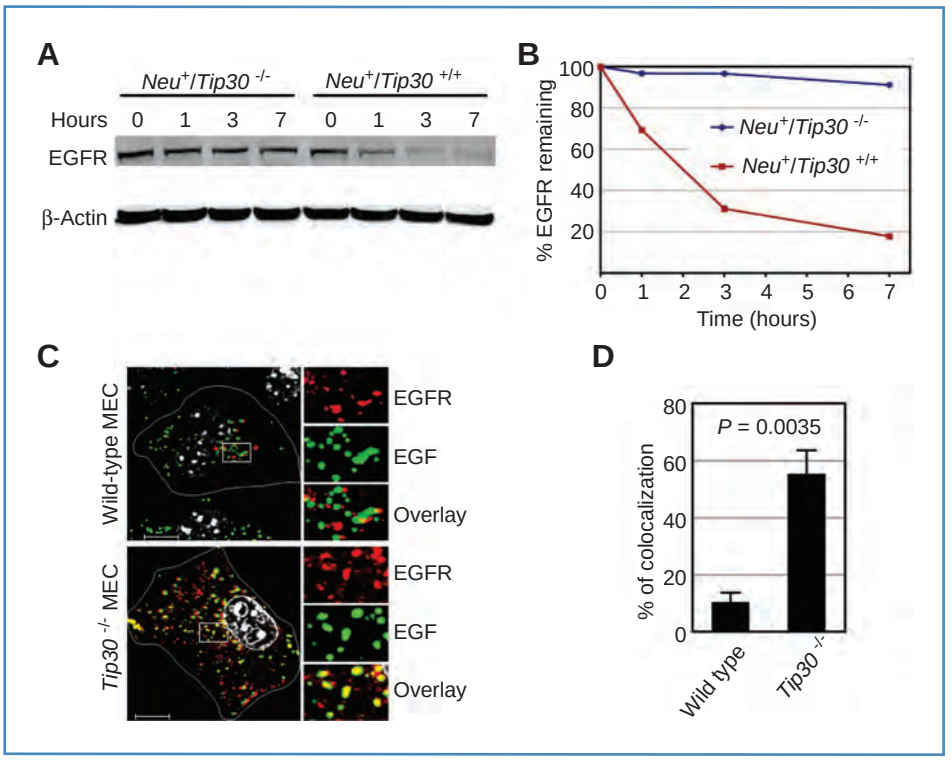

Figure 6. Deletion of *Tip30* in MECs leads to delayed EGFR degradation. A, *Neu*$^{+}$/*Tip30*$^{-/-}$ and *Neu*$^{+}$/*Tip30*$^{+/+}$ mammary tumor cells were incubated with 100 ng/mL of EGF for 1 hour on ice, followed by washing with cold PBS and incubating in serum-free medium containing cycloheximide (20 μg/mL) for the indicated times. Whole-cell lysates were blotted with the indicated antibodies. B, quantification of EGFR protein levels in (A) using Odyssey 2.1 software. C, primary *Tip30*$^{+/+}$ and *Tip30*$^{-/-}$ MECs were subjected to EGFR internalization analysis. Representative confocal microscopy images show the localization of EGFR (red) in endosomes after 2 hours of Alexa^{488}-EGF (green) internalization. Results are typical and representative of 3 experiments on primary cells from 2 mice of each genotype. Boxed areas are magnified. Representative cells are outlined in white. The colocalization of EGF and EGFR (yellow) in *Tip30*$^{-/-}$ cells is indicative of delayed endocytic degradation of EGFR; the nucleus was stained with DAPI (gray). Scale bar, 10 μm. D, quantitative analysis of EGF and EGFR colocalization. Twenty cells in each group were analyzed using MBF_imageJ. Pearson's colocalization coefficients were calculated and converted to percentages. $P = 0.035$.

deletion may promote the development of ER+ mammary tumors by enhancing Akt activation and increasing active ERα-positive cells. Consistent with this scenario, a previous study showed that Akt overexpression could increase the intensity of ERα staining, the number of ERα-positive cells, and the frequency of ER+ tumors in DMBA-treated mice (31), although it did not show whether these tumors were PR positive. Moreover, expression and phosphorylation of ERα in ER+ human breast cells are enhanced by the activation of Akt (21, 31). It should be noted that enhanced Akt activation alone is insufficient for driving the tumorigenic process in mouse MECs *in vivo* (32); therefore, other mechanisms such as increased expression of c-Myc and IGF-1 induced by *Tip30* deletion may also contribute to the formation of ER+/PR− mammary tumors in MMTV-Neu mouse models (14, 15).

Even thought tumors arising in *Neu*$^{+}$/*Tip30*$^{-/-}$ mice were stained negatively for PRs and did not display significantly more PR-A/PR-B mRNAs according to our quantitative RT-PCR analysis (data not shown), these ER+/PR− tumors were sensitive to progesterone stimulation and RU486 inhibition, and PR-A proteins were detectable in cultured ER+/PR− tumor cells when proteasomes were inhibited. One explanation for these observations is that PR-A is expressed in ER+/PR− tumors but rapidly turns over due to enhanced activation of EGFR and HER2/Neu *in vivo*. This explanation is supported by previous reports that PR degradation by the 26S proteasome is mediated by MAPK/ERK-induced phosphorylation at Ser294 in cultured breast cancer cells (20). It has been shown that ERK1/2 activation in human cancer cells induces PR-B Ser294 phosphorylation and blocks PR-B sumoylation, which leads to 2 coupled events, hyperactive transcription activity and rapid turnover of PR-B proteins. PR-A was shown to be relatively resistant to these events compared with PR-B (20, 33–35). In agreement with these results, we also observed significantly enhanced ERK1/2 activation at *Neu*$^{+}$/*Tip30*$^{-/-}$ tumor periphery compared with *Neu*$^{+}$/*Tip30*$^{+/+}$ tumor periphery (Supplementary Fig. 2). Notably, we detected only PR-A after treatment with proteasome inhibitor (Fig. 3D), possibly because PR-A is the dominant form in the mammary glands of mature virgin mice whereas human breast cells express both PR-A and PR-B (36). Our observation that ER+/PR− tumors were responsive to progesterone and RU486 indicates a critical role of progesterone signaling in the growth of ER+/PR− tumors and implicates that intervention of ER+/PR− breast cancers may be achieved, in part, through suppression of PR function.

DOI:10.1158/0008-5472.CAN-10-3057

Our data seem to support the hypothesis that ER^+ breast cancers arise from ER+ or otherwise estrogen-responsive progenitor cells (37). However, our data do not exclude the possibility that *Tip30* deletion may cause ER−/PR− cells to reexpress ERα or promote transformed ER−/PR− luminal progenitor cells to differentiate to ER+/PR− epithelial cells. Studies on the origin of tumor cells in MMTV-Neu mice have suggested that tumor cells from this model originate from transformed luminal progenitor cells committing to ER−/PR− cells (38). Therefore, the cell origin of ER+/PR− tumors arising in $Neu^+/Tip30^{-/-}$ mice remains to be determined.

Currently, there remains a profound need for more effective therapies for treating HER2+/ER+/PR− breast cancers because of their poor response and development of resistance to existing therapies. Nonetheless, the majority of preclinical studies of ER-positive breast cancer have relied on cultured cell lines or on xenograft tumor models, in which breast tumor development and progression do not accurately represent clinical human breast cancer. Alternatively, the use of genetically engineered mouse models of breast cancer has major advantages for investigating the molecular mechanism of mammary tumorigenesis as well as developing anticancer agents. To date, there have been many mouse mammary cancer models generated by overexpression or deletion of specific genes that are associated with human breast cancer. Unfortunately, most mammary tumors arising in those animal models are ER−/PR− and do not morphologically resemble the major subtype of human breast cancer (ER+ ductal carcinoma); ER+ mammary tumors are observed in only a few genetically engineered mouse models (39–42). To our knowledge, there has been no animal model of HER2+/ER+/PR− mammary tumors reported. Therefore, our mouse model of HER2+/ER+/PR− breast cancer provides a valuable tool for deciphering the mechanisms of HER2+/ER+/PR− breast cancer development and for testing single or combination therapies.

Disclosure of Potential Conflicts of Interest

No potential conflicts of interest were disclosed.

Acknowledgments

We are grateful to Jill Pecha, for backcrossing *Tip30* deletion allele into FBV mice, and Ryan Brooks, Adam C. Edmunds, George Chen, for the excellent technical assistance. We thank Ying Qin for histopathologic expertise and Eran Andrechek for critical reading of the manuscript.

The contents of this work are solely the responsibility of the authors and do not necessarily represent the official views of the NIDDK, National Institute of Environment Health Science, or National Cancer Institute, National Institutes of Health.

Grant Support

This work was supported by grants RO1 DK066110-01 and W81XWH-08-1-0377 (to H.X.) from the NIDDK and Department of Defense and grant U01 ES/CA 012800 (to S.Z.H.) from the National Institute of Environment Health Science and the National Cancer Institute, National Institutes of Health, Department of Health and Human Services.

The costs of publication of this article were defrayed in part by the payment of page charges. This article must therefore be hereby marked *advertisement* in accordance with 18 U.S.C. Section 1734 solely to indicate this fact.

Received 08/19/2010; revised 10/11/2010; accepted 10/15/2010; published online 12/15/2010.

References

1. Osborne CK, Schiff R, Arpino G, Lee AS, Hilsenbeck VG. Endocrine responsiveness: understanding how progesterone receptor can be used to select endocrine therapy. Breast 2005;14:458–65.
2. Ponzone R, Montemurro F, Maggiorotto F, Robba C, Gregori D, Jacomuzzi ME, et al. Clinical outcome of adjuvant endocrine treatment according to PR and HER-2 status in early breast cancer. Ann Oncol 2006;17:1631–6.
3. Arpino G, Weiss H, Lee AV, Schiff R, De Placido S, Osborne CK, et al. Estrogen receptor-positive, progesterone receptor-negative breast cancer: association with growth factor receptor expression and tamoxifen resistance. J Natl Cancer Inst 2005;97:1254–61.
4. Creighton CJ, Kent Osborne C, van de Vijver MJ, Foekens JA, Klijn JG, Horlings HM, et al. Molecular profiles of progesterone receptor loss in human breast tumors. Breast Cancer Res Treat 2009;114:287–99.
5. Kim HJ, Cui X, Hilsenbeck SG, Lee AV. Progesterone receptor loss correlates with human epidermal growth factor receptor 2 overexpression in estrogen receptor-positive breast cancer. Clin Cancer Res 2006;12:1013s–8s.
6. Cui X, Schiff R, Arpino G, Osborne CK, Lee AV. Biology of progesterone receptor loss in breast cancer and its implications for endocrine therapy. J Clin Oncol. 2005;23:7721–35.
7. Dowsett M, Johnston S, Martin LA, Salter J, Hills M, Detre S, et al. Growth factor signalling and response to endocrine therapy: the Royal Marsden Experience. Endocr Relat Cancer 2005;12Suppl 1:S113–7.
8. Konecny G, Pauletti G, Pegram M, Untch M, Dandekar S, Aguilar Z, et al. Quantitative association between HER-2/neu and steroid hormone receptors in hormone receptor-positive primary breast cancer. J Natl Cancer Inst 2003;95:142–53.
9. Xiao H, Tao Y, Greenblatt J, Roeder RG. A cofactor, TIP30, specifically enhances HIV-1 Tat-activated transcription. Proc Natl Acad Sci USA 1998;95:2146–51.
10. Ito M, Jiang C, Krumm K, Zhang X, Pecha J, Zhao J, et al. TIP30 deficiency increases susceptibility to tumorigenesis. Cancer Res 2003;63:8763–7.
11. Lee LW, Zhang DH, Lee KT, Koay ES, Hewitt RE. CC3/TIP30 expression was strongly associated with HER-2/NEU status in breast cancer. Ann Acad Med Singapore 2004;33:S30–2.
12. Tong X, Li K, Luo Z, Lu B, Liu X, Wang T, et al. Decreased TIP30 expression promotes tumor metastasis in lung cancer. Am J Pathol 2009;174:1931–9.
13. Zhao J, Ni H, Ma Y, Dong L, Dai J, Zhao F, et al. TIP30/CC3 expression in breast carcinoma: relation to metastasis, clinicopathologic parameters, and P53 expression. Hum Pathol 2007;38:293–8.
14. Pecha J, Ankrapp D, Jiang C, Tang W, Hoshino I, Bruck K, et al. Deletion of Tip30 leads to rapid immortalization of murine mammary epithelial cells and ductal hyperplasia in the mammary gland. Oncogene 2007;26:7423–31.
15. Jiang C, Ito M, Piening V, Bruck K, Roeder RG, Xiao H. TIP30 interacts with an estrogen receptor alpha-interacting coactivator CIA and regulates c-myc transcription. J Biol Chem 2004;279:27781–9.
16. Zhao J, Lu B, Xu H, Tong X, Wu G, Zhang X, et al. Thirty-kilodalton Tat-interacting protein suppresses tumor metastasis by inhibition of osteopontin transcription in human hepatocellular carcinoma. Hepatology 2008;48:265–75.
17. King FW, Shtivelman E. Inhibition of nuclear import by the proapoptotic protein CC3. Mol Cell Biol 2004;24:7091–101.
18. Guy CT, Webster MA, Schaller M, Parsons TJ, Cardiff RD, Muller WJ. Expression of the neu protooncogene in the mammary epithelium of

DOI:10.1158/0008-5472.CAN-10-3057

transgenic mice induces metastatic disease. Proc Natl Acad Sci US A 1992;89:10578–82.
19. Huang S, Li Y, Chen Y, Podsypanina K, Chamorro M, Olshen AB, et al. Changes in gene expression during the development of mammary tumors in MMTV-Wnt-1 transgenic mice. Genome Biol 2005;6:R84.
20. Lange CA, Shen T, Horwitz KB. Phosphorylation of human progesterone receptors at serine-294 by mitogen-activated protein kinase signals their degradation by the 26S proteasome. Proc Natl Acad Sci U S A 2000;97:1032–7.
21. Campbell RA, Bhat-Nakshatri P, Patel NM, Constantinidou D, Ali S, Nakshatri H. Phosphatidylinositol 3-kinase/AKT-mediated activation of estrogen receptor alpha: a new model for anti-estrogen resistance. J Biol Chem 2001;276:9817–24.
22. Lannigan DA. Estrogen receptor phosphorylation. Steroids 2003; 68:1–9.
23. Hutchinson JN, Jin J, Cardiff RD, Woodgett JR, Muller WJ. Activation of Akt-1 (PKB-alpha) can accelerate ErbB-2-mediated mammary tumorigenesis but suppresses tumor invasion. Cancer Res 2004;64:3171–8.
24. Ju X, Katiyar S, Wang C, Liu M, Jiao X, Li S, et al. Akt1 governs breast cancer progression *in vivo*. Proc Natl Acad Sci USA 2007;104: 7438–43.
25. Maroulakou IG, Oemler W, Naber SP, Tsichlis PN. Akt1 ablation inhibits, whereas Akt2 ablation accelerates, the development of mammary adenocarcinomas in mouse mammary tumor virus (MMTV)-ErbB2/neu and MMTV-polyoma middle T transgenic mice. Cancer Res 2007;67:167–77.
26. Nardulli AM, Katzenellenbogen BS. Progesterone receptor regulation in T47D human breast cancer cells: analysis by density labeling of progesterone receptor synthesis and degradation and their modulation by progestin. Endocrinology 1988;122:1532–40.
27. Mellman I. Membranes and sorting. Curr Opin Cell Biol 1996;8:497–8.
28. Sorkin A, Goh LK. Endocytosis and intracellular trafficking of ErbBs. Exp Cell Res 2009;315:683–96.
29. Forgac M. Vacuolar ATPases: rotary proton pumps in physiology and pathophysiology. Nat Rev Mol Cell Biol 2007;8:917–29.
30. Murphy JE, Padilla BE, Hasdemir B, Cottrell GS, Bunnett NW. Endosomes: a legitimate platform for the signaling train. Proc Natl Acad Sci U S A 2009;106:17615–22.
31. Blanco-Aparicio C, Perez-Gallego L, Pequeno B, Leal JF, Renner O, Carnero A. Mice expressing myrAKT1 in the mammary gland develop carcinogen-induced ER-positive mammary tumors that mimic human breast cancer. Carcinogenesis 2007;28:584–94.
32. Hutchinson J, Jin J, Cardiff RD, Woodgett JR, Muller WJ. Activation of Akt (protein kinase B) in mammary epithelium provides a critical cell survival signal required for tumor progression. Mol Cell Biol 2001; 21:2203–12.
33. Shen T, Horwitz KB, Lange CA. Transcriptional hyperactivity of human progesterone receptors is coupled to their ligand-dependent down-regulation by mitogen-activated protein kinase-dependent phosphorylation of serine 294. Mol Cell Biol 2001;21:6122–31.
34. Qiu M, Lange CA. MAP kinases couple multiple functions of human progesterone receptors: degradation, transcriptional synergy, and nuclear association. J Steroid Biochem Mol Biol 2003;85: 147–57.
35. Daniel AR, Faivre EJ, Lange CA. Phosphorylation-dependent antagonism of sumoylation derepresses progesterone receptor action in breast cancer cells. Mol Endocrinol 2007;21:2890–906.
36. Aupperlee MD, Smith KT, Kariagina A, Haslam SZ. Progesterone receptor isoforms A and B: temporal and spatial differences in expression during murine mammary gland development. Endocrinology 2005;146:3577–88.
37. Allred DC, Brown P, Medina D. The origins of estrogen receptor alpha-positive and estrogen receptor alpha-negative human breast cancer. Breast Cancer Res 2004;6:240–5.
38. Vaillant F, Asselin-Labat ML, Shackleton M, Forrest NC, Lindeman GJ, Visvader JE. The mammary progenitor marker CD61/beta3 integrin identifies cancer stem cells in mouse models of mammary tumorigenesis. Cancer Res 2008;68:7711–7.
39. Liu S, Umezu-Goto M, Murph M, Lu Y, Liu W, Zhang F, et al. Expression of autotaxin and lysophosphatidic acid receptors increases mammary tumorigenesis, invasion, and metastases. Cancer Cell 2009;15:539–50.
40. Medina D, Kittrell FS, Shepard A, Stephens LC, Jiang C, Lu J, et al. Biological and genetic properties of the p53 null preneoplastic mammary epithelium. FASEB J 2002;16:881–3.
41. Rose-Hellekant TA, Schroeder MD, Brockman JL, Zhdankin O, Bolstad R, Chen KS, et al. Estrogen receptor-positive mammary tumorigenesis in TGFalpha transgenic mice progresses with progesterone receptor loss. Oncogene 2007;26:5238–46.
42. Zhang X, Podsypanina K, Huang S, Mohsin SK, Chamness GC, Hatsell S, et al. Estrogen receptor positivity in mammary tumors of Wnt-1 transgenic mice is influenced by collaborating oncogenic mutations. Oncogene 2005;24:4220–31.
43. Medina D, Kittrell F. Establishment of Mouse Mammary Cell Lines. New York: Kluwer Academic/Plenum Publishers; 2000.
44. Jiang C, Pecha J, Hoshino I, Ankrapp D, Xiao H. TIP30 mutant derived from hepatocellular carcinoma specimens promotes growth of HepG2 cells through up-regulation of N-cadherin. Cancer Res 2007;67: 3574–82.
45. Ku NO, Omary MB. Keratins turn over by ubiquitination in a phosphorylation-modulated fashion. J Cell Biol 2000;149:547–52.

Figure S1

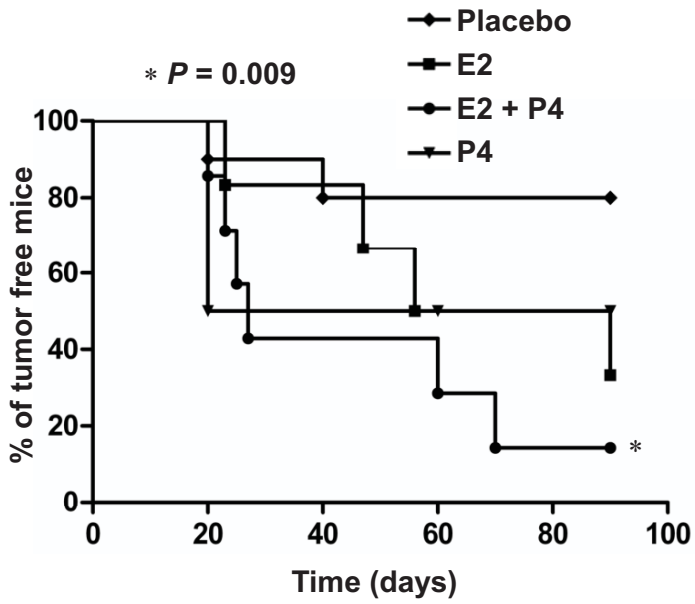

Legend to Supplementary Figure 1:
Two ER+/PR- mammary tumors from *Neu*+/*Tip30*$^{-/-}$ mice were minced and inoculated s.c. in the front flanks of ovariectomized mice supplemented with Placebo (n = 10), estrogen (E2, n = 6), progesterone (P4, n = 6) or E2 plus P4 (n = 7) pellets. Kaplan-Meier analysis of mammary-tumor free-survival was performed based on the time of tumors becoming 1 cm^3 in volume or tumors becoming $\geq$ 0.25 cm^3 by the end of three months. *P* = 0.009 (placebo *vs.* E2 + P4), log-rank test.

Figure S2

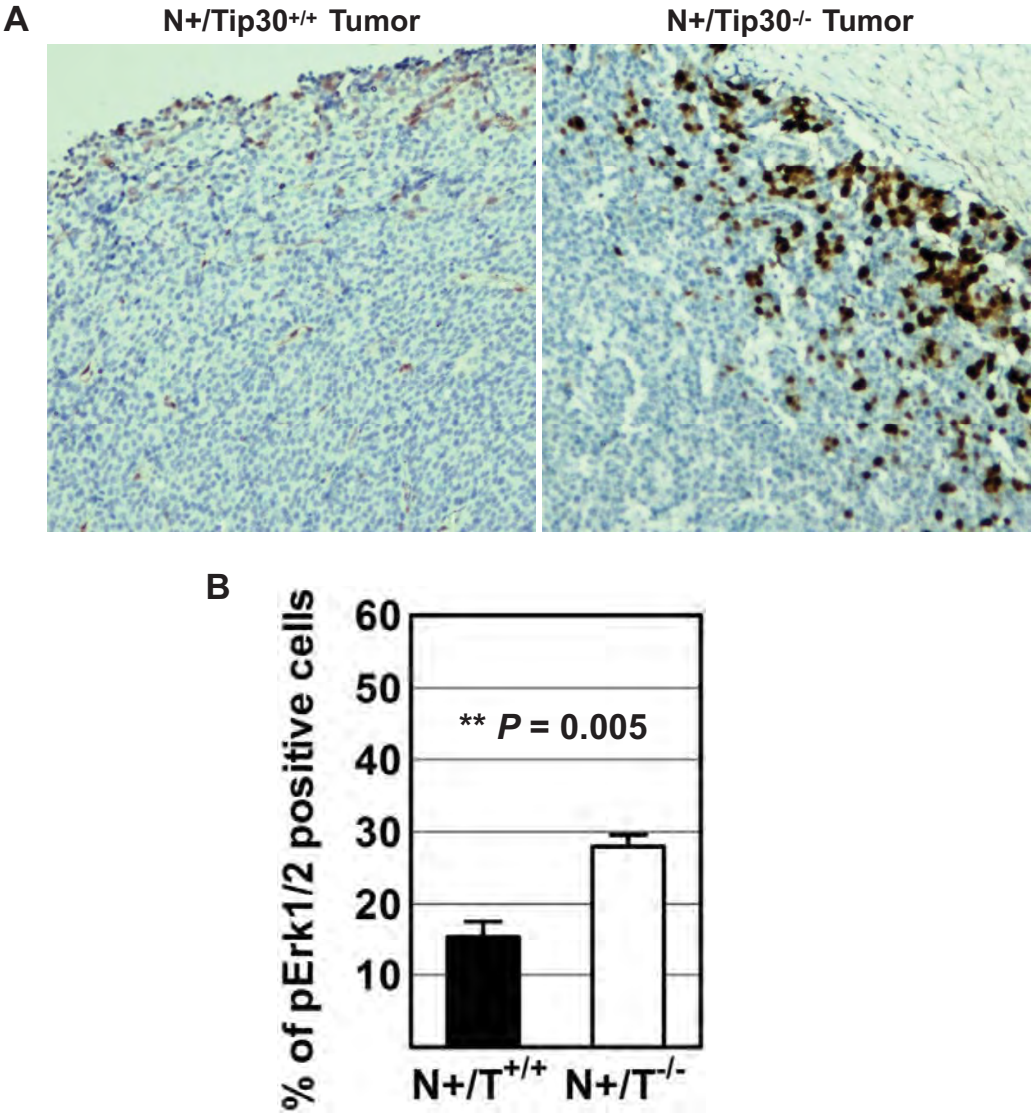

Legend to Supplementary Figure 2:

(A) Representative immunohistochemical staining images show enhanced phosphorylation of ERK1/2 at Thr202/Tyr204 in mammary tumors from Neu+/Tip30$^{-/-}$ mice (n = 3) compared with those from Neu+/Tip30$^{+/+}$ mice (n = 3).

(B) Quantification of pERK1/2 positive cells. Since very few cells at the tumor core were stained positive for pERK, cells within 120 μm distance from the edge were counted. *P* = 0.005; t test.

THE JOURNAL OF BIOLOGICAL CHEMISTRY VOL. 286, NO. 11, pp. 9373–9381, March 18, 2011

A Novel TIP30 Protein Complex Regulates EGF Receptor Signaling and Endocytic Degradation*[S]

Received for publication, December 1, 2010, and in revised form, January 18, 2011 Published, JBC Papers in Press, January 20, 2011, DOI 10.1074/jbc.M110.207720

Chengliang Zhang[‡§], Aimin Li[‡¶], Xinchun Zhang[§], and Hua Xiao[‡1]

From the [‡]Department of Biomedical and Integrative Physiology and [§]Genetics Program, Michigan State University, East Lansing, Michigan 48824 and the [¶]Department of Oncology, Nanfang Hospital, Southern Medical University, Guangzhou 510515, China

Activated epidermal growth factor receptor (EGFR) continues to signal in the early endosome, but how this signaling process is regulated is less well understood. Here we describe a protein complex consisting of TIP30, endophilin B1, and acyl-CoA synthetase long chain family member 4 (ACSL4) that interacts with Rab5a and regulates EGFR endocytosis and signaling. These proteins are required for the proper endocytic trafficking of EGF-EGFR. Knockdown of TIP30, ACSL4, endophilin B1, or Rab5a in human liver cancer cells or genetic knock-out of Tip30 in mouse primary hepatocytes results in the trapping of EGF-EGFR complexes in early endosomes, leading to delayed EGFR degradation and prolonged EGFR signaling. Furthermore, we show that Rab5a colocalizes with vacuolar (H^+)-ATPases (V-ATPases) on transport vesicles. The TIP30 complex facilitates trafficking of Rab5a and V-ATPases to EEA1-positve endosomes in response to EGF. Together, these results suggest that this TIP30 complex regulates EGFR endocytosis by facilitating the transport of V-ATPases from trans-Golgi network to early endosomes.

Receptor-mediated endocytosis is a mechanism utilized by eukaryotic cells to rapidly take up specific nutrients and reduce receptor signaling at the plasma membrane. Internalized ligand-receptor complexes are enclosed in early endosomes, also called sorting endosomes, where they are either recycled or delivered to lysosomes for destruction (1, 2). Signaling receptors continue to activate certain downstream pathways from early endosomes (3–6) until ligand-receptor complexes dissociate due to lower luminal pH created by vacuolar V-ATPases,[2] the major proton pump responsible for endosomal and lysosomal acidification (2, 7–9). Inactivation of V-ATPases blocks the transition from early to late endosomes (10). Therefore, the proper endosomal targeting and activity of V-ATPases contribute to the tight regulation of both endocytic trafficking and receptor endosomal signaling.

Acidic luminal pH in early endosomes is the driving force for receptors to release their ligands, such as insulin and low density lipoprotein (LDL) (1, 2). On the basis of individually tracking EGF and EGFR, it has long been considered that EGFR travels together with EGF until they reach lysosomes (11, 12). However, it is unclear whether they remain bound to each other on the way to lysosomes. Recent studies have suggested that EGFR is inactivated before being degraded and that EGF dissociates from EGFR prior to lysosomal transfer (6, 13–15).

Rab5a is a small GTPase that regulates early endosome fusion *in vitro* (16), motility of early endosomes on microtubules (17), and the traffic between endosomes and lysosomes (18). Deletion of Rab5a in cells inhibits the transport of EGFR from early endosomes to lysosomes and consequently causes sustained EGFR signaling and delayed EGFR degradation (19). Despite its importance to endocytic transport, how Rab5a mediates down-regulation of receptor signaling remains unclear.

TIP30, also known as HTATIP2 or CC3 (20, 21), is a tumor suppressor that has been demonstrated to act as a transcription cofactor to repress transcription in the nucleus (22, 23) and to localize at the nuclear envelope to block nuclear importing (24). However, TIP30 also localizes in the cytoplasm, where its function is not known (25–28).

Here we report that a newly identified protein complex containing TIP30, ACSL4, and Endo B1 drives EGF-EGFR complex endocytic trafficking by facilitating the localization of Rab5a and V-ATPases to early endosomes. Rab5a and V-ATPase reside in vesicles devoid of the early endosomal marker EEA1 and the recycling endosomal marker transferrin receptor (TfR), suggesting that these vesicles are post-trans-Golgi network vesicles responsible for the transport of integral membrane protein V-ATPases. Our data suggest a mechanism by which Rab5a in cooperation with other proteins in the TIP30 complex transports V-ATPases to early endosomes and induces the dissociation of EGF from EGFR and the termination of EGFR endosomal signaling.

EXPERIMENTAL PROCEDURES

Cell Culture—PLC/PRF/5 and HepG2 cell lines were purchased from ATCC. Cells were cultured in DMEM (Invitrogen) supplemented with 10% fetal bovine serum and penicillin/streptomycin (Invitrogen) at 37 °C in 5% CO_2.

DNA Constructs and shRNAs—The pSin-EF2 vector (29) was converted to destination vectors by cloning the Gateway cassette RfA (reading frame A, Invitrogen) with either N-terminal or C-terminal HA tag, CFP, EYFP, or DsRed fluorescent proteins into blunted SpeI and EcoRI sites. Human Rab5a, ACSL4,

* This work was supported, in whole or in part, by National Institutes of Health Grants RO1 DK066110-01 and W81XWH-08-1-0377 from the NIDDK (to H. X.). This work was also supported by a grant from the Department of Defense.

[S] The on-line version of this article (available at http://www.jbc.org) contains supplemental Figs. S1–S2.

[1] To whom correspondence should be addressed: 3193 Biomedical and Physical Sciences Bldg., East Lansing, MI 48824-3320. Fax: 517-355-5125; E-mail: xiaoh@msu.edu.

[2] The abbreviations used are: V-ATPase, vacuolar (H^+)-ATPase; EGFR, epidermal growth factor receptor; Endo B1, endophilin B1; TfR, transferrin receptor.

and EndoB1 were amplified using RT-PCR from mRNA isolated from PLC/PRF/5 cells. TIP30 was subcloned from pFlag7-TIP30 and pFlag7-TIP30M (30). For bimolecular fluorescence complementation assays, VC155 and VN173 (31) were cloned into pCDNA3.1 and pSin-EF2, respectively, and both were also converted to destination vectors. Lentiviral plasmids producing shRNAs against TIP30, Rab5a, and ACSL4 were from Sigma-Aldrich. Lentiviral plasmids for shRNAs against Endo B1 were from Open Biosystems.

Antibodies—HA (HA-7), β-actin (AC-15), and Endo B1 antibodies were from Sigma-Aldrich. AKT, AKT-pS473, EEA1, and Rab5a antibodies were from Cell Signaling. EGFR-pY845, TfR, Alexa Fluor 546 goat anti-mouse, and Alexa Fluor 594 goat anti-rabbit antibodies were from Invitrogen. Anti-EGFR antibody was from Millipore. ATP6V1H antibody was from Santa Cruz Biotechnology. LAMP1 antibody was purchased from The Developmental Studies Hybridoma Bank at University of Iowa.

EGFR Internalization and Immunofluorescence—PLC/PRF/5 cells were infected by lentiviruses producing shRNA against indicated genes. Cells were pooled after being selected for 4 days with 2 μg/ml puromycin. At least two confirmed knockdown pools for each targeted gene were used for the experiments in Figs. 4–8. Control and knockdown cells were cultured on cover glass and were serum-starved for 24 h in DMEM. Wild type and *Tip30*$^{-/-}$ primary hepatocytes were starved for 3 h. Cells were incubated with 100 ng/ml Alexa-488-conjugated EGF (Alexa^{488}-EGF) (Invitrogen) and 20 μg/ml cycloheximide on ice for 1 h and then were washed four times with cold PBS and incubated in DMEM with 20 μg/ml cycloheximide at 37 °C for different time periods. Cells were fixed in 4% paraformaldehyde in PBS for 15 min, permeabilized with 0.1% Triton X-100 for 2 min, and stained for the indicated proteins. Images were obtained with a Zeiss LSM 510 Meta confocal microscope (Carl Zeiss) using Plan-Apochromat 63×/1.40 oil objective. Pinhole size was set to 1 airy unit for all channels. All images are representative single optical sections. To determine EGFR stability upon EGF treatment, cells were cultured in 6-cm dishes and treated as above except that unlabeled EGF was used, and the cells were collected for immunoblot at various time points.

Immunoprecipitation—PLC/PRF/5 cells were transfected with indicated constructs. Whole cell extracts were prepared from pooled stable clones as described previously with modifications (32). Briefly, cells were homogenized by 20 strokes in two packed cell pellet volumes of buffer A (10 mM Hepes, pH 7.9, 10 mM KCl, 0.5 mM DTT, protease inhibitor mixture) using a Kontes homogenizer (B pestle). Another 20 strokes were applied after adding 1.5 cell pellet volumes of buffer B (50 mM Hepes, pH 7.9, 0.6 mM EDTA, 1.5 mM DTT, 1.26 M NaCl, 75% glycerol) followed by centrifugation at 100,000 × *g* for 1 h. The supernatant was dialyzed against BC300 (20 mM Hepes, pH 7.9, 20% glycerol, 0.2 mM EDTA, 0.5 mM DTT, 0.3 M KCl) (33) and centrifuged at 15,000 rpm for 20 min followed by rotating with anti-HA agarose beads (Roche Diagnostics) overnight at 4 °C. The beads were centrifuged and extensively washed using BC300 buffer. Immunoprecipitates were eluted with HA peptides (Roche Diagnostics), denatured, resolved on SDS-PAGE, and subjected to silver stain, immunoblot, or LC-MS/MS spectral analyses (The MSU Proteomics Facility, Michigan State University).

Mouse Hepatocyte Isolation—Primary hepatocytes were isolated from 8-week-old wild type and *Tip30*$^{-/-}$ mice as described (34) with modifications. Briefly, the inferior vena cava was cannulated, and the liver was first perfused *in situ* with an oxygenated Krebs-Ringer buffer (115 mM NaCl, 5.9 mM KCl, 25 mM $NaHCO_3$, 10 mM glucose, 20 mM Hepes, pH 7.4) with 0.1 mM EGTA at 37 °C followed by perfusion with oxygenated Krebs-Ringer buffer containing 0.25 mM $CaCl_2$ and 20 μg/ml Liberase Blendzyme 3 (Roche Applied Science). Liver was removed and then gently minced in ice-cold Krebs-Ringer buffer. Liver cell suspension was then filtered with Falcon cell strainers (BD Biosciences) and washed three times by centrifugation at 50 × *g* for 2 min at 4 °C. Cell viability was determined by trypan blue exclusion. Cells were cultured in DMEM (with 10% FBS and 1× penicillin/streptomycin) at 37 °C with 5% CO_2.

RESULTS

TIP30 Forms a Complex with Rab5a, Endo B1, and ACSL4—To identify cytosolic proteins that interact with TIP30, we stably expressed TIP30 protein with an HA tag fused to its C-terminal end (TIP30-HA) in human hepatocellular carcinoma cells (PLC/PRF/5). Co-immunoprecipitation assays were performed using whole cell extracts generated from cells expressing TIP30-HA or control vector. Mass spectrometric analysis identified Rab5a, ACSL4, and EndoB1 (also known as Bif-1) in the immunoprecipitates. Association of these proteins with TIP30-HA was confirmed by immunoblot analysis using specific antibodies (Fig. 1*A*). The interactions were further confirmed by reciprocal immunoprecipitation. When Rab5a, Endo B1, or ACSL4 were HA-tagged, each could be specifically co-immunoprecipitated with endogenous TIP30 and the other three endogenous proteins (Fig. 1*B*). Although Endo B1 failed to be immunoprecipitated with ACSL4-HA, possibly due to the interference of HA at its C terminus, endogenous ACSL4 was detected in Endo B1-HA immunoprecipitates. Notably, Rab5a was co-immunoprecipitated with these proteins in the presence of 0.2 mM EDTA, implying that the interaction is independent of its nucleotide binding status. We next used bimolecular fluorescence complementation analysis (31) to visualize the association of TIP30 with these proteins in living cells. We observed that co-expression of TIP30-VC155 with VN173-Rab5a, ACSL4-VN173, or Endo B1-VN173 in cells reconstituted fluorescence, whereas co-expression of TIP30-VC155 and control VN173 did not (Fig. 1*C*), indicating that TIP30 directly or indirectly interacts with these proteins in living cells.

To determine whether endogenous TIP30 associates with endogenous ACSL4 and EndoB1, we did glycerol gradient sedimentation and observed that these proteins co-sedimented at a position between the 150- and 443-kDa marker proteins in a 15–35% glycerol gradient (Fig. 2*A*). The majority of TIP30 and part of Endo B1 appeared in fractions containing proteins smaller than 66 kDa, suggesting that these two proteins may exist mainly as a heterodimer or as separated homodimers. An *in vitro* binding assay showed that bacterially expressed recom-

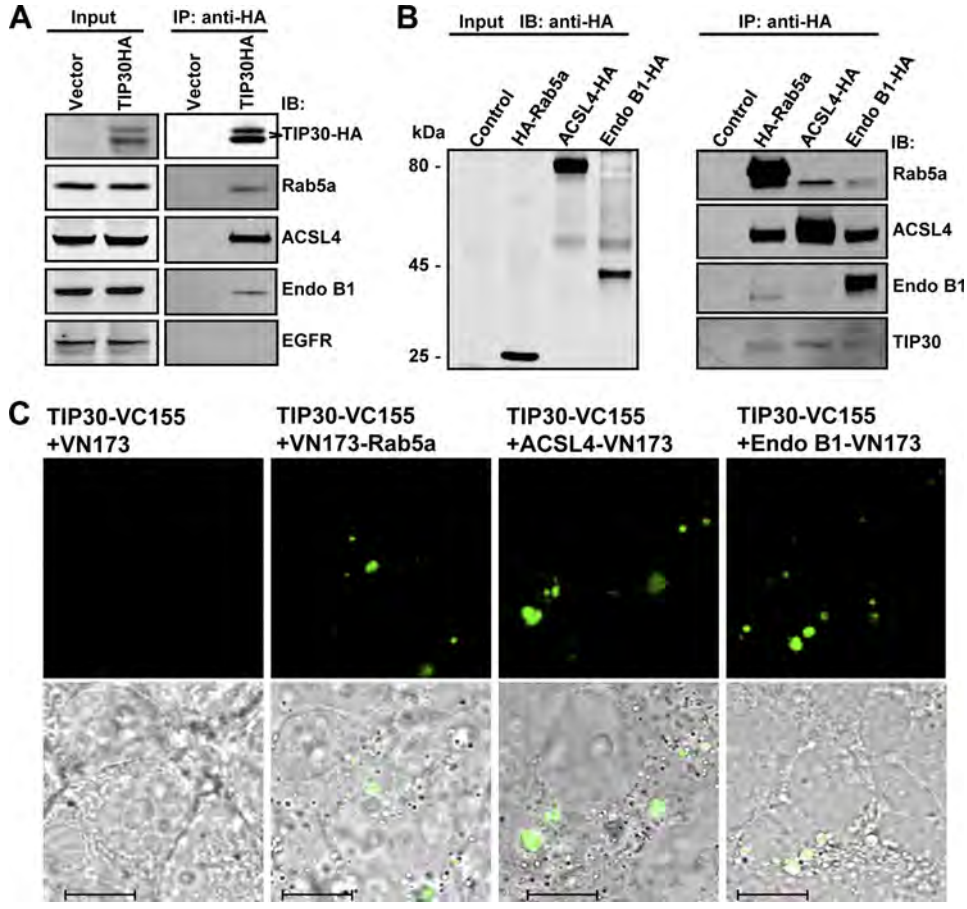

FIGURE 1. **TIP30 interacts with Rab5a, ACSL4, and Endo B1.** *A*, immunoblot confirmed the association of Rab5a, ACSL4, and Endo B1 with TIP30. The immunoprecipitates were resolved on SDS-PAGE and analyzed by immunoblotting (*IB*) with the indicated antibodies. The two polypeptides that reacted with anti-HA antibodies might result from posttranslational modifications on TIP30. *Input* was 10% (equals 70 μg of protein) of the volume of lysates used in the immunoprecipitation (*IP*) assays. The EGFR blot serves as a negative control. *B*, reciprocal co-immunoprecipitation. Whole cell extracts made from cells expressing HA-Rab5a, ACSL4-HA, Endo B1-HA, or empty vector were subjected to co-immunoprecipitation with α-HA-agarose beads. The immunoprecipitates were subjected to immunoblot analysis with the indicated antibodies. *Input* was 10% of the volume of lysates used in the immunoprecipitation assays. *C*, bimolecular fluorescence complementation analysis was performed on 293T cells by co-expressing TIP30-VC155 with VN173, VN173-Rab5a, ACSL4-VN173, or Endo B1-VN173. *Green* indicates fluorescent signal from Venus, a GFP variant. *Bottom panels* show overlays of differential interference contrast and representative confocal microscope images. *Scale bars*, 10 μm.

binant ACSL4 and Endo B1 were able to directly bind purified baculovirus-expressed recombinant TIP30 (Fig. 2*B*). These results indicate that TIP30, ACSL4, and Endo B1 may form a protein complex to interact with Rab5a.

Rab5a colocalizes with EGFR in endosomes in response to EGF (35, 36). To test whether TIP30 is also targeted to endosomes, we co-expressed TIP30-CFP and EGFR-DsRed fusion proteins and examined their localization in HepG2 cells lacking detectable endogenous TIP30 and EGFR. Confocal microscopy analysis showed that TIP30-CFP partially colocalized with EGF and EGFR-DsRed in endosomes 10 min after cells were treated with Alexa-647-conjugated EGF (Alexa^{647}-EGF; Fig. 2*C*), suggesting that TIP30 was also targeted to endosomes. Consistently, immunostaining of endogenous TIP30 and EGFR revealed that TIP30 was partially localized to EGF-EGFR-positive endosomes (Fig. 2*D*). Taken together, our protein-protein interaction and colocalization studies suggest that TIP30, ACSL4, and Endo B1 form a protein complex and may function together with Rab5a on the endocytic pathway.

Inhibition of TIP30, ACSL4, or Endo B1 Leads to Delayed EGFR Degradation and Sustained EGFR Signaling—Knockdown of Rab5a expression in HeLa cells retards EGFR transport from early endosomes to late endosomes and delays the degradation of EGFR (19). The interaction of TIP30, ACSL4, and Endo B1 with Rab5a raises the possibility that these proteins may also function in endocytic pathways. We performed EGFR internalization analysis to investigate whether the inhibition of TIP30, ACSL4, or Endo B1 affects the endocytic down-regulation of EGFR. Instead of continuous incubation with EGF, serum-starved cells were first incubated with EGF on ice to allow for binding of ligand to receptors, and then they were washed to remove unbound EGF before being moved to 37 °C for internalization. Nascent protein synthesis was blocked by cycloheximide in the culture medium. This approach eliminates the interference from continuous ligand entrance and new receptor synthesis, thus enabling us to monitor both the traffic and the fate of EGF-EGFR complexes. We found that knockdown of TIP30, Rab5a, ACSL4, or Endo B1 in PLC/PRF/5 cells (Fig. 3, *A*–*D*) resulted in a slower reduction of total EGFR

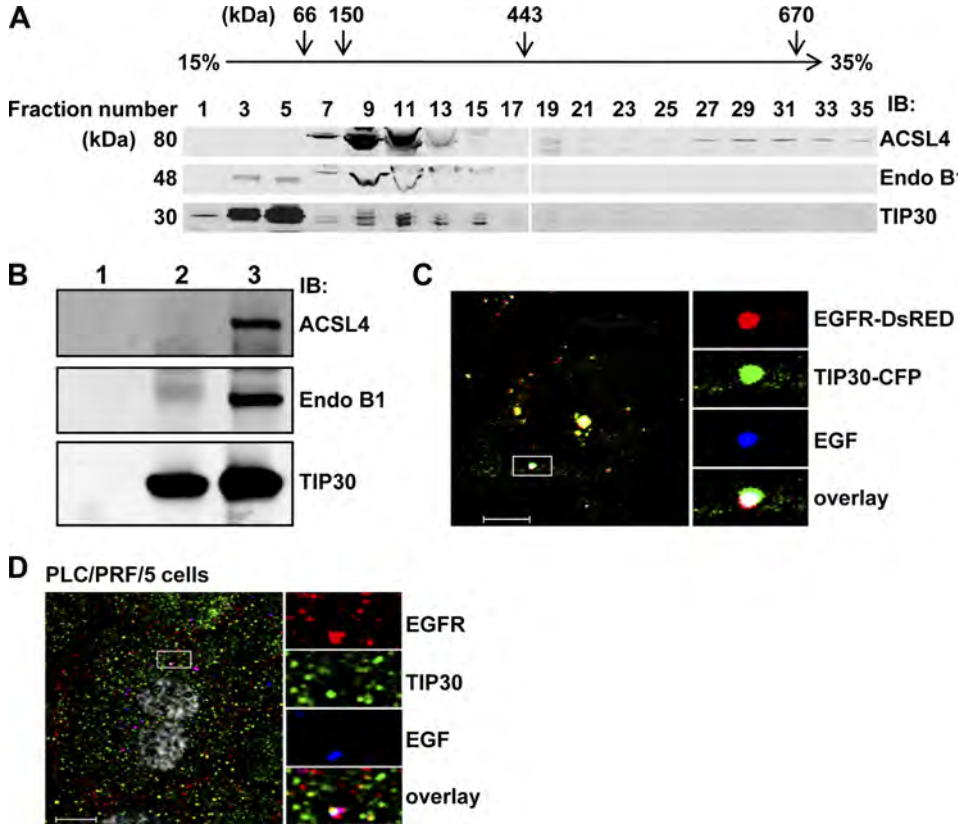

FIGURE 2. **Endogenous TIP30, ACSL4, and Endo B1 associate together.** *A*, endogenous TIP30, ACSL4, and Endo B1 were co-sedimented in a glycerol gradient. Whole cell extracts of PLC/PRF/5 cells and protein markers were loaded on the top of linear 10–35% (v/v) glycerol gradients (10 ml) formed from the bottom of 12-ml Beckman tubes. The buffer throughout the gradients was 20 mM Hepes-KOH (pH 7.0), 100 mM KCl, 1 mM dithiothreitol. The gradients were centrifuged at 200,000 × *g* in a SW41 Ti rotor (Beckman) at 4 °C for 20 h. After centrifugation, fractions were collected, concentrated, and subjected to immunoblot (*IB*) analysis. Albumin (66 kDa), alcohol dehydrogenase (150 kDa) apoferritin (443 kDa), thyroglobulin (670 kDa), and blue dextran (2,000 kDa) were run in parallel as molecular mass indicators. *B*, direct interaction of TIP30, ACSL4, and Endo B1. GST-ACSL4 and His-Endo B1 (*lane 1*), FLAG-TIP30 (*lane 2*), or GST-ACSL4, His-Endo B1, and FLAG-TIP30 (*lane 3*) were subjected to anti-FLAG M2 immunoprecipitation. 100 ng of each protein was used. Aliquots of precipitates were resolved on SDS-PAGE and analyzed by immunoblot with the indicated antibodies. Purified FLAG-TIP30 was described previously (30). Bacterially expressed GST-ACSL4 was purchased from Abnova. His-Endo B1 was expressed in BL21. *C*, TIP30 and EGF-EGFR are colocalized in endosomes in response to EGF treatment. HepG2 cells co-expressing TIP30-CFP (*green*) and EGFR-DsRed (*red*) were treated with 10 ng/ml Alexa^{647}-EGF (*blue*) for 10 min and then analyzed by confocal microscopy. A typical image is shown. The *boxed areas* are magnified. *Scale bar*, 10 μm. *D*, TIP30 is localized to EGFR-positive endosomes. PLC/PRF/5 cells were immunostained with antibodies for EGFR (*red*) and TIP30 (*green*) after 30 min of Alexa^{488}-EGF (*blue*) internalization. The *boxed areas* are magnified. *Scale bar*, 10 μm.

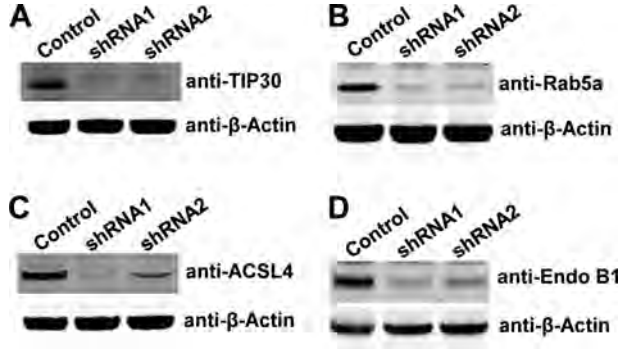

FIGURE 3. **Knockdown of TIP30, Rab5a, ACSL4, and Endo B1 in PLC/PRF/5 cells.** *A–D*, immunoblot analyses show knockdown of TIP30, Rab5a, ACSL4, or Endo B1 in PLC/PRF/5 cell. Whole cell lysates were made from cells expressing a scramble shRNA or shRNA against TIP30 (*A*), Rab5a (*B*), ACSL4 (*C*), or Endo B1 (*D*). Two shRNAs against each gene were used, and equal amounts of protein were loaded per lane.

protein levels (Fig. 4, *A–F*). To corroborate these findings, we further examined whether phosphorylation of EGFR at Tyr-845 (EGFR-pY845) and phosphorylation of AKT at Ser-473 (AKT-pS473), a downstream target of EGFR signaling, were affected. Remarkably, the levels of EGFR-pY845 and AKT-pS473 were sustained much longer in TIP30, ACSL4, Endo B1, or Rab5a knockdown cells than in control cells (Fig. 4, *A–F*). Of note, Akt phosphorylation was rapidly increased followed by a decline and then increased again after a 3-h internalization (Fig. 4, *A–D*). Although the exact mechanism to explain this phenomenon remains to be tested, one can envisage that it may reflect the autonomic balance of kinase and phosphatase activities for Akt in cells.

To assess the effect of TIP30 deletion on EGFR endocytic down-regulation in normal cells and to exclude off-target effects of shRNAs, we performed EGFR internalization analysis using primary hepatocytes isolated from wild type and Tip30 knock-out mouse littermates. Deletion of *Tip30* in primary hepatocytes delayed EGF-induced EGFR degradation (Fig. 4, *G* and *H*), and the phosphorylation of EGFR at Tyr-845 and Akt at Ser-473 was higher and sustained longer in *Tip30*$^{-/-}$ hepatocytes than in wild type hepatocytes. Together, these data provide strong evidence that TIP30, ACSL4, Endo B1, and Rab5a not only physically associate but also function together in promoting the endocytic down-regulation of EGFR protein level and signaling.

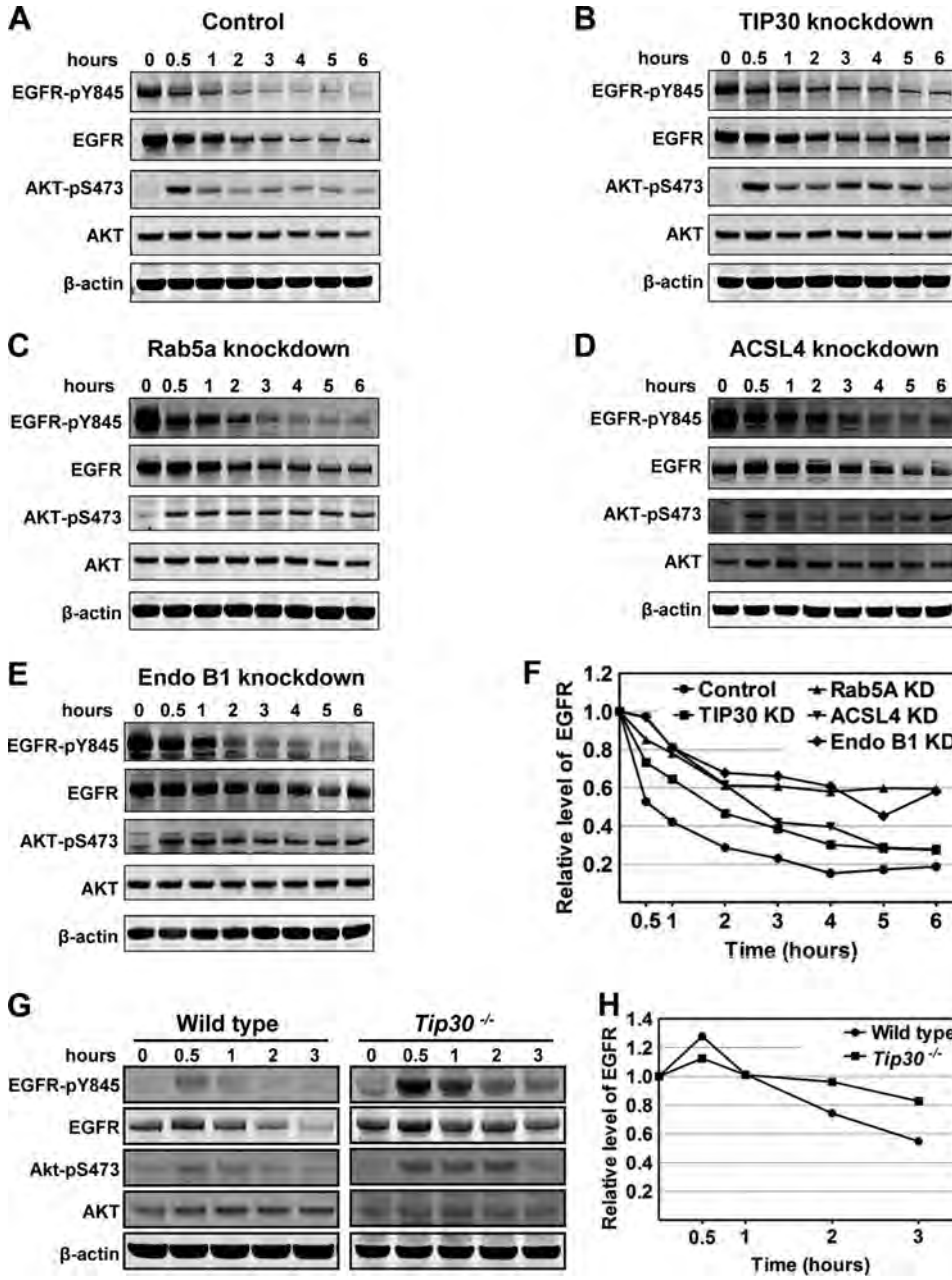

FIGURE 4. **TIP30, Rab5a, ACSL4, and Endo B1 promote the endocytic down-regulation of EGFR.** *A–E*, knockdown of TIP30, Rab5a, ACSL4, or Endo B1 results in delayed EGFR degradation and sustained EGFR signaling. Control PLC/PRF/5 cells (*A*), TIP30 (*B*), Rab5a (*C*), Endo B1 (*D*), and ACSL4 (*E*) knockdown cells were incubated with 100 ng/ml EGF after being serum-starved for 24 h and then were washed with cold PBS and incubated with cycloheximide at 37 °C. Cells were collected at various time points after EGF internalization and subjected to immunoblot analysis with the indicated antibodies. Results are typical and representative of experiments on cells from two different shRNAs. *F*, quantification of EGFR protein levels in *A–E* using Odyssey 2.1 software. *KD*, knockdown. *G*, deletion of *Tip30* in mouse primary hepatocytes leads to delayed EGFR degradation and sustained EGFR signaling. Primary hepatocytes were isolated from wild type and *Tip30*$^{-/-}$ mice. Endocytosis-induced EGFR degradation was analyzed as described in *A–E*. *H*, quantification of EGFR protein levels in *G* using Odyssey 2.1 software.

TIP30, ACSL4, Endo B1, and Rab5a Are Required for EGF-EGFR Endocytic Trafficking—An early study showed that EGF dissociates from EGFR at later stages of endocytosis (37). Moreover, it has been suggested that EGFR is inactivated before being transferred to lysosomes and degraded (6, 13–15). To test whether depletion of TIP30, ACSL4, Endo B1, or Rab5a affects EGF dissociation from EGFR, we simultaneously tracked Alexa^{488}-EGF and EGFR at different time points after internalization using confocal microscopy. We found that fluorescent EGF partially colocalizes with EGFR and Rab5a in control cells after 15 and 30 min of internalization (supplemental Fig. S1*A*). Interestingly, Alexa^{488}-EGF exited in membrane-bound vesicles from EGFR-positive endosomes in control cells after 60 min of internalization (Fig. 5*A*). In contrast, the majority of EGF remained colocalized with EGFR in TIP30 or Rab5a knockdown cells (control cells, 7 ± 3%; TIP30 knockdown cells, 36 ± 4%; Rab5a knockdown cells, 46 ± 5%; $n = 60$, $p < 0.01$ *versus* control cells; Fig. 5, *A* and *C*). The EGF vesicles were devoid of

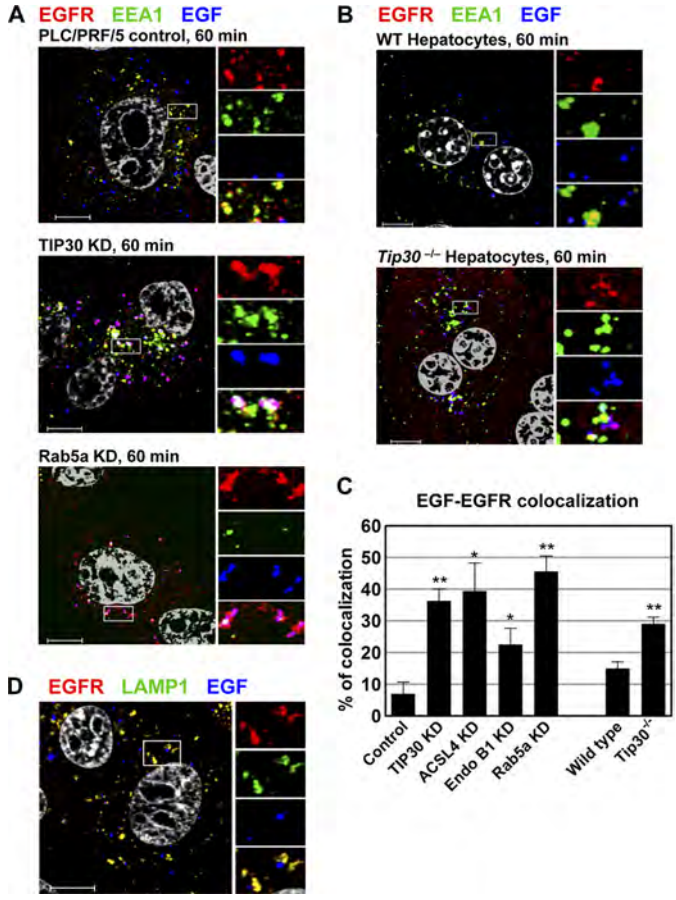

FIGURE 5. **TIP30 and Rab5a depletion delays the exit of EGF from early endosomes.** *A*, knockdown (*KD*) of TIP30 or Rab5a causes delayed exit of Alexa^{488}-EGF from early endosomes. Cells expressing control shRNA or shRNA against TIP30 or Rab5a were subjected to EGFR internalization analysis. After internalization of Alexa^{488}-EGF (*blue*) for 60 min, cells were fixed and double-immunostained for EGFR (*red*) and EEA1 (*green*). Nucleus was stained by DAPI (*gray*). *Magenta* results from overlap between *red* and *blue*. Results are representative of at least three independent experiments on cells expressing two different shRNAs. The *boxed areas* are magnified. *Scale bars*, 10 μm. *B*, deletion of *Tip30* in mouse primary hepatocytes leads to trapping of EGF in early endosomes. Wild type and *Tip30*$^{-/-}$ primary hepatocytes were subjected to the same EGFR internalization analysis as described in *A*. The *boxed areas* are magnified. *Scale bars*, 10 μm. *C*, quantitative analysis of EGF-EGFR colocalization 60 min after EGF internalization. 60 cells represented by Fig. 5, *A* and *B*, and Fig. 6*A* in each group were analyzed using MBF_ImageJ. Pearson's colocalization coefficients were calculated and converted to percentages. Data represent means ± S.E. *, $p < 0.05$, **, $p < 0.01$, relative to control or wild type cells; Student's *t* test. *D*, EGF exits endosomes in LAMP1-negative vesicles. Cells were stained for EGFR and LAMP1 60 min after EGF internalization. *Scale bar*, 10 μm.

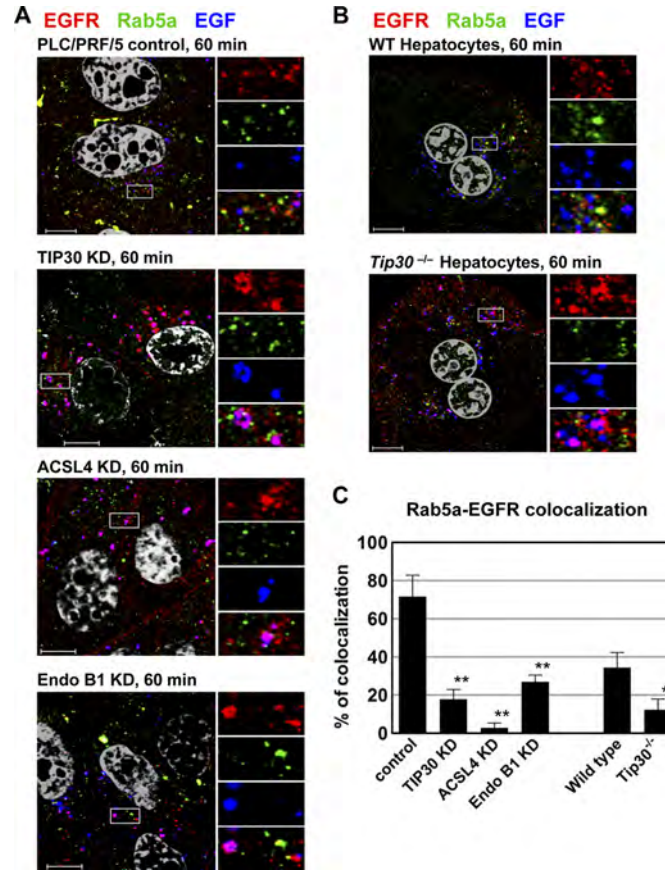

FIGURE 6. **TIP30, ACSL4, and Endo B1 are required for the localization of Rab5a to early endosomes.** *A*, knockdown (*KD*) of TIP30, ACSL4, or Endo B1 inhibits the localization of Rab5a to early endosomes. Control cells and TIP30, ACSL4, or Endo B1 knockdown cells were subjected to EGFR internalization analysis. 60 min after internalization of Alexa^{488}-EGF (*blue*), cells were immunostained for EGFR (*red*) and Rab5a (*green*). Nucleus is stained by DAPI (*gray*). Results are typical and representative of three experiments on cells from two different shRNAs. The *boxed areas* are magnified. *Scale bars*, 10 μm. *B*, *Tip30* deletion in primary hepatocytes inhibits the recruitment of Rab5a to early endosomes. Primary hepatocytes were stained for EGFR (*red*) and Rab5a (*green*) after 60 min of EGF (*blue*) internalization. The *boxed areas* are magnified. *Scale bars*, 10 μm. *C*, quantitative analysis of Rab5a-EGFR colocalization after 60 min of EGF internalization was performed as described in the legend for Fig. 2. Data represent means ± S.E. *, $p < 0.05$, **, $p < 0.01$, relative to control or wild type cells; Student's *t* test.

early endosomal markers EEA1 and Rab5a, as well as late endosomal and lysosomal marker LAMP1 (Fig. 5*D*), indicating that they are neither early/late endosomes nor lysosomes.

We next performed EGFR internalization analysis using wild type and *Tip30*$^{-/-}$ primary hepatocytes. Consistently, *Tip30* deletion increased the colocalization of EGF and EGFR nearly 2-fold (wild type primary hepatocytes, 15 ± 2%; *Tip30*$^{-/-}$ primary hepatocytes, 29 ± 2%; $n = 20$, $p < 0.01$; Fig. 5, *B* and *C*).

Likewise, knockdown of ACSL4 or Endo B1 expression also increased the colocalization of EGF and EGFR (ACSL4 knockdown cells, 40 ± 8%; Endo B1 knockdown cells, 23 ± 5%; $n = 60$, $p < 0.05$ *versus* control cells; Figs. 5*C* and 6*A*). The majority of EGF colocalized with EGFR even after 120 min of internalization in knockdown and *Tip30*$^{-/-}$ cells (supplemental Fig. S1, *A–C*). Taken together, these results suggest that TIP30, ACSL4, Endo B1, and Rab5a are involved in promoting EGF dissociation from EGFR during endocytic trafficking.

TIP30, ACSL4, and Endo B1 Promote the Loading of Rab5a on Early Endosomes—Endocytic vesicles gain Rab5a dynamically mostly by membrane fusion with Rab5-positive endosomes in the course of cargo transport (38). This is further supported by the observation that Rab5a is mainly localized on numerous vesicles in the perinuclear region of cells under steady state condition and is rapidly recruited to early endocytic vesicles at the cell periphery in response to EGF (35, 36). The similar effects of TIP30 and Rab5a knockdown on EGFR endocytosis prompted us to test whether TIP30 is involved in the loading of Rab5a on early endosomes. In control cells, Rab5a appeared in EGFR-positive endosomes from which EGF had exited after 60 min of EGF internalization (Fig. 6*A*). By contrast, the colocalization of Rab5a and EGFR was significantly decreased in TIP30

knockdown cells (control cells, 72 ± 11%; TIP30 knockdown cells, 18 ± 5%; $n = 60$, $p < 0.01$; Fig. 6, *A* and *C*) and *Tip30*$^{-/-}$ primary hepatocytes (wild type hepatocytes, 34 ± 8%; *Tip30*$^{-/-}$ hepatocytes, 12 ± 5%; $n = 20$, $p < 0.05$; Fig. 6, *B* and *C*). Similar results were obtained with ACSL4 or Endo B1 knockdown cells (ACSL4 knockdown cells, 3 ± 2%; Endo B1 knockdown cells, 27 ± 4%; $n = 60$, $p < 0.01$ *versus* control cells; Fig. 6, *A* and *C*). Interestingly, there were a few Rab5a-positive early endosomes in Endo B1 knockdown cells, which was probably the result of incomplete knockdown. However, these Rab5a-positive endosomes appeared different from those in control cells. They did not release EGF even after 120 min of internalization (supplemental Fig. S1*B*), indicating that Endo B1 has an additional function after Rab5a recruitment. This provides a possible explanation for the observation that Endo B1 knockdown cells have less EGF-EGFR colocalization and more Rab5a-EGFR overlap but have longer lasting EGFR stability when compared with TIP30 and ACSL4 knockdown cells (Figs. 4, *A–F*, 5*C*, and 6*C*). Together, these results indicate that TIP30, ACSL4, and Endo B1 promote efficient Rab5a localization to early endosomes.

Rab5a Vesicles Transport V-ATPases to Early Endosomes—Intriguingly, we noted that Rab5a appeared in vesicles when it was not localized to EGFR-positive endosomes (Fig. 6, *A* and *B*). To further characterize those EGFR-negative Rab5a vesicles, we co-stained EEA1 and Rab5a in wild type mouse primary hepatocytes 30 min after EGF internalization. The EGFR-negative Rab5a vesicles were also negative for EEA1 and TfR (Fig. 7, *A* and *B*), suggesting that they are neither plasma membrane-derived endocytic vesicles nor recycling endosomes, but likely transporting vesicles that originate from the trans-Golgi network.

Dissociation of ligand-receptor complexes inside endosomes is caused by the low luminal pH created by V-ATPases. Our previously presented results showed that lack of Rab5a in early endosomes was concomitant with delayed EGF-EGFR dissociation induced by loss of TIP30 or its interacting proteins. Rab5a did not coexist with EGF in EGFR-positive endosomes, suggesting that Rab5a vesicles may deliver V-ATPases to early endosomes to drive EGF-EGFR dissociation. To test this hypothesis, we examined the intracellular localization of V-ATPases by staining for the regulatory subunit H (ATP6V1H). ATP6V1H-positive staining was observed in Rab5a vesicles lacking EGF and EGFR in TIP30 knockdown cells (Fig. 7*C*). Significant reduction of ATP6V1H localization to EGFR-positive endosomes was observed in TIP30, Rab5a, ACSL4, or Endo B1 knockdown cells (control cells, 46 ± 7%; TIP30 knockdown cells, 25 ± 4%; Rab5a knockdown cells, 19 ± 1%; ACSL4 knockdown cells, 19 ± 2%; Endo B1 knockdown cells, 21 ± 1%; $n = 60$, $p < 0.05$ *versus* control cells; Fig. 8, *A* and *C*) and in *Tip30*$^{-/-}$ primary hepatocytes (wild type hepatocytes, 61 ± 4%; *Tip30*$^{-/-}$ hepatocytes, 23 ± 6%; $n = 20$, $p < 0.01$; Fig. 8, *B* and *C*). Moreover, in live PLC/PRF/5 cells co-expressing EYFP-Rab5a and ATP6V1H-DsRed, EGF-positive endosomes fused with Rab5a-ATP6V1H vesicles at 11 min after EGF internalization and released Alexa^{647}-EGF 3 min after the merge (Fig. 8*D*).

To determine whether mislocalization of V-ATPases affects endosomal acidification, we monitored endosomal pH after

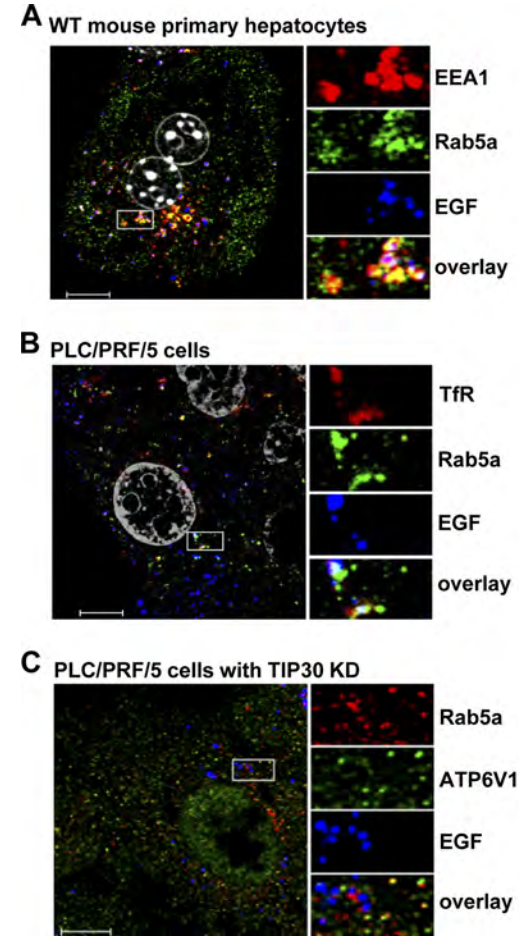

FIGURE 7. **Rab5a vesicles carry V-ATPases and are devoid of EEA1 and TfR.** *A*, EGFR-negative Rab5a vesicles are not early endosomes. Wild type mouse primary hepatocytes were immunostained for EEA1 (*red*) and Rab5a (*green*) after 30 min of EGF (*blue*) internalization. *Scale bar*, 10 μm. *B*, TfR partially colocalizes with Rab5a. PLC/PRF/5 cells were immunostained for TfR (*red*) and Rab5a (*green*) after 10 min of EGF (*blue*) internalization. *Scale bar*, 10 μm. *C*, V-ATPases colocalize with Rab5a in transport vesicles. TIP30 knockdown (*KD*) cells were immunostained for V-ATPase (*red*) and Rab5a (*green*) after 30 min of EGF (*blue*) internalization. *Scale bar*, 10 μm.

pHrodo-EGF:Alexa^{647}-EGF (7:3) internalization (39). Indeed, TIP30 knockdown resulted in significantly less acidic endosomes (supplemental Fig. S2, *A* and *B*). Taken together, these data indicate that Rab5a contribute to endosomal acidification by transporting V-ATPases to endocytic vesicles and that TIP30, ACSL4, and Endo B1 are required for efficient transport.

DISCUSSION

The present study describes a novel protein complex consisting of TIP30, ACSL4, and Endo B1 that interacts with Rab5a and regulates EGFR endocytic trafficking. Down-regulation of these proteins results in trapping of EGF-EGFR complexes in early endosomes, which enabled us to further dissect the EGFR endocytic pathway. We uncovered two consecutive events following EGF-EGFR entrance into the early endosomes because these two events became obviously detectable when the function of the TIP30 complex was inhibited. First, newly formed endosomes are devoid of V-ATPases and Rab5a. V-ATPases are delivered to early endosomes by the Rab5a vesicles. Second, localization of Rab5a and V-ATPases to the early endosomes

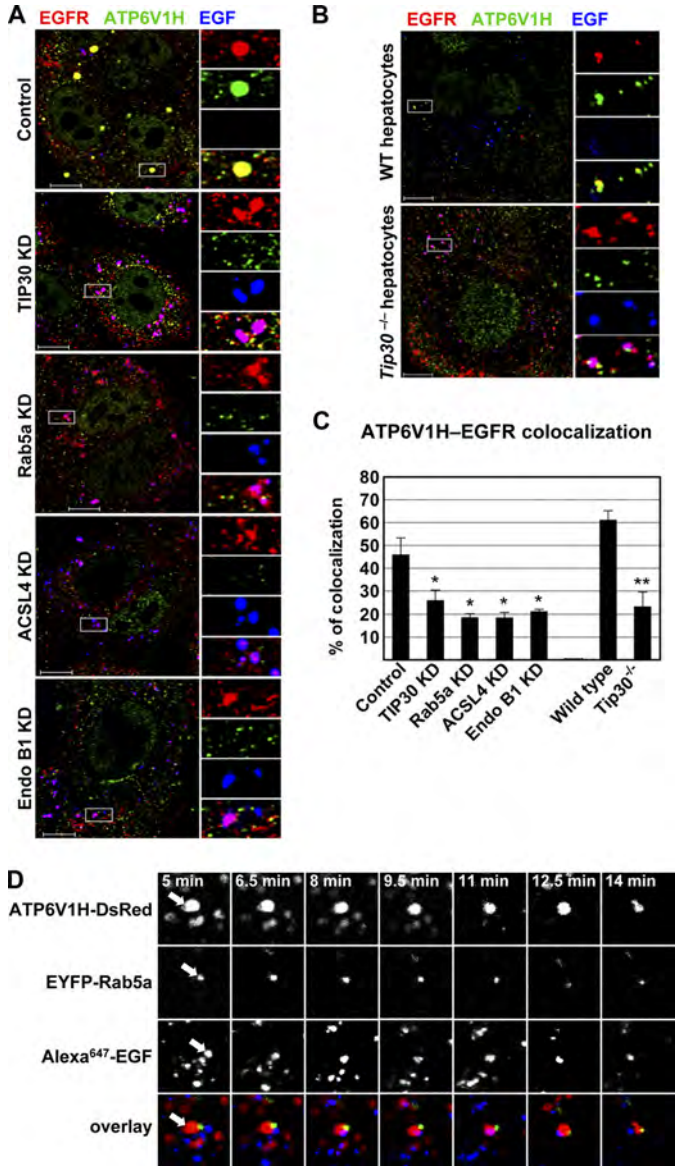

FIGURE 8. **Rab5a vesicles transport V-ATPases to early endosomes.** *A*, depletion of TIP30, ACSL4, or Endo B1 inhibits the loading of V-ATPases on endocytic vesicles. Cells were immunostained for EGFR (*red*) and ATP6V1H (*green*) after 60 min of EGF (*blue*) internalization. Results are typical and representative of three experiments on cells from two different shRNAs. The *boxed areas* are magnified. *Scale bars*, 10 μm. *KD*, knockdown. *B*, deletion of *Tip30* in mouse primary hepatocytes results in mislocalization of V-ATPases. Immunostaining was performed as described in *A*. *Scale bars*, 10 μm. *C*, colocalization between V-ATPases and EGFR was analyzed using MBF_ImageJ. Pearson's colocalization coefficients were calculated and converted to percentages. *, $p < 0.05$, **, $p < 0.01$, relative to control or wild type cells; Student's *t* test. *D*, Alexa^{647}-EGF is released after EGF endocytic vesicles merge with Rab5a vesicles. Live cells expressing ATP6V1H-DsRed (*red*) and EYFP-Rab5a (*green*) were imaged by confocal microscopy at the indicated times after Alexa^{647}-EGF internalization, and images of a single focal plane were acquired. A typical EGF endocytic vesicle movement was shown. *Arrows* point toward the two vesicles undergoing merge and EGF release.

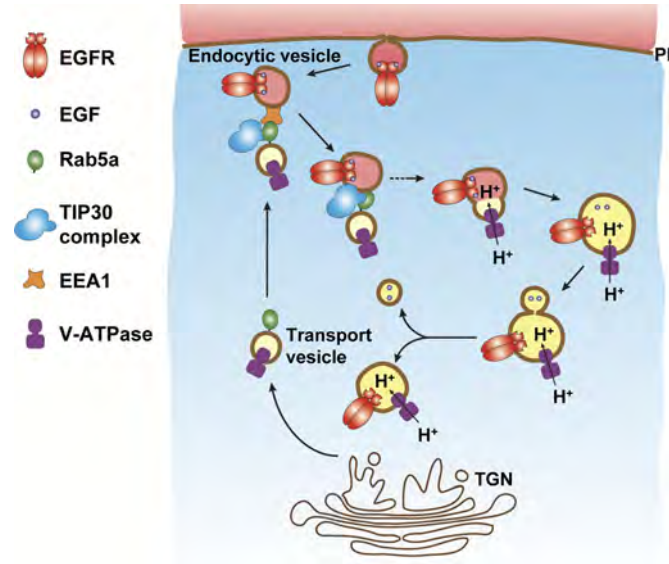

FIGURE 9. **Proposed model shows the regulation of Rab5a vesicle-mediated transport of V-ATPases to endocytic vesicles in EGFR endocytic trafficking.** Rab5a directs the trans-Golgi network (*TGN*)-originated vesicles carrying V-ATPases toward the cell peripheral and recognizes endocytic vesicles presumably by interacting with EEA1 (48, 49). Then, the TIP30 complex facilitates the fusion of the two vesicles to help load V-ATPases, which can start pump H^+ into endosomes. EGF dissociates from EGFR due to lower pH created by V-ATPases and might exit endosomes in membrane-bound vesicles.

results in the termination of EGFR endosomal signaling. Clearly, inhibiting the function of the TIP30 complex can block the transport of V-ATPases to endosomes, leading to EGF-bound EGFR detention in endosomes, delayed EGFR endocytic degradation, and sustained activation of Akt. Given that EGF-bound EGFR enclosed in endosomes is sufficient to activate downstream molecules and to induce cell survival (40), our results indicate that enhanced EGFR signaling by inhibition of TIP30, ACSL4 and EndoB1 may contribute to the initiation and progression of cancers. Indeed, we have recently reported that *Tip30* deletion in MMTV-Neu mice leads to enhanced EGFR signaling and development of estrogen receptor-positive and progesterone receptor-negative mammary tumors (41). Thus, the regulation of EGFR-mediated endocytosis by the TIP30 complex may serve as a general mechanism to govern EGFR signaling and suppress tumorigenesis.

Endo B1 belongs to a family of proteins containing N-terminal Bin-Amphiphysin-Rvs (BAR) domains and is involved in apoptosis, autophagy, mitochondrial fission, and endocytic trafficking (42). The role of Endo B1 in EGFR endocytosis is consistent with a previous report that Endo B1 colocalizes with EEA1 in the early endosome of neural cells in response to nerve growth factor (43). It is noteworthy that Endo B1 knock-out mice exhibited spontaneous development of lymphomas, hepatocellular carcinomas, and mammary tumors (44). These phenotypes resemble the phenotypes of *Tip30* knock-out mice (25).[3] Thus, we speculate that TIP30 and Endo B1 may act in concert to suppress tumorigenesis, at least in part, through the regulation of EGFR-mediated endocytosis. With the identification of the interaction between TIP30 and Endo B1, this hypothesis can now be addressed.

Rab family proteins have been well known to be essential for vesicle targeting (45). Rab5a is recruited to the early endosomes, where it promotes the endocytic down-regulation of EGFR and transition from endosome to lysosome. Before entering endosomes, Rab5a was found in smaller vesicles localized in the perinuclear region (36, 46). These Rab5 vesicles are redistributed to the cell periphery region, where they colocalize with

[3] A. Li, J. Pecha, and H. Xiao, unpublished data.

EGFR in early endosomes in response to EGF treatment (17, 35, 36). Notably, newly formed endocytic vesicles containing transferrin, LDL, EGF, or influenza virus were devoid of Rab5a and acquired Rab5a through merging with Rab5a vesicles (35). Our data support these observations and clearly show that besides the EEA1- and EGFR-positive endocytic vesicles, there is a population of Rab5a-positive vesicles that are negative for EEA1 and EGFR but positive for V-ATPases. Given that intracellular trafficking of EGF-EGFR or entry of dengue and West Nile viruses into HeLa cells by clathrin-mediated endocytosis requires vacuolar acidic pH and Rab5a (47), we propose that Rab5a is involved in post-trans-Golgi network transport of integral membrane proteins and helps create acidic endosomal pH by targeting V-ATPases to endosomes, thereby providing the driving force for EGFR endocytic trafficking and viral entry into host cells (Fig. 9).

We were surprised to see that Alexa^{488}-EGF vesicles pinched off from endosomes shortly after internalization. This event was observed in both human liver cancer cells and mouse primary hepatocytes. The Alexa^{488}-EGF vesicles are previously uncharacterized vesicles that are devoid of early endosomal, recycling endosomal, and lysosomal markers, implying that EGF might exit endosomes after the dissociation with EGFR. Nevertheless, it will be important to determine whether Alexa^{488}-EGF in these vesicles is intact or degraded.

Acknowledgments—We thank Dr. Stephen Prescott for generously sharing anti-ACSL4 antibody, Dr. Chang-deng Hu for generously sharing bimolecular fluorescence complementation plasmids, and Drs. Richard Schlegel and Frank Suprynowicz for generously sharing pHrodo-EGF. We are grateful to Drs. Sandra Haslam, Hans Cheng, Jerry Dodgson, Karen Friderici, and Richard Schwartz for critical reading of the manuscript.

REFERENCES

1. Mellman, I. (1996) *Annu. Rev. Cell Dev. Biol.* **12,** 575–625
2. Maxfield, F. R., and McGraw, T. E. (2004) *Nat. Rev. Mol. Cell Biol.* **5,** 121–132
3. Miaczynska, M., Pelkmans, L., and Zerial, M. (2004) *Curr. Opin. Cell Biol.* **16,** 400–406
4. Polo, S., and Di Fiore, P. P. (2006) *Cell* **124,** 897–900
5. Sorkin, A., and von Zastrow, M. (2009) *Nat. Rev. Mol. Cell Biol.* **10,** 609–622
6. Murphy, J. E., Padilla, B. E., Hasdemir, B., Cottrell, G. S., and Bunnett, N. W. (2009) *Proc. Natl. Acad. Sci. U.S.A.* **106,** 17615–17622
7. Yamashiro, D. J., Tycko, B., Fluss, S. R., and Maxfield, F. R. (1984) *Cell* **37,** 789–800
8. Backer, J. M., Kahn, C. R., and White, M. F. (1990) *J. Biol. Chem.* **265,** 14828–14835
9. Nishi, T., and Forgac, M. (2002) *Nat. Rev. Mol. Cell Biol.* **3,** 94–103
10. Clague, M. J., Urbé, S., Aniento, F., and Gruenberg, J. (1994) *J. Biol. Chem.* **269,** 21–24
11. Carpenter, G., and Cohen, S. (1979) *Annu. Rev. Biochem.* **48,** 193–216
12. Carpenter, G., and Cohen, S. (1976) *J. Cell Biol.* **71,** 159–171
13. Authier, F., and Chauvet, G. (1999) *FEBS Lett.* **461,** 25–31
14. Burke, P., Schooler, K., and Wiley, H. S. (2001) *Mol. Biol. Cell* **12,** 1897–1910
15. Umebayashi, K., Stenmark, H., and Yoshimori, T. (2008) *Mol. Biol. Cell* **19,** 3454–3462
16. Gorvel, J. P., Chavrier, P., Zerial, M., and Gruenberg, J. (1991) *Cell* **64,** 915–925
17. Nielsen, E., Severin, F., Backer, J. M., Hyman, A. A., and Zerial, M. (1999) *Nat. Cell Biol.* **1,** 376–382
18. Rosenfeld, J. L., Moore, R. H., Zimmer, K. P., Alpizar-Foster, E., Dai, W., Zarka, M. N., and Knoll, B. J. (2001) *J. Cell Sci.* **114,** 4499–4508
19. Chen, P. I., Kong, C., Su, X., and Stahl, P. D. (2009) *J. Biol. Chem.* **284,** 30328–30338
20. Shtivelman, E. (1997) *Oncogene* **14,** 2167–2173
21. Xiao, H., Tao, Y., Greenblatt, J., and Roeder, R. G. (1998) *Proc. Natl. Acad. Sci. U.S.A.* **95,** 2146–2151
22. Jiang, C., Ito, M., Piening, V., Bruck, K., Roeder, R. G., and Xiao, H. (2004) *J. Biol. Chem.* **279,** 27781–27789
23. Zhao, J., Lu, B., Xu, H., Tong, X., Wu, G., Zhang, X., Liang, A., Cong, W., Dai, J., Wang, H., Wu, M., and Guo, Y. (2008) *Hepatology* **48,** 265–275
24. King, F. W., and Shtivelman, E. (2004) *Mol. Cell. Biol.* **24,** 7091–7101
25. Ito, M., Jiang, C., Krumm, K., Zhang, X., Pecha, J., Zhao, J., Guo, Y., Roeder, R. G., and Xiao, H. (2003) *Cancer Res.* **63,** 8763–8767
26. Lee, L. W., Zhang, D. H., Lee, K. T., Koay, E. S., and Hewitt, R. E. (2004) *Ann. Acad. Med. Singapore* **33,** S30–32
27. Tong, X., Li, K., Luo, Z., Lu, B., Liu, X., Wang, T., Pang, M., Liang, B., Tan, M., Wu, M., Zhao, J., and Guo, Y. (2009) *Am. J. Pathol.* **174,** 1931–1939
28. Zhao, J., Ni, H., Ma, Y., Dong, L., Dai, J., Zhao, F., Yan, X., Lu, B., Xu, H., and Guo, Y. (2007) *Hum. Pathol.* **38,** 293–298
29. Yu, J., Vodyanik, M. A., Smuga-Otto, K., Antosiewicz-Bourget, J., Frane, J. L., Tian, S., Nie, J., Jonsdottir, G. A., Ruotti, V., Stewart, R., Slukvin, I. I., and Thomson, J. A. (2007) *Science* **318,** 1917–1920
30. Xiao, H., Palhan, V., Yang, Y., and Roeder, R. G. (2000) *EMBO J.* **19,** 956–963
31. Hu, C. D., Grinberg, A. V., and Kerppola, T. K. (2005) in *Current Protocols in Protein Science* (Coligan, J. E., Dunn, B. M., Speicher, D. W., and Wingfield, P. T., eds) pp. 19.10.1–19.10.2, John Wiley & Sons, Inc., Somerset, NJ
32. Stringer, K. F., Ingles, C. J., and Greenblatt, J. (1990) *Nature* **345,** 783–786
33. Chiang, C. M., and Roeder, R. G. (1995) *Science* **267,** 531–536
34. Seglen, P. O. (1972) *Exp. Cell Res.* **74,** 450–454
35. Lakadamyali, M., Rust, M. J., and Zhuang, X. (2006) *Cell* **124,** 997–1009
36. Leonard, D., Hayakawa, A., Lawe, D., Lambright, D., Bellve, K. D., Standley, C., Lifshitz, L. M., Fogarty, K. E., and Corvera, S. (2008) *J. Cell Sci.* **121,** 3445–3458
37. Carter, R. E., and Sorkin, A. (1998) *J. Biol. Chem.* **273,** 35000–35007
38. Rink, J., Ghigo, E., Kalaidzidis, Y., and Zerial, M. (2005) *Cell* **122,** 735–749
39. Suprynowicz, F. A., Krawczyk, E., Hebert, J. D., Sudarshan, S. R., Simic, V., Kamonjoh, C. M., and Schlegel, R. (2010) *J. Virol.* **84,** 10619–10629
40. Wang, Y., Pennock, S., Chen, X., and Wang, Z. (2002) *Mol. Cell. Biol.* **22,** 7279–7290
41. Zhang, C., Mori, M., Gao, S., Li, A., Hoshino, I., Aupperlee, M. D., Haslam, S. Z., and Xiao, H. (2010) *Cancer Res.* **70,** 10224–10233
42. Takahashi, Y., Meyerkord, C. L., and Wang, H. G. (2009) *Cell Death Differ.* **16,** 947–955
43. Wan, J., Cheung, A. Y., Fu, W. Y., Wu, C., Zhang, M., Mobley, W. C., Cheung, Z. H., and Ip, N. Y. (2008) *J. Neurosci.* **28,** 9002–9012
44. Takahashi, Y., Meyerkord, C. L., and Wang, H. G. (2008) *Autophagy* **4,** 121–124
45. Pfeffer, S. R. (2001) *Trends Cell Biol.* **11,** 487–491
46. Bucci, C., Parton, R. G., Mather, I. H., Stunnenberg, H., Simons, K., Hoflack, B., and Zerial, M. (1992) *Cell* **70,** 715–728
47. Krishnan, M. N., Sukumaran, B., Pal, U., Agaisse, H., Murray, J. L., Hodge, T. W., and Fikrig, E. (2007) *J. Virol.* **81,** 4881–4885
48. Lawe, D. C., Chawla, A., Merithew, E., Dumas, J., Carrington, W., Fogarty, K., Lifshitz, L., Tuft, R., Lambright, D., and Corvera, S. (2002) *J. Biol. Chem.* **277,** 8611–8617
49. Simonsen, A., Lippé, R., Christoforidis, S., Gaullier, J. M., Brech, A., Callaghan, J., Toh, B. H., Murphy, C., Zerial, M., and Stenmark, H. (1998) *Nature* **394,** 494–498

Figure S1. Deletion of TIP30, ACSL4, or Endo B1 Delays EGF-EGFR dissociation and inhibits the recruitment of Rab5a to endocytic vesicles

A-B, TIP30, ACSL4, or Endo B1 knockdown delays EGF-EGFR dissociation and inhibits the recruitment of Rab5a to endocytic vesicles. Localization of EGFR (red) and Rab5a (green) in control, TIP30 KD, ACSL4 KD and Endo B1 KD cells were monitored 120 min after $Alexa^{488}$-EGF (blue) internalization. Nucleus is stained by DAPI (gray). Typical images of cells in each group are shown. Boxed areas are magnified. Magenta represents red and blue overlap. Bars, 10 μm.
C, TIP30 deletion in primary hepatocytes leads to delayed EGF-EGFR dissociation and inhibits the recruitment of Rab5a to endocytic vesicles. Wild type and *Tip30*$^{-/-}$ primary hepatocytes were subjected to EGFR internalization analysis and were immunostained for EGFR (red) and Rab5a (green) 120 min after $Alexa^{488}$-EGF (blue) internalization. Bars, 10 μm.

Figure S2. Knockdown of TIP30 inhibits endosomal acidification.

A, Monitoring endosomal acidification in living cells. Control and TIP30 Knockdown cells were starved overnight and EGFR internalization analyses were performed by using Alex647-EGF (red) and pHrodo-EGF (green) that were mixed in a ratio of 3:7. Fluorescence from pHrodo indicates endosomal acidification. Images were acquired at the indicated time points. Bars, 5 μm.
B, Quantification of endosomal acidification. Alex647- and pHrodo-positive endosomes in 5 cells of each group were counted and percentage of pHrodo-positive endosomes was calculated. $^{**}P < 0.01$, relative to control cells; t test.

Figure S1

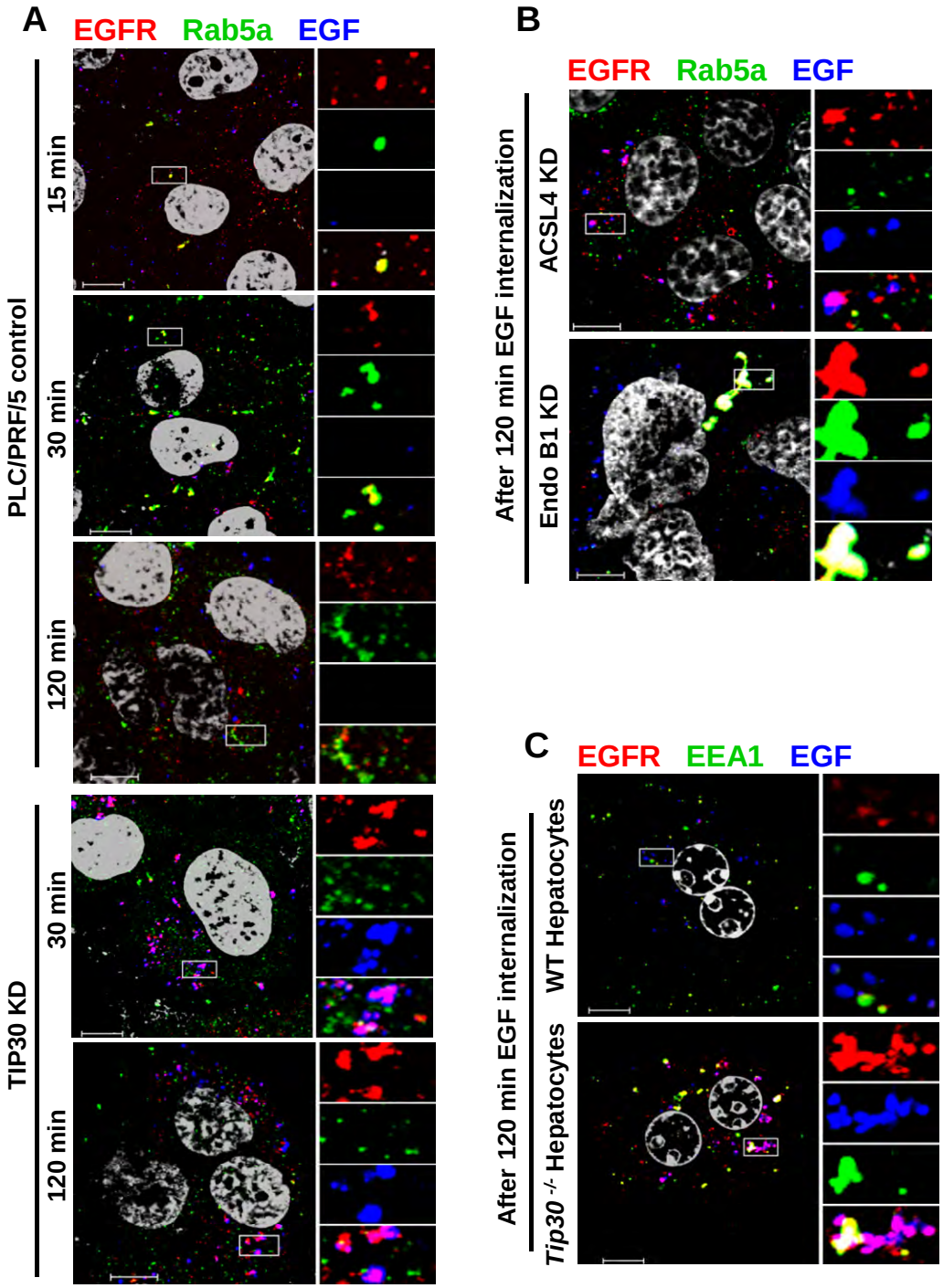
A
EGFR Rab5a EGF
PLC/PRF/5 control
15 min
30 min
120 min
TIP30 KD
30 min
120 min
B
EGFR Rab5a EGF
After 120 min EGF internalization
ACSL4 KD
Endo B1 KD
C
EGFR EEA1 EGF
After 120 min EGF internalization
WT Hepatocytes
Tip30 -/- Hepatocytes

Figure S2

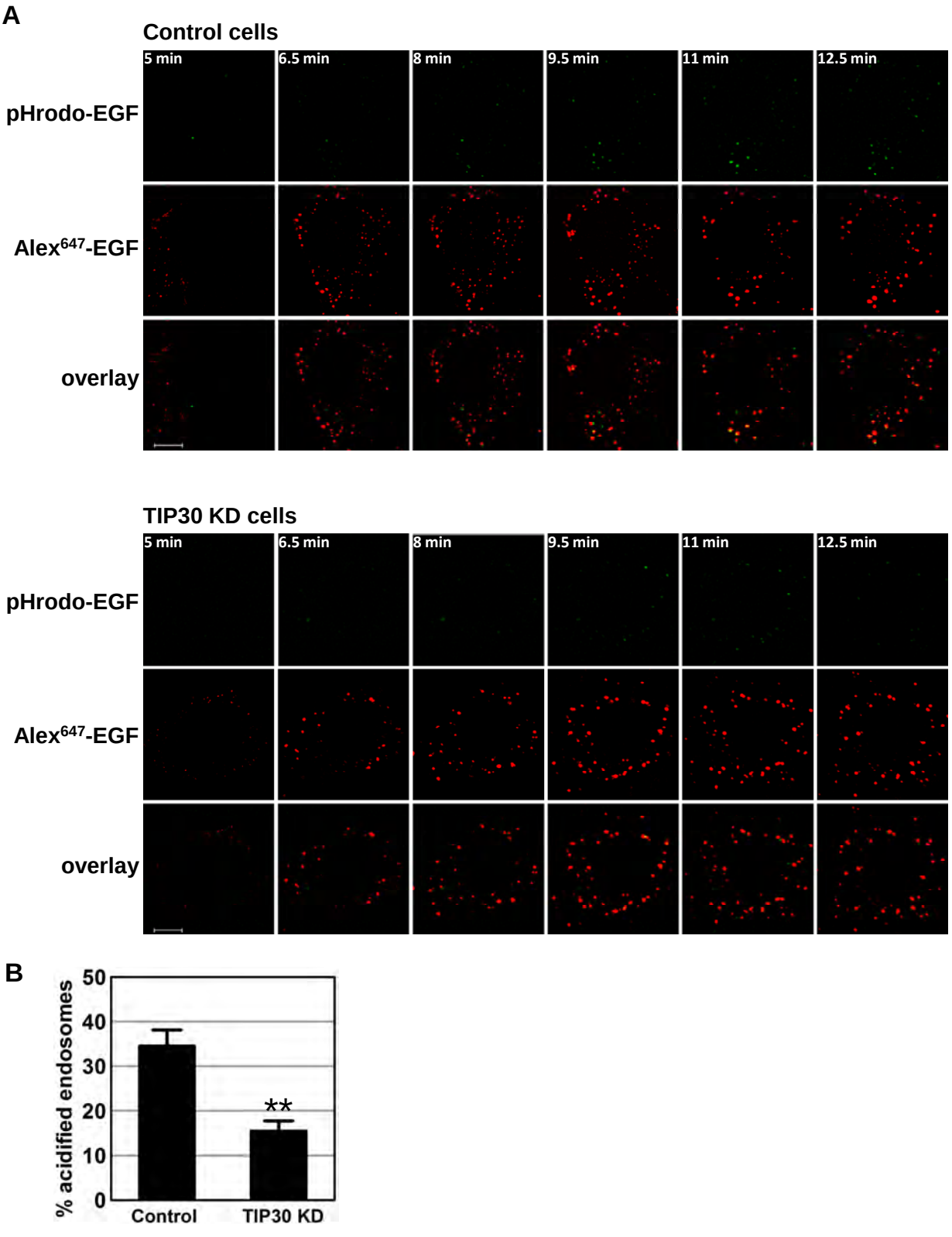
A
Control cells
5 min
6.5 min
8 min
9.5 min
11 min
12.5 min
pHrodo-EGF
Alex647-EGF
overlay
TIP30 KD cells
5 min
6.5 min
8 min
9.5 min
11 min
12.5 min
pHrodo-EGF
Alex647-EGF
overlay
B
% acidified endosomes
50
40
30
20
10
0
**
Control
TIP30 KD

OPEN ACCESS Freely available online

PLoS one

The TIP30 Protein Complex, Arachidonic Acid and Coenzyme A Are Required for Vesicle Membrane Fusion

Chengliang Zhang[1,2], Aimin Li[1,3], Shenglan Gao[1], Xinchun Zhang[2], Hua Xiao[1]*

1 Department of Biomedical and Integrative Physiology, Michigan State University, East Lansing, Michigan, United States of America, **2** Genetics Program, Michigan State University, East Lansing, Michigan, United States of America, **3** Department of Oncology, Nanfang Hospital, Southern Medical University, Guangzhou, Guangdong, People's Republic of China

Abstract

Efficient membrane fusion has been successfully mimicked *in vitro* using artificial membranes and a number of cellular proteins that are currently known to participate in membrane fusion. However, these proteins are not sufficient to promote efficient fusion between biological membranes, indicating that critical fusogenic factors remain unidentified. We have recently identified a TIP30 protein complex containing TIP30, acyl-CoA synthetase long-chain family member 4 (ACSL4) and Endophilin B1 (Endo B1) that promotes the fusion of endocytic vesicles with Rab5a vesicles, which transport endosomal acidification enzymes vacuolar (H^+)-ATPases (V-ATPases) to the early endosomes *in vivo*. Here, we demonstrate that the TIP30 protein complex facilitates the fusion of endocytic vesicles with Rab5a vesicles *in vitro*. Fusion of the two vesicles also depends on arachidonic acid, coenzyme A and the synthesis of arachidonyl-CoA by ACSL4. Moreover, the TIP30 complex is able to transfer arachidonyl groups onto phosphatidic acid (PA), producing a new lipid species that is capable of inducing close contact between membranes. Together, our data suggest that the TIP30 complex facilitates biological membrane fusion through modification of PA on membranes.

Citation: Zhang C, Li A, Gao S, Zhang X, Xiao H (2011) The TIP30 Protein Complex, Arachidonic Acid and Coenzyme A Are Required for Vesicle Membrane Fusion. PLoS ONE 6(6): e21233. doi:10.1371/journal.pone.0021233

Editor: Anna Maria Delprato, Institut Européen de Chimie et Biologie, France

Received December 13, 2010; **Accepted** May 24, 2011; **Published** June 24, 2011

Funding: The study was funded by RO1 DK066110-01 from the NIDDK, http://www2.niddk.nih.gov/, and W81XWH-08-1-0377 (to H.X.) from the Department of Defense, www.defense.gov/. The funders had no role in study design, data collection and analysis, decision to publish, or preparation of the manuscript.

Competing Interests: The authors have declared that no competing interests exist.

* E-mail: xiaoh@msu.edu

Introduction

Membrane fusion is well known as one of the most fundamental cellular processes in living organisms. It generally requires cellular factors to bring donor and recipient membranes into close proximity, increase membrane curvature, and disturb lipid bilayers [1,2]. Extensive studies during the past decades have led to the identification of a number of fusogenic proteins and lipids. In addition to lipids such as acyl-CoA [3,4], arachidonic acid [5,6], phosphoinositides, phosphotidic acid and diacylglycerol [7,8,9], many proteins including Rab5, Rab5 effectors, SNARE proteins and SNARE accessory factors are necessary for various membrane fusion events [10,11].

Recently, efficient endosome fusion was successfully mimicked using proteoliposomes reconstituted with 17 recombinant core fusion proteins [2,12]. Notably, however, these proteins are not sufficient to promote efficient fusion between biological membranes, indicating that biological membrane fusion requires more cellular factors than artificial membrane fusion. Given that purified endosomes contain the core SNARE proteins Syntaxin6, Syntaxin13, Vti1a and VAMP4, it is likely that factors needed for initiating membrane fusion have yet been identified.

Among the lipids that play key roles in membrane fusion, arachidonic acid has been shown to be required for endosome fusion *in vitro* [6], and is the most effective fusogen in chromaffin granule fusion [13]. In addition, membrane-bound arachidonic acid can drive annexin II-mediated membrane fusion of the lamellar body with the plasma membrane during the exocytosis [5].

We have recently identified a protein complex containing TIP30, ACSL4 and Endo B1 that interacts with Rab5a and facilitates the loading of V-ATPases on endocytics vesicles. Inhibiting any of these proteins causes the mislocalization of V-ATPases, thus leading to the trapping of EGF-EGFR complexes in endocytic vesicles, delayed EGFR degradation and sustained EGFR endosomal signaling [14]. In addition, we have shown that Rab5a and V-ATPase reside in vesicles devoid of EGFR, the early endosomal marker EEA1 and the recycling endosomal marker transferrin receptor (TfR), suggesting that Rab5a functions as a identity tag for vesicles that deliver V-ATPases to endosomes [14]. Given that localization of integral membrane proteins to their target membranes requires vesicle membrane fusion [15], we therefore examined if the TIP30 protein complex can promote vesicle membrane fusion *in vitro*. Since ACSL4 was identified in the protein complex and it is an acyl-CoA synthetase that prefers arachidonic acid as the reaction substrate, we included both arachidonic acid and coenzyme A in the *in vitro* membrane fusion reactions. We found that the TIP30 complex and the synthesis of arachidonyl-CoA from arachidonic acid and coenzyme A are required for efficient fusion of Rab5a vesicles with endocytic vesicles. The TIP30 complex may initiate membrane fusion by modifying membrane PA.

Results

The TIP30 complex, arachidonic acid and coenzyme A promote fusion between endocytic and Rab5a vesicles

To investigate whether the TIP30 complex can promote membrane fusion *in vitro*, we used a confocal microscopy-based *in vitro*

fusion assay [16,17] to monitor fusion between endocytic and Rab5a vesicles in an initial pilot experiment. Endocytic and Rab5a vesicles were prepared from HepG2 cells that do not contain detectable endogenous TIP30 and EGFR. Rab5a vesicles were labeled by expressing EYFP-Rab5a fusion proteins and prepared from serum-starved cells. Endocytic vesicles were labeled by expressing EGFR-DsRed fusion proteins and prepared from EGF treated cells. The two types of vesicles that contain equal amount of proteins were incubated in the fusion buffer at 37°C followed by examination with confocal microscopy. Vesicle fusion and aggregation were represented by the fluorescence overlap between EGFR-DsRed and EYFP-Rab5a.

Since ACSL4 is an acyl-CoA ligase with high substrate preference for arachidonic acid (C20:4) [18], we first tested if arachidonic acid and coenzyme A are needed. Vesicles resulting from reactions that were kept on ice were evenly distributed on the slides, appearing as small vesicles with low fluorescence intensity and no fluorescence overlap (Figure 1A, lane 1; Figure 1B). Similarly, no fluorescence overlap was observed in the absence of arachidonic acid or in the presence of triacsin C (10 uM), a potent inhibitor of ACSL4 (Figure 1A, lanes 4 and 6; Figure 1B). In contrast, in the presence of arachidonic acid and coenzyme A, immunopurified TIP30 complex caused vesicle enlargement and significantly increased fluorescence overlap (TIP30 complex: 50± 6%; control eluates: 20±3%; omitting coenzyme A: 17± 2%; omitting GTP: 16±4%; n = 6 representative confocal images of 143×143 μm, $p<0.01$ versus TIP30 complex; Figure 1A and 1B), thereby resulting in much intensified fluorescence. Rab5a vesicles attached to aggregated endocytic vesicles, but remained as small particles when the TIP30 complex, coenzyme A, or GTP was omitted. The effect of GTP exclusion is consistent with the fact that GTP is a known membrane fusion factor and required for Rab5a function. We next screened for other fatty acids that might promote membrane fusion, including palmitic, palmitoleic, oleic, linoleic, linolenic, eicosapentaenoic, and docosahexaenoic acids. None of these fatty acids could promote vesicle enlargement and fluorescence overlap (data not shown). Furthermore, arachidonic acid significantly increased fluorescence overlap in the presence of HeLa cell cytoplasmic S100 extracts that containing the TIP30 complex (HeLa S100: 2±2%; HeLa S100+arachidonic acid: 50±5%; n = 6 representative confocal images of 143×143 μm, $p<0.01$ versus HeLa S100; Figure 1C). These results suggest that arachidonic acid and the TIP30 complex are involved in membrane aggregation and/or fusion, which are consistent with our *in vivo* data [14] and previous reports that arachidonic acid is essential for vesicle membrane fusion [6,13].

To determine whether that vesicle enlargement and fluorescence overlap were due to membrane fusion or aggregation, we examined the vesicles that resulted from fusion reactions by transmission electron microscopy (TEM). Without the addition of arachidonic acid, all vesicles appeared spherical and ranged in diameter from 50 to 300 nm. In contrast, the complete fusion reaction led to the production of vesicles enlarged to more than 1 μm in diameter (Figure 2A); the larger vesicles were not found in reactions without arachidonic acid. Ongoing fusion could also be observed. Quantitative analysis revealed a significant increase in the amount of enlarged vesicles (with arachidonic acid: 300–500 nm, 24±2%; >500 nm, 16.5±1.5%; without arachidonic acid: 300–500 nm, 1±0.2%; >500 nm, 0; n = 150, $p<0.01$; Figure 2B). Given the fluorescent overlap between two types of vesicles in the complete reactions shown in Figure 1, these results indicate that the TIP30 complex and synthesis of arachidonyl-CoA are essential for the fusion of Rab5a vesicles with endocytic vesicles.

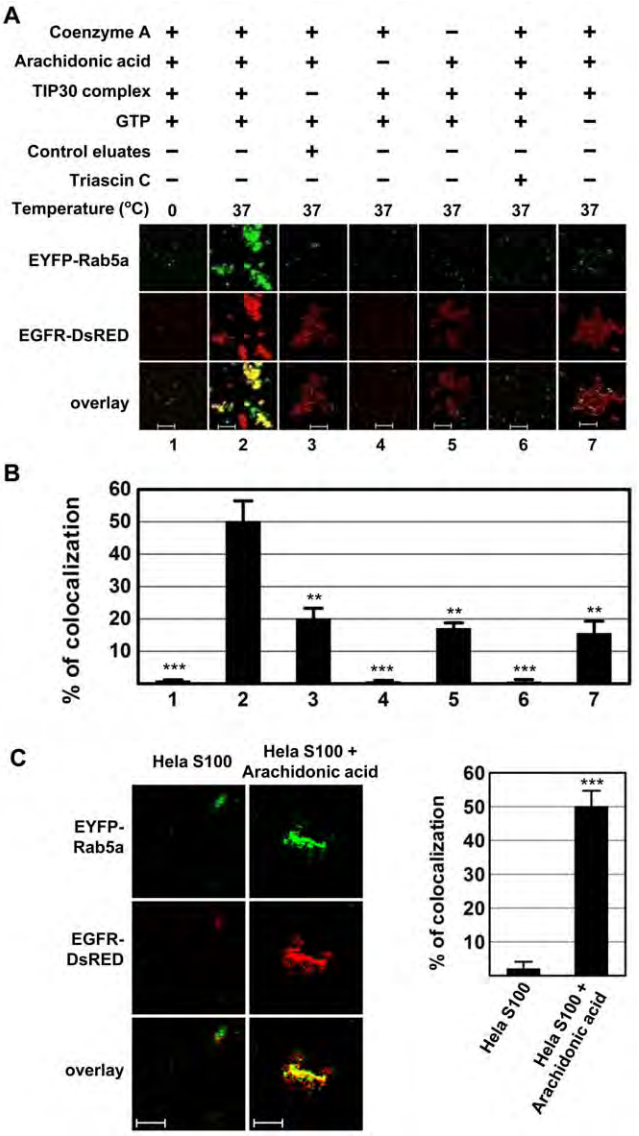

Figure 1. The TIP30 protein complex, arachidonic acid and coenzyme A promote the fusion between endocytic and Rab5a vesicles. (**A**) Aliquots of isolated EGFR-DsRed and EYFP-Rab5a vesicles (both contain 20 μg of proteins) were mixed and incubated in reactions (20 μl) with the indicated components. The resulting fusion products were spotted on glass slides and images were taken using confocal microscope. Panels 1, 4 and 6 were scanned with 3× amplification gain setting due to lower fluorescence intensity of individual vesicles. Arachidonic acid (100 nmol) was used in the reactions. Images are single plane and are representative for at least three independent experiments. Scale bars, 5 μm. (**B**) Signal overlap was quantified using MBF_ImageJ. Pearson's colocalization coefficients were calculated from three independent experiments and were converted to percentages. Data represent means ± SEM. $^{**}P<0.01$, $^{***}P<0.001$; t test. (**C**) Arachidonic acid promotes the vesicle fusion induced by HeLa cell S100. S100 fractions (4 mg/ml) of HeLa cells were incubated with isolated EGFR-DsRed and EYFP-Rab5a vesicles (both contain 20 μg proteins) in the absence or presence of 100 nmol arachidonic acid. Resulting vesicles were examined using confocal microscopy (left panel) and fluorescence overlaps were quantified (right panel).
doi:10.1371/journal.pone.0021233.g001

Recombinant TIP30, ACSL4 and Endo B1 can replace the TIP30 complex in promoting fusion of endocytic vesicles with Rab5a vesicles

To exclude possible influences of other associated or contaminating proteins in immunopurified TIP30 complexes, we replaced

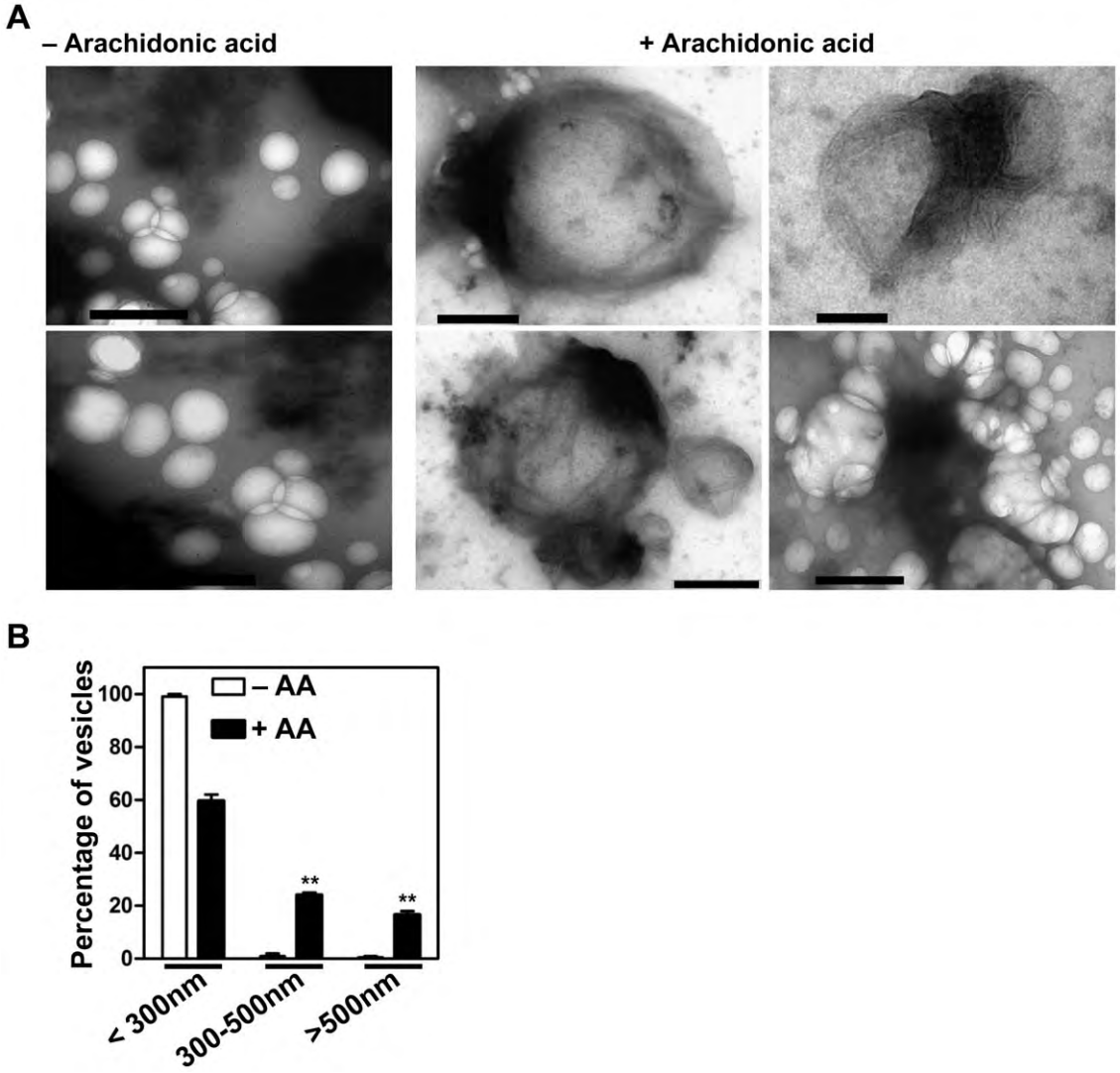

Figure 2. Transmission electron microscopy analysis of products from in vitro vesicle fusion assays. (**A**) EGFR-DsRed and EYFP-Rab5a vesicles were incubated with immunopurified TIP30 complex in the fusion buffer with (right panel) or without (left panel) 100 nmol of arachidonic acid. Resulting vesicles were stained with uranyl acetate and examined using TEM. Scale bars, 500 nm. (**B**) The graphs show the percentages of vesicles with different diameters. At least 6 images from two independent experiments were counted. Data represent means ± SEM. n = 150; $^{**}P<0.01$, t test.
doi:10.1371/journal.pone.0021233.g002

the immuno-complexes with bacterially-expressed recombinant TIP30, ACSL4 and Endo B1 in cell free assays. The three highly purified recombinant proteins (Figure 3A) can efficiently promote fluorescence overlap (75±6%), whereas lack of any of these proteins led to significantly less overlap (TIP30: 18±1%; TIP30 and ACSL4: 23±1%; Endo B1: 35±3%; ACSL4 and EndoB1: 8±2%; ACSL4: 20±5%; n = 6 representative images of 143×143 μm; $p<0.01$ versus TIP30, ACSL4 and Endo B1; Figure 3B and 3C). TIP30M, a TIP30 mutant with a mutated putative nucleotide binding motif (GXXGXXG) [19], only promoted 24±2% overlap (n = 6 representative images of 143×143 μm; $p<0.01$ versus TIP30, ACSL4 and Endo B1; Figure 3B and 3C, panel 4). These data suggest that TIP30, ACSL4 and Endo B1 together can substitute for the TIP30 complex in promoting the fusion between endocytic and Rab5a vesicles.

Vesicle tethering and stacking induced by acylation of phosphatidic acid

To gain further insight into how TIP30 and its interacting proteins mediate membrane fusion, we first used ^{3}H-arachidonic acid to label membrane lipids and found that at least one lipid species in purified early endosomes was specifically labeled by the TIP30 complex (Figure 4A, lane 2). The production of the labeled lipid was significantly less in the reaction using control eluates (lane 1) or TIP30M immunoprecipitates (lane 3), and was blocked by triacsin C (lane 5). The new lipid species was not observed when Rab5a vesicles were used in the reactions (data not shown). These data indicate that lipids on endocytic vesicles are the specific recipients of the arachidonyl group.

To identify the lipids that are modified, we performed protein-lipid overlay assays using membrane strips prespotted with 15 cellular membrane lipids (Figure 4B). TIP30 and Endo B1 specifically bind phosphatidic acid (PA) and cardiolipin. Endo B1 also binds phosphatidylinositol 4-phosphate (PtdIns(4)P; Figure 4C). ACSL4 and Rab5a did not bind any lipids spotted on the strips (data not shown). Cardiolipin is found predominantly in the inner mitochondrial membrane, whereas PA has been implicated in the fusion of various intracellular membranes [7,20]. Therefore, we focused on PA and tested whether the TIP30 complex could convert PA to PA-derivatives. Lipids extracted from the acylation

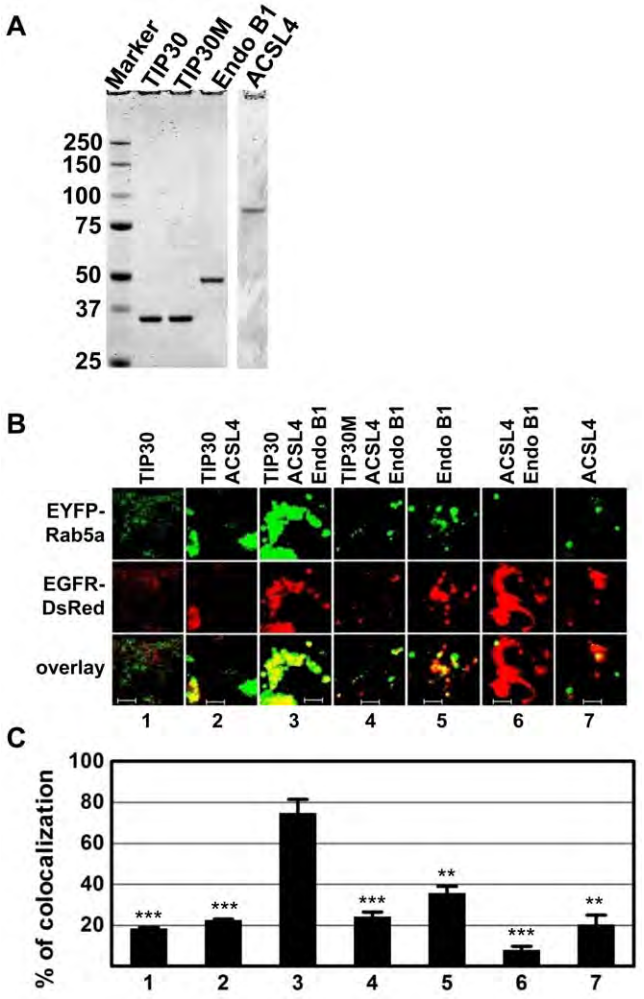

Figure 3. Bacterially expressed recombinant TIP30, ACSL4 and Endo B1 can replace the TIP30 complex in promoting efficient vesicle fusion. (**A**) Recombinant proteins were expressed in BL21 cells and were purified using cobalt affinity resins. Eluted proteins were subjected to SDS-PAGE analysis followed by Coomassie blue staining. Images were acquired using a Li-Cor scanner. (**B**) EGFR-DsRed and EYFP-Rab5a vesicles were incubated with the indicated recombinant proteins (20 ng each) in the fusion buffer. Resulting fusion products were examined using confocal microscope. Scale bars, 5 μm. (**C**) Quantification of images represented in (B). Signal overlap was quantified using MBF_ImageJ. Pearson's colocalization coefficients were calculated from three independent experiments and converted to percentages. Data represent means ± SEM. $^{**}P<0.01$, $^{***}P<0.001$; t test.
doi:10.1371/journal.pone.0021233.g003

reactions with PA and arachidonic acid as substrates were subjected to MS/MS and LC-MS/MS spectrometry analyses (Figure 5A–5C). The flow injection precursor scan in both modes revealed one predominant peak with an m/z (mass-to-charge ratio) value of 940.2, which does not match the exact mass of any known lipids in the database (lipidmaps.org). Thus, the identity of lipid product of the TIP30 complex remains unknown. However, since its mass is very close to the mass (940.85) of triacylglycerols ($C_{61}H_{112}O_6$), we speculate that it might be a triacylglycerol.

To determine how PA derivatives *per se* would affect membrane fusion, we carried out acylation reactions by incubating PA or phosphoinositide (PI) with the TIP30 complex in the fusion buffer. The resulting lipids were purified, resuspended by sonication, and incubated with vesicles. Interestingly, the PA derivatives promoted dramatic fluorescence overlap among endocytic and Rab5a vesicles on ice (Figure 6). In contrast, PA incubated with control eluates did not promote significant fluorescence overlap among the vesicles, nor did phosphoinositide (PI) that was prepared with the same procedure as the PA derivative. A triacylglycerol (1,2-Dilinoleoyl-3-palmitoyl-*rac*-glycerol) with a palmitoyl tail at the sn-3 position also increases significant fluorescence overlap (Figure 6). . These results indicate that the PA derivatives possibly promote membrane aggregation and/or fusion.

Finally, we used electron microscopy to examine the vesicles after incubation with PA derivatives that were generated by either immunopurified or recombinant protein-reconstituted TIP30 complexes (Figure 7). PA derivatives caused vesicle tethering and stacking, which is marked by dramatic deformation (Figure 7B and 7C). In contrast, the vesicle aggregation caused by triacylglycerol seemed due only to tethering (Figure 7E), indicating that these specific commercially available triacyglycerols do not have the ability to induce vesicle stacking; therefore do not represent the new lipid species generated by the TIP30 complex. Consistent with the confocal microscopy data, PA treated with control eluates (Figure 7A) or PI treated with immunpurified TIP30 complex (Figure 7D) had no apparent effect.

Nonetheless, we did not observe complete fluorescence overlap and enlarged endosomes (>0.5 μm in diameter) as seen in Figure 2, suggesting that additional activities of the TIP30 complex or other proteins on the membranes, such as SNAREs, SNARE accessory factors, Rab5a and its effectors, are needed to accomplish the fusion steps following close membrane contact. Collectively, these data indicate that TIP30, ACSL4, and Endo B1 promote vesicle membrane fusion by fatty acylating PA.

Discussion

Elucidating the molecular basis of intracellular trafficking and protein sorting requires the identification of the critical components participating in these processes. Our earlier studies demonstrated that proteins in the TIP30 protein complex are required for the fusion of endocytic and Rab5a vesicles *in vivo*. In the present study, using both confocal microscopy and transmission electron microscopy, we demonstrated that the TIP30 complex promotes membrane fusion *in vitro* and that arachidonyl-CoA synthesis by ACSL4, a component in the TIP30 complex, is essential for membrane fusion.

Arachidonic acid has been shown to be involved in vesicle membrane fusion [6,13]. Previous reconstituted approaches *in vitro* have contributed greatly to our understanding of membrane fusion. However, to our knowledge, efficient fusion between biological membranes has hardly been achieved *in vitro* in cell free assays without using cytosol fractions or arachidonic acid, further emphasizing the important role of arachidonic acid during membrane fusion. How does arachidonic acid promote membrane fusion? Arachidonic acid has been proposed to stimulate SNARE complex assembly [21,22,23]. Our data seem support these observations by showing that endocytic vesicles recognize Rab5a vesicles only after arachidonic acid was added to the reactions. Interestingly, fusion did not occur in the absence of the TIP30 complex or in the presence of the ACSL4 inhibitor. These results suggest that in addition to directly promoting SNARE complex assembly, arachidonic acid must be activated by esterification to stimulate membrane fusion.

We further showed that the arachidonyl group is transferred to endosomal PA to generate a new lipid species that induce vesicle tethering and stacking. Thus, we suggest a hypothesis that arachidonic acid promotes membrane fusion by contributing to both PA

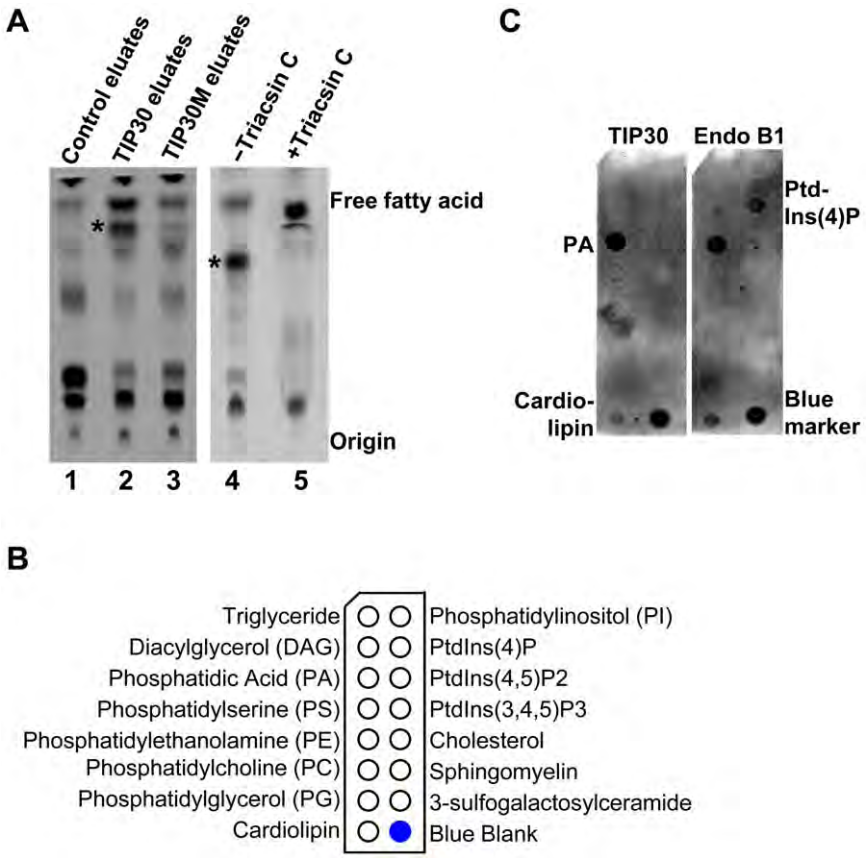

Figure 4. TIP30 and Endo B1 strongly bind phosphatidic acid. (**A**) Fatty acylation of endosomal lipids by the TIP30 complex. [^{3}H]-arachidonic acid can be transferred to endosomal membrane lipids by the TIP30 complex, but not by TIP30M immunoprecipitates or control immunoprecipitates (left panel). The transfer was blocked by 10 μM triacsin C (right panel). Image was acquired by scanning lipids resolved on TLC plate with a Molecular Dynamics Storm 860. * indicates the radiolabeled lipid. (**B**) The schematic diagram shows the lipid species pre-spotted on membranes that are used in lipid-protein overlay assays. (**C**) TIP30 and Endo B1 strongly bind phosphatidic acid (PA). Protein-lipid overlay assays were carried out by incubating recombinant proteins with membrane strips containing 15 pre-spotted lipids. Membranes were scanned using a Li-Cor scanner after being sequentially overlaid with primary and fluorescent secondary antibodies.
doi:10.1371/journal.pone.0021233.g004

acylation and SNARE complex assembly. Consistent with this view, PA and its synthetase phospholipase D (PLD) are known to participate in membrane fusion during vesicle transport [20,24]. Moreover, as integral components of many biological membranes, triacylglycerols have been demonstrated to possess great potency to promote spontaneous curvature in an acyl chain length dependent manner [25], which may alter membrane structure to support membrane fusion [1,2]. We speculate that the addition of the hydrophobic acyl chain to endosomal PA may help to overcome the repulsive hydration force generated from water bound to the lipid headgroups. In addition, triacylglycerols can exhibit an extended conformation [26] with the 3-arachidonyl group in the opposite direction of the other two acyl chains, thereby allowing for attachment and fusion between two membranes [27,28]. Our results suggest that as an initiation event, acylation of endosomal PA enables the close contact between donor and recipient membranes, thus allowing for fusion to be accomplished by SNAREs, SNARE accessory factors, Rab5 and its effectors. Nevertheless, although we favor this hypothesis to explain the role of TIP30 in membrane fusion and endocytic trafficking, we do not rule out other possible hypotheses that may also explain the actions of the TIP30 complex. Undoubtedly, efficient fusion could be achieved using artificial membranes in the absence of arachidonic acid. This may be due to the fact that artificial membranes are far less complex than biological membranes in terms of membrane composition, organization and dynamics, thereby requiring much less factors to fuse. This view is supported by the observation that the same set of proteins could promote efficient fusion of artificial membranes but incapable of inducing efficient biological membrane fusion [12]. Furthermore, our data suggest that the TIP30 complex modifies lipids to initiate membrane fusion. This step may have been bypassed during the processes of lipid extraction and membrane reconstitution. It would be interesting to find out whether addition of arachidonic acid, CoA and the TIP30 complex could enhance artificial membrane fusion.

Clearly, more work is needed to determine how fatty acylated PA and other lipid derivatives cooperate with the action of SNAREs, Rab5 and their effectors in membrane fusion. Future studies may also focus on finding out how the TIP30 complex acylates PA and what the exact identity of the fusion products is. It is expected that a more precise mechanism underlying membrane fusion will emerge by integrating information from studies of both lipids and proteins.

Materials and Methods

Reagents

DMEM, fetal bovine serum, trypsin, penicillin, and streptomycin were purchased from Invitrogen. Anti-HA agarose beads were from Roche Applied Science. Polyclonal rabbit anti-human Rab5a

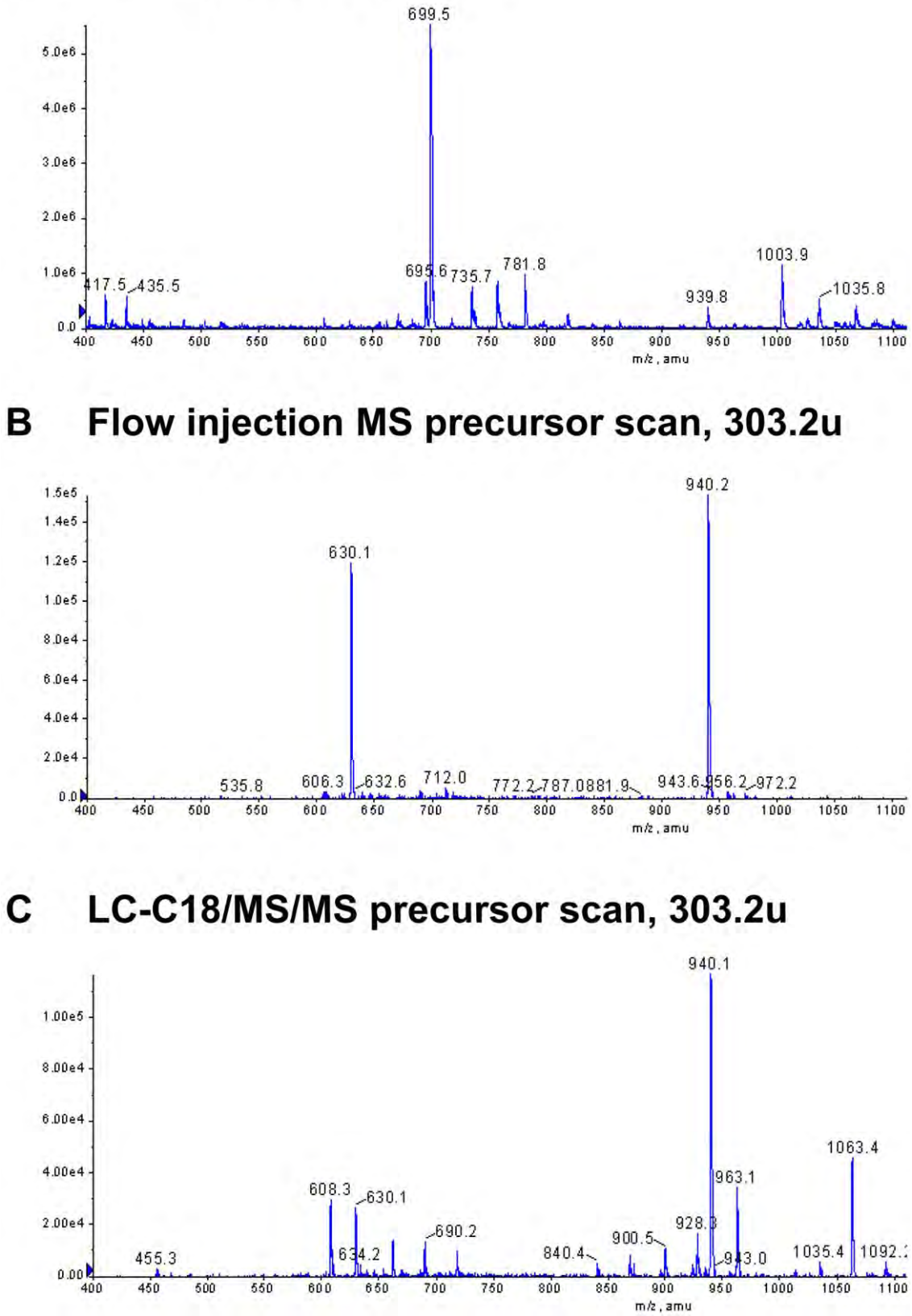

Figure 5. Arachidonyl group was transferred onto phosphatidic acid. (**A**) PA was incubated with the TIP30 protein complex in the fusion buffer. Resulting lipids were purified and subjected to flow injection negative scan in the range of 400–1400 u. A predominant peak of 699.5 was

detected. Atomic mass: arachidonic acid, 304.5 u; 18:1 PA, 699.5 u. The lipids in the smaller peaks have molecular weights that do not match any of the expected PA derivatives. (**B**) The flow injection negative precursor scan for 303.2 u over a mass range of 400–1400 u. (**C**) The LC-C18 negative precursor scan for 303.2 u over a mass range of 400–1400 u. The lipids after the acylation reaction was extracted and chromatographed on a C-18 column to reduce possible adduction mechanisms of compounds detected in the flow injection negative precursor scan of 303.2 u.
doi:10.1371/journal.pone.0021233.g005

antibody was from Cell Signaling. Polyclonal rabbit anti-human ACSL4 was a generous gift from Stephen Prescott (University of Utah). Polyclonal rabbit anti-human Endo B1, LPA, triacylglycerol (1,2-Dilinoleoyl-3-palmitoyl-*rac*-glycerol), arachidonic acid and CoA were from Sigma-Aldrich. PA (1,2-dioleoyl-sn-glycero-3-phosphate) were purchased from Avanti Polar Lipids. [^{3}H]-arachidonic acid was from PerkinElmer.

Cell culture

PLC/PRF/5 and HepG2 cell lines were purchased from ATCC and cultured in DMEM supplemented with 10% fetal bovine serum and penicillin/streptomycin at 37°C in 5% CO_2.

Immunoprecipitation

Immunoprecipitations were performed as previously described [14].

Purification of endocytic and Rab5a vesicles

HepG2 cells were transduced by the lentivirus carrying vector pSin-EGFR-DsRed or pSin-EYFP-Rab5a and were selected for 4 days with 2 μg/ml puromycin. To prepare endosomes carrying EGFR-DsRed, we treated cells with 10 ng/ml EGF at 37°C for 10 minutes and purified early endosomes on the flotation gradient essentially as described [29]. Briefly, cells were incubated with 10 ng/ml EGF for 10 min at 37°C. After several washings, cells were scraped and pelleted at 4°C before being subjected to needle breakdown in homogenization buffer (250 mM sucrose, 3 mM imidazole, pH 7.4, 1 mM EDTA) at 4°C. Homogenates were centrifuged at 3000 rpm for 10 min at 4°C and post-nuclear supernatants (PNS) were collected. PNSs were then suspended in 40.6% sucrose by adding a stock solution (62% sucrose, 3 mM imidazole, pH 7.4, 1 mM EDTA) and loaded at the bottom of a SW40 centrifugation tube. The load was then sequentially overlaid with 1.5 ml of 35% sucrose in 3 mM imidazole, pH 7.4 with 1 mM EDTA; 1 ml of 25% sucrose in 3 mM imidazole, pH 7.4 with 1 mM EDTA; and at the top with 0.5 ml of homogenization buffer. The gradient was centrifuged at 125000 g for 60 min at 4°C. Early endosomal fractions were collected at the 35%/25% sucrose interface.

Rab5 vesicles containing EYFP-Rab5a were prepared as described [30]. Briefly, HepG2 cells expressing pSin-EYFP-Rab5a were starved for 24 hours before being scraped and pelleted at 4°C. PNSs were prepared as described above. PNSs were then centrifuged at 10000 rpm at 4°C using a bench top centrifuge. The post mitochondria supernatants were loaded on top of homogenization buffer in SW40 centrifugation tubes with 0.5 ml cushion solution (62% sucrose, 3 mM imidazole, pH 7.4, 1 mM EDTA) at the bottom. Centrifugation was done at 100000 g for 60 min at 4°C and Rab5a vesicles were collected on top of the cushion solution.

In vitro vesicle fusion assay

The assay was performed as described previously with modifications [16,17]. Briefly, EGFR-DsRED endocytic vesicles and EYFP-Rab5a vesicles (aliquotes of both contain 20 μg proteins) were gently mixed in a total volume of 20 μl fusion buffer (10 mM Hepes, pH 7.4, 1.5 mM MgOAc, 1 mM DTT, 50 mM KOAc, 100 nmol arachidonic acid, 1 mM coenzyme A, 5 mM GTP, complemented with 4 μl of an ATP-regenerating system containing 1:1:1 mixture of 100 mM ATP, 600 mM creatine phosphate, and 4 mg/ml creatine phosphokinase). After incubating with indicated purified proteins at 37°C for 40 min, a portion of the reactions were spotted on slides and examined using Zeiss LSM 510 Meta confocal microscope. All images are representative single optical sections. Colocalization analysis was done using MBF_ImageJ. For reactions in Figure 5, PA and PI were incubated with control eluates or the TIP30 complex in a total volume of 200 μl fusion buffer. Resulting lipids were purified using Bligh-Dyer Method [31] and incubated with vesicles in homogenization buffer (250 mM sucrose, 5 mM Hepes, pH 7.4) on ice.

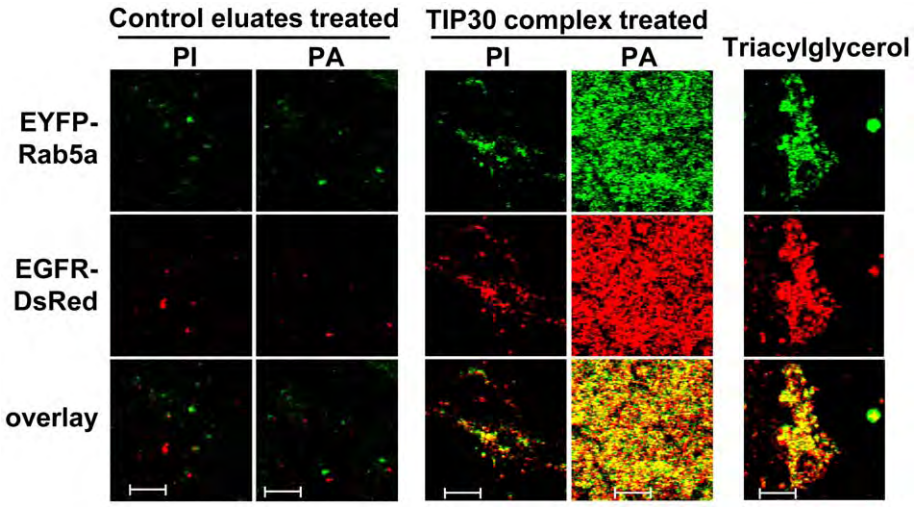

Figure 6. Fatty acylation of phosphatidic acid promotes vesicle aggregation. Lipids were extracted after incubating 100 nmol PA or phosphatidylinositol (PI) with 100 nmol arachidonic acid the TIP30 complex or control eluates. Lipids were resuspended in homogenization buffer by sonication and were mixed with EGFR-DsRed and EYFP-Rab5a vesicles in *in vitro* fusion buffer at 37°C. Resulting vesicles were spotted on glass slides and images were taken using confocal microscope. Scale bars, 5 μm.
doi:10.1371/journal.pone.0021233.g006

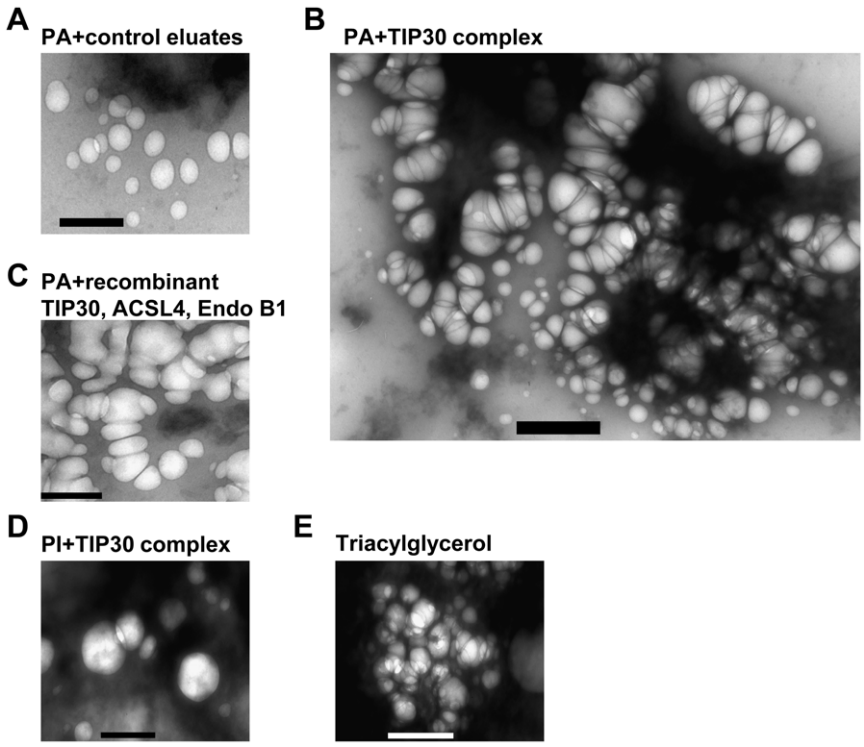

Figure 7. Fatty acylation of phosphatidic acid induce vesicle tethering and stacking. Effects of acylated PA on vesicle fusion were determined using electron microscope. Lipids were extracted after incubating PA with control immunoprecipitates (A), PA with immunopurified TIP30 complex (B), PA with recombinant TIP30, ACSL4, and Endo B1 (C) or PI with immunopurified TIP30 complex (D). Each of these lipids or triacylglycerol (E) was suspended in homogenization buffer and incubated on ice with EGFR-DsRed and EYFP-Rab5a vesicles. The resulting vesicles were examined using TEM. Scale bars, 500 nm.
doi:10.1371/journal.pone.0021233.g007

Electron microscopy studies was performed as described previously using TEM JEOL 100CX [12].

Protein-lipid overlay assays

Protein-lipid overlay assays were performed essentially as previously described [32]. Briefly, membrane strips (Echelon Biosciences Inc.) containing 15 pre-spotted lipids were incubated overnight at 4°C with recombinant proteins (10 μg/ml) in TBST with 5% milk. After being washed with TBST 10 min each for 3 times, the strips were incubated overnight at 4°C with specific primary antibodies against the recombinant proteins in TBST with 5% milk. The strips then were washed again and incubated with corresponding fluorescent secondary antibodies at room temperature for 1 hour. Images were acquired by scanning the strips using a Li-Cor scanner.

Lipid acylation

Purified endocytic vesicles (aliquots containing 20 μg proteins) were incubated with indicated proteins and [^{3}H]-arachidonic acid (PerkinElmer) in the presence or absence of 10 μM triacsin C at 37°C for 1 hour in a total volume of 200 μl fusion buffer. Lipids were extracted using Bligh-Dyer Method [31] and resolved on silica gel 60 TLC plate with chloroform/ethanol/water/triethylamine (30/35/7/35) as the solvent. The TLC plate was exposed to Kodak Tritium Sensitive Storage Phosphor Screen. Images were acquired by scanning the screen using a Molecular Dynamics Storm 860. For preparation of lipid derivatives from PA, PI or LPA, 100 nmol lipids were incubated with immunopurified TIP30 complex or recombinant TIP30, ACSL4 and Endo B1 in the fusion buffer. Resulting lipids were purified using Bligh-Dyer Method [31].

MS/MS spectrometry analysis

MS/MS spectrometry analysis of PA derivatives were performed in Avanti Polar Lipids Inc. Briefly, PA derivatives were extracted according to Bligh-Dyer method and redissoved in methanol/chloroform (85/18) with 10 mM NH_4OAC and 1 ug/ml NH_4OH. First, standards of 17:0–20:4 PA and 17:0–20:4 PI were prepared in the above solution and infused in the API 4000 QTrap triple quadrupole with linear ion trap instrument for optimization of collisional energy to provide mass fragments of arachidonic acid (20:4) at 303.2 u. Then samples were flow injected into the MS/MS in negative scan mode to discover products from the described reaction. The m/z value was used to search the most likely molecular species at http://www.lipidmaps.org.

Statistical analysis

All statistical tests were two-tailed t-test. Data represent means ± SEM. *$P<0.05$, **$P<0.01$.

Acknowledgments

We are grateful to Stephen Prescott for generously sharing ACSL4 antibody. We thank Drs. Hans Cheng, Jerry Dodgson, Karen Friderici and Richard Schwartz for critical reading of the manuscript and Alicia Pastor for electron microscopy analysis.

Author Contributions

Conceived and designed the experiments: CZ HX. Performed the experiments: CZ AL SG XZ. Analyzed the data: CZ HX XZ. Wrote the paper: CZ HX.

References

1. Martens S, McMahon HT (2008) Mechanisms of membrane fusion: disparate players and common principles. Nat Rev Mol Cell Biol 9: 543–556.
2. McMahon HT, Kozlov MM, Martens S (2010) Membrane Curvature in Synaptic Vesicle Fusion and Beyond. Cell 140: 601–605.
3. Pfanner N, Glick BS, Arden SR, Rothman JE (1990) Fatty acylation promotes fusion of transport vesicles with Golgi cisternae. J Cell Biol 110: 955–961.
4. Pfanner N, Orci L, Glick BS, Amherdt M, Arden SR, et al. (1989) Fatty acyl-coenzyme a is required for budding of transport vesicles from Golgi cisternae. Cell 59: 95–102.
5. Chattopadhyay S, Sun P, Wang P, Abonyo B, Cross NL, et al. (2003) Fusion of Lamellar Body with Plasma Membrane Is Driven by the Dual Action of Annexin II Tetramer and Arachidonic Acid. Journal of Biological Chemistry 278: 39675–39683.
6. Mayorga LS, Colombo MI, Lennartz M, Brown EJ, Rahman KH, et al. (1993) Inhibition of endosome fusion by phospholipase A2 (PLA2) inhibitors points to a role for PLA2 in endocytosis. Proc Natl Acad Sci U S A 90: 10255–10259.
7. Haucke V, Di Paolo G (2007) Lipids and lipid modifications in the regulation of membrane traffic. Curr Opin Cell Biol 19: 426–435.
8. Jun Y, Fratti RA, Wickner W (2004) Diacylglycerol and Its Formation by Phospholipase C Regulate Rab- and SNARE-dependent Yeast Vacuole Fusion. Journal of Biological Chemistry 279: 53186–53195.
9. Mima J, Hickey CM, Xu H, Jun Y, Wickner W (2008) Reconstituted membrane fusion requires regulatory lipids, SNAREs and synergistic SNARE chaperones. EMBO J 27: 2031–2042.
10. Stenmark H (2009) Rab GTPases as coordinators of vesicle traffic. Nat Rev Mol Cell Biol 10: 513–525.
11. Wickner W, Schekman R (2008) Membrane fusion. Nat Struct Mol Biol 15: 658–664.
12. Ohya T, Miaczynska M, Coskun U, Lommer B, Runge A, et al. (2009) Reconstitution of Rab- and SNARE-dependent membrane fusion by synthetic endosomes. Nature 459: 1091–1097.
13. Creutz CE (1981) cis-Unsaturated Fatty Acids Induce the Fusion of Chromaffin Granules Aggregated by Synexin. The Journal of Cell Biology 91: 247–256.
14. Zhang C, Li A, Zhang X, Xiao H (2011) A novel TIP30 protein complex regulates EGF receptor signaling and endocytic degradation. J Biol Chem 286: 9373–9381.
15. Pryer NK, Wuestehube LJ, Schekman R (1992) Vesicle-mediated protein sorting. Annu Rev Biochem 61: 471–516.
16. Bethani I, Werner A, Kadian C, Geumann U, Jahn R, et al. (2009) Endosomal fusion upon SNARE knockdown is maintained by residual SNARE activity and enhanced docking. Traffic 10: 1543–1559.
17. Brandhorst D, Zwilling D, Rizzoli SO, Lippert U, Lang T, et al. (2006) Homotypic fusion of early endosomes: SNAREs do not determine fusion specificity. Proc Natl Acad Sci U S A 103: 2701–2706.
18. Cao Y, Traer E, Zimmerman GA, McIntyre TM, Prescott SM (1998) Cloning, Expression, and Chromosomal Localization of Human Long-Chain Fatty Acid-CoA Ligase 4 (FACL4). Genomics 49: 327–330.
19. Xiao H, Palhan V, Yang Y, Roeder RG (2000) TIP30 has an intrinsic kinase activity required for up-regulation of a subset of apoptotic genes. Embo J 19: 956–963.
20. Jenkins G, Frohman M (2005) Phospholipase D: a lipid centric review. Cellular and Molecular Life Sciences 62: 2305–2316.
21. Connell E, Darios F, Broersen K, Gatsby N, Peak-Chew SY, et al. (2007) Mechanism of arachidonic acid action on syntaxin-Munc18. EMBO Rep 8: 414–419.
22. Latham CF, Osborne SL, Cryle MJ, Meunier FA (2007) Arachidonic acid potentiates exocytosis and allows neuronal SNARE complex to interact with Munc18a. J Neurochem 100: 1543–1554.
23. Rickman C, Davletov B (2005) Arachidonic acid allows SNARE complex formation in the presence of Munc18. Chem Biol 12: 545–553.
24. Jones D, Morgan C, Cockcroft S (1999) Phospholipase D and membrane traffic: Potential roles in regulated exocytosis, membrane delivery and vesicle budding. Biochimica et Biophysica Acta (BBA) - Molecular and Cell Biology of Lipids 1439: 229–244.
25. Lee YC, Zheng YO, Taraschi TF, Janes N (1996) Hydrophobic alkyl headgroups strongly promote membrane curvature and violate the headgroup volume correlation due to "headgroup" insertion. Biochemistry 35: 3677–3684.
26. Fahey DA, Small DM (1986) Surface properties of 1,2-dipalmitoyl-3-acyl-sn-glycerols. Biochemistry 25: 4468–4472.
27. Kinnunen PK, Holopainen JM (2000) Mechanisms of initiation of membrane fusion: role of lipids. Biosci Rep 20: 465–482.
28. Kinnunen PK (1992) Fusion of lipid bilayers: a model involving mechanistic connection to HII phase forming lipids. Chem Phys Lipids 63: 251–258.
29. Gorvel JP, Escola JM, Stang E, Bakke O (1995) Invariant chain induces a delayed transport from early to late endosomes. J Biol Chem 270: 2741–2746.
30. Fuchs R, Ellinger I (2002) Free-flow electrophoretic analysis of endosome subpopulations of rat hepatocytes. Curr Protoc Cell Biol Chapter 3: Unit 3 11.
31. Bligh EG, Dyer WJ (1959) A rapid method of total lipid extraction and purification. Can J Biochem Physiol 37: 911–917.
32. Dowler S, Kular G, Alessi DR (2002) Protein lipid overlay assay. Sci STKE 2002: pl6.